

Report No. CG-D-09-95



A Review of Selected Modular Maneuvering Models

Robert D. Sedat
and
Nathan R. Fuller

U.S. Coast Guard
Research and Development Center
1082 Shennecossett Road
Groton, CT 06340-6096



FINAL REPORT
NOVEMBER 1994

This document is available to the U.S. public through the
National Technical Information Service, Springfield, Virginia 22161

Prepared for:

U.S. Department of Transportation
United States Coast Guard
Office of Engineering, Logistics, and Development
Washington, DC 20593-0001

19950515 104

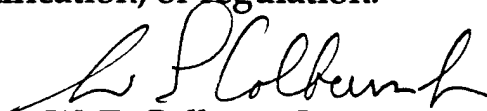
DTIC QUALITY INSPECTED 5

NOTICE

This document is disseminated under the sponsorship of the Department of Transportation in the interest of information exchange. The United States Government assumes no liability for its contents or use thereof.

The United States Government does not endorse products or manufacturers. Trade or manufacturers' names appear herein solely because they are considered essential to the object of this report.

The contents of this report reflect the views of the Coast Guard Research & Development Center. This report does not constitute a standard, specification, or regulation.



W. E. Colburn, Jr.

Technical Director, Acting
United States Coast Guard
Research & Development Center
1082 Shennecossett Road
Groton, CT 06340-6096

Technical Report Documentation Page

1. Report No. CG-D-09-95		2. Government Accession No.		3. Recipient's Catalog No.	
4. Title and Subtitle A Review of Selected Modular Maneuvering Models				5. Report Date November 1994	
				6. Performing Organization Code	
7. Author(s) Robert D. Sedat and Nathan R. Fuller				8. Performing Organization Report No. R&DC 32/94	
				10. Work Unit No. (TRAIS)	
9. Performing Organization Name and Address U.S. Coast Guard Research and Development Center 1082 Shennecossett Road Groton, Connecticut 06340-6096				11. Contract or Grant No.	
				13. Type of Report and Period Covered Final Report	
				14. Sponsoring Agency Code	
12. Sponsoring Agency Name and Address Department of Transportation U.S. Coast Guard Office of Engineering, Logistics, and Development Washington, D.C. 20593-0001					
15. Supplementary Notes Robert Sedat (203) 441-2684 of the CG R & D Center was the COTR for the projects described by this report. Nathan Fuller (202) 267-2015 of Coast Guard Headquarters (G-ENE) provided technical support.					
16. Abstract This report summarizes rotating arm model tests performed on a small and large-scale MARINER model, and on a systematic series of 14 small models based on variations of the MARINER hull form. Forces and moments on all the fully fixed models were recorded. In the large-scale MARINER tests, data on rudder inflow velocities, and the effect of the rudder and propeller on hull forces and moment were also obtained. The report then describes full-scale maneuvering trials performed on a MARINER class ship. Finally, maneuvering calculations based on modular principles are presented, and show satisfactory agreement with the trials' results. Such calculations can be performed during preliminary design to predict the effects of various hull, propeller and rudder geometries on vessel maneuverability.					
17. Key Words maneuvering modular rotating arm scale effects MARINER trials simulation propeller rudder systematic series				18. Distribution Statement Document is available to the U.S. public through the National Technical Information Service, Springfield, Virginia 22161	
19. Security Classif. (of this report) UNCLASSIFIED		20. SECURITY CLASSIF. (of this page) UNCLASSIFIED		21. No. of Pages	
				22. Price	

METRIC CONVERSION FACTORS

Approximate Conversions to Metric Measures

Symbol	When You Know	Multiply By	To Find	Symbol
LENGTH				
in	inches	* 2.5	centimeters	cm
ft	feet	30	centimeters	cm
yd	yards	0.9	meters	m
mi	miles	1.6	kilometers	km
AREA				
in ²	square inches	6.5	square centimeters	cm ²
ft ²	square feet	0.09	square meters	m ²
yd ²	square yards	0.8	square meters	m ²
mi ²	square miles	2.6	square kilometers	km ²
	acres	0.4	hectares	ha
MASS (WEIGHT)				
oz	ounces	28	grams	g
lb	pounds	0.45	kilograms	kg
	short tons (2000 lb)	0.9	tonnes	t
VOLUME				
tsp	teaspoons	5	milliliters	ml
tbsp	tablespoons	15	milliliters	ml
fl oz	fluid ounces	30	milliliters	ml
c	cups	0.24	liters	l
pt	pints	0.47	liters	l
qt	quarts	0.95	liters	l
gal	gallons	3.8	liters	l
ft ³	cubic feet	0.03	cubic meters	m ³
yd ³	cubic yards	0.76	cubic meters	m ³
TEMPERATURE (EXACT)				
°F	Fahrenheit temperature	5/9 (after subtracting 32)	Celsius temperature	°C

*1 in = 2.54 (exactly).

Approximate Conversions from Metric Measures

Symbol	When You Know	Multiply By	To Find	Symbol
LENGTH				
mm	millimeters	0.04	inches	in
cm	centimeters	0.4	inches	in
m	meters	3.3	feet	ft
m	meters	1.1	yards	yd
km	kilometers	0.6	miles	mi
AREA				
cm ²	square centimeters	0.16	square inches	in ²
m ²	square meters	1.2	square yards	yd ²
km ²	square kilometers	0.4	square miles	mi ²
ha	hectares (10,000 m ²)	2.5	acres	
MASS (WEIGHT)				
g	grams	0.035	ounces	oz
kg	kilograms	2.2	pounds	lb
t	tonnes (1000 kg)	1.1	short tons	
VOLUME				
ml	milliliters	0.03	fluid ounces	fl oz
l	liters	0.125	cups	c
l	liters	2.1	pints	pt
l	liters	1.06	quarts	qt
l	liters	0.26	gallons	gal
m ³	cubic meters	35	cubic feet	ft ³
m ³	cubic meters	1.3	cubic yards	yd ³
TEMPERATURE (EXACT)				
°C	Celsius temperature	9/5 (then add 32)	Fahrenheit temperature	°F

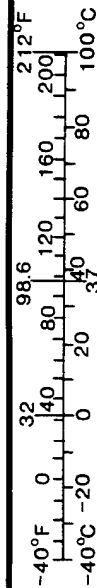


Table of Contents

	<u>Page</u>
List of Figures.....	vii
List of Tables.....	x
Nomenclature.....	xi
Background.....	1
Equations of Motion.....	3
The Japanese Mathematical Modeling Group (MMG).....	9
Coast Guard Experimental Program.....	9
Stevens Institute of Technology Test Program.....	10
Comparison of Bare Hull Forces and Moment to Existing Data and Development of New Regression Equations.....	12
David Taylor Research Center Test Program.....	67
Propeller Inflow and Propeller Forces.....	76
Rudder Inflow Velocity and Direction.....	82
Rudder Forces and Moment.....	87
Simplified Steady State Turning Circle Predictions.....	88
A Desktop Ship Maneuvering Simulator (DSMS).....	88
Full-Scale Trials.....	89
Comparison of Simulation to Full-Scale Trials.....	89
Conclusions.....	94
Recommendations.....	95
References.....	96

Accession For	
NTIS CRA&I	<input checked="" type="checkbox"/>
DTIC TAB	<input type="checkbox"/>
Unannounced	<input type="checkbox"/>
Justification	
By	
Distribution /	
Availability Codes	
Dist	Avail and/or Special
A-1	

Table of Contents (Cont'd)

	<u>Page</u>
Appendix A: IMO Interim Standards for Ship Maneuverability.....	A-1
Appendix B: Added Mass Values.....	B-1
Appendix C: Commercially Available PC-based Maneuvering Simulators.....	C-1
Appendix D: Steady-State Diagram of Steering.....	D-1

Acknowledgement: Special thanks to the late Dr. Volf Asinovsky, who originated the Coast Guard model tests described herein, and provided challenging technical leadership in this research effort until his untimely death in 1989. Thanks also to G-MTH-4 and G-ENE-5 for supporting this work, and to the staffs at DTRC and SIT for conducting the model tests.

List of Figures

<u>Figure</u>	<u>Page</u>
1. Coordinate System and Sign Conventions.....	4
2. Increase of Resistance Augmentation with Propeller Load.....	7
3. Non-Dimensional Side Force on MARINER Model.....	13
4. Non-Dimensional Yaw Moment on MARINER Model.....	14
5. Non-Dimensional Axial Force on MARINER Model.....	15
6. Non-Dimensional Side Force on Parent Model.....	16
7. Non-Dimensional Yaw Moment on Parent Model.....	17
8. Non-Dimensional Axial Force on Parent Model.....	18
9. Non-Dimensional Side Force on Model A1.....	19
10. Non-Dimensional Yaw Moment on Model A1.....	20
11. Non-Dimensional Axial Force on Model A1.....	21
12. Non-Dimensional Side Force on Model A2.....	22
13. Non-Dimensional Yaw Moment on Model A2.....	23
14. Non-Dimensional Axial Force on Model A2.....	24
15. Non-Dimensional Side Force on Model B1.....	25
16. Non-Dimensional Yaw Moment on Model B1.....	26
17. Non-Dimensional Axial Force on Model B1.....	27
18. Non-Dimensional Side Force on Model B2.....	28
19. Non-Dimensional Yaw Moment on Model B2.....	29
20. Non-Dimensional Axial Force on Model B2.....	30
21. Non-Dimensional Side Force on Model C1.....	31
22. Non-Dimensional Yaw Moment on Model C1.....	32
23. Non-Dimensional Axial Force on Model C1.....	33
24. Non-Dimensional Side Force on Model C2.....	34

<u>Figure</u>	<u>Page</u>
25. Non-Dimensional Yaw Moment on Model C2.....	35
26. Non-Dimensional Axial Force on Model C2.....	36
27. Non-Dimensional Side Force on Model C3.....	37
28. Non-Dimensional Yaw Moment on Model C3.....	38
29. Non-Dimensional Axial Force on Model C3.....	39
30. Non-Dimensional Side Force on Model D1.....	40
31. Non-Dimensional Yaw Moment on Model D1.....	41
32. Non-Dimensional Axial Force on Model D1.....	42
33. Non-Dimensional Side Force on Model D2.....	43
34. Non-Dimensional Yaw Moment on Model D2.....	44
35. Non-Dimensional Axial Force on Model D2.....	45
36. Non-Dimensional Side Force on Model D3.....	46
37. Non-Dimensional Yaw Moment on Model D3.....	47
38. Non-Dimensional Axial Force on Model D3.....	48
39. Non-Dimensional Side Force on Model E1.....	49
40. Non-Dimensional Yaw Moment on Model E1.....	50
41. Non-Dimensional Axial Force on Model E1.....	51
42. Non-Dimensional Side Force on Model E2.....	52
43. Non-Dimensional Yaw Moment on Model E2.....	53
44. Non-Dimensional Axial Force on Model E2.....	54
45. Non-Dimensional Side Force on Model E3.....	55
46. Non-Dimensional Yaw Moment on Model E3.....	56
47. Non-Dimensional Axial Force on Model E3.....	57
48. Non-Dimensional Side Force at Large Drift Angles for MARINER Model.....	58
49. Non-Dimensional Yaw Moment at Large Drift Angles for MARINER Model.....	59

<u>Figure</u>	<u>Page</u>
50. Non-Dimensional Axial Force at Large Drift Angles for MARINER Model.....	60
51. Comparison of Present Regression Equation and Canadian Model for Axial Force on Parent Model.....	62
52. Comparison of Present Regression Equation and Inoue's Regression Equation for Side Force on Parent Model.....	63
53. Comparison of Present Regression Equation and Inoue's Regression Equation for Yaw Moment on Parent Model.....	64
54. Effect of Model Scale on Side Force Data.....	69
55. Effect of Model Scale on Yaw Moment Data.....	70
56. Effect of Model Scale on Axial Force Data.....	71
57. Effect of Rudder Angle of Attack on MARINER Side Force and Moment.....	73
58. Stern Geometry with Pitot Tube Rudder, and Propulsion Data.....	74
59. Schematic Illustration of Flow Straightening Effect...	75
60. Flag Rudder Angle vs. Geometric Rudder Drift Angle (with and without Propeller).....	77
61. Propeller Inflow Velocity vs. Geometric Propeller Drift Angle.....	79
62. Propeller Inflow Angle vs. Geometric Propeller Drift Angle.....	80
63. Rudder Inflow Angle vs. Geometric Rudder Drift Angle.....	84
64. Rudder Inflow Velocity vs. Geometric Rudder Drift Angle.....	85
65. Axial Velocity Induced by the Propeller on the Rudder.....	86
66. Comparison of Predicted and Measured Turning Circles.....	91
67. Predicted 10-10 Zig-Zag (20 Knot Approach Speed).....	92

<u>Figure</u>	<u>Page</u>
68. Measured 10-10 Zig-Zag (20 Knot Approach Speed).....	93

List of Tables

<u>Table</u>	<u>Page</u>
1. USCG Series - Hull Characteristics.....	11
2. Coefficients for Present Regression Equations.....	66
3. Characteristics of Full-Scale MARINER and DTRC Model...	68
D-1. Diagram of Steering for MARINER Class Ship.....	D-4
D-2. Diagram of Steering for MARINER Class Ship with Reduced Rudder Size.....	D-5

NOMENCLATURE

a	hull resistance augmentation factor
A_p	area of propeller disk = $\pi D^2/4$
B	maximum beam at waterline
C_{aca}	aft lateral area coefficient = twice projected underwater lateral area aft of midships/(LH)
C_b	block coefficient = $V/(LBH)$
C_{fca}	forward lateral area coefficient = twice projected underwater lateral area forward of midships/(LH)
C_{FM}	model coefficient of frictional resistance
C_{FS}	ship coefficient of frictional resistance
CG	center of gravity
C_M	midship area coefficient = area of midship section/(BH)
C_P	prismatic coefficient = C_b/C_M
C_T	propeller loading coefficient = $T/(\rho/2 A_p V_a^2)$
D	propeller diameter
EAR	propeller expanded area ratio
F	generalized force
Fr	Froude number = $V/(gL)^{1/2}$
GM	transverse metacentric height
g	gravitational acceleration
H	draft at midships
I	generalized moment of inertia
I_{pp}	propeller rotational moment of inertia
I_{xx}	hull moment of inertia about x axis
J	propeller advance coefficient = $V_a/(nD)$
J_{pp}	propeller added moment of inertia

Nomenclature (Cont'd)

K_T	propeller thrust coefficient = $T/(\rho/2 n^2 D^4)$
K_Q	propeller torque coefficient = $Q/(\rho/2 n^2 D^5)$
L	waterline length
LCG	x-distance from midships to longitudinal center of gravity (negative if LCG aft of midships)
LOA	overall length
M	generalized moment
m	vessel mass
m_{ij}	added mass ($i=1-6$, $j=1-6$: subscripts 1-3 refer to translations about x, y and z axes respectively, 3-6 refer to rotations about x, y and z respectively)
N	measured bare-hull hydrodynamic yaw moment about amidships
N'	non-dimensional bare-hull hydrodynamic yaw moment about amidships = $N/(\rho/2 V^2 L^3)$
N''	Inoue's non-dimensional bare-hull hydrodynamic yaw moment about amidships = $N/(\rho/2 V^2 H L^2)$
N_H	viscosity-induced hydrodynamic yaw moment about CG due to hull (including interaction effects)
N_P	viscosity-induced hydrodynamic yaw moment about CG due to propeller (including interaction effects)
N_R	viscosity-induced hydrodynamic yaw moment about CG due to rudder (including interaction effects)
n	propeller revolutions per second
Q	propeller torque
Q_d	delivered engine torque
Q_f	torque due to bearing friction
R	instantaneous radius of curvature (or rotating arm length)
r	dimensional yaw rate (radians/sec.)

Nomenclature (Cont'd)

r'	non-dimensional yaw rate = $rL/V = L/R$
t	thrust deduction factor
T	propeller thrust
u	velocity in x-direction
u_a	axial velocity induced by propeller (see Figure 65)
V	magnitude of ships velocity vector
V_a	propeller speed of advance = $V (1-w_p)$
V_p	effective propeller inflow velocity
V_R	effective rudder inflow velocity
VCG	vertical center of gravity (above baseline)
V_a	propeller speed of advance = $V (1-w_p)$
v	velocity in y-direction
w_p	effective wake fraction at propeller
w_{p0}	effective wake fraction at propeller (on straight steady course)
w_R	effective wake fraction at rudder
w_{R0}	effective wake fraction at rudder on straight steady course
X	measured bare-hull hydrodynamic force in x-direction (with centrifugal force deducted)
X'	non-dimensional bare-hull hydrodynamic X-force = $X/(\rho/2 L^2 V^2)$
X_H	viscosity-induced hydrodynamic surge force on hull (including interaction effects)
X_P	viscosity-induced hydrodynamic surge force on propeller (including interaction effects)
X_R	viscosity-induced hydrodynamic surge force on rudder (including interaction effects)
x	surge direction on ship-fixed axis system

Nomenclature (Cont'd)

x_P	x-distance from LCG to propeller plane (generally negative)
x_R	x-distance from LCG to rudder quarter chord point (generally negative)
Y	measured bare-hull hydrodynamic force in y-direction (with centrifugal force deducted)
Y'	non-dimensional bare-hull hydrodynamic Y-force $= Y/(\rho/2 V^2 L^2)$
Y''	Inoue's bare-hull non-dimensional hydrodynamic Y-force $= Y/(\rho/2 V^2 L H)$
Y_H	viscosity-induced hydrodynamic sway force on hull (including interaction effects)
Y_P	viscosity-induced hydrodynamic sway force on propeller (including interaction effects)
Y_R	viscosity-induced hydrodynamic sway force on rudder (including interaction effects)
y	sway direction on ship-fixed axis system
z	yaw axis (positive downwards)

Greek Symbols

α_P	effective propeller inflow angle
α_R	effective rudder inflow angle
β	geometric drift angle at midships
β_{cg}	geometric drift angle at LCG
β_P	geometric drift angle at propeller
β_R	geometric drift angle at rudder (same sign convention as β_P , see Figure 1)
β_x	geometric drift angle at a distance, x , positive forward of tow point
δ	rudder angle
Δ	ship weight

Background

Many current methods for the prediction of ship maneuvering have serious limitations. While the equations of motion are well known, the critical hydrodynamic force and moment terms are usually obtained by experiment. These terms may be expressed by a truncated Taylor series expansion about conditions of zero surge, sway, yaw and rudder angle [Abkowitz]. While appropriate for stability analysis, such truncated expansions are only accurate over a limited range of variables. Other polynomial forms, sometimes including absolute value terms, have also been proposed. Whichever model is chosen, the coefficients (or hydrodynamic derivatives) are generally obtained from rotating arm or planar motion mechanism data using least squares or other curve-fitting methods. Many reports give only the fitted coefficients, which obscures the quality of fit, the range of variables covered, and makes comparison between different models awkward.

Model tests are very expensive, may be subject to scale effects, and are strictly applicable only to the particular hull/rudder/propeller combination tested. Little attempt is made to study the flow field, or to isolate the contributions of these components to the total forces and moments. Thus, it is often prohibitively expensive, during preliminary design, to examine the effect of a different rudder design, propeller size or stern configuration on a ship's maneuverability. As [Dand] concludes, such a model "performs satisfactorily when taken as a whole, but ...does not allow individual elements to be changed as the design is changed. It is a powerful tool for training, but a less useful tool for design." An excellent summary of the overall maneuvering problem is given in the paper by [Oltmann and Sharma].

The International Maritime Organization has recently adopted Interim Standards for Ship Maneuverability, which are presented

in Appendix A. Therefore, it becomes increasingly important for naval architects to be able to predict these characteristics early in the design process. Note that the IMO criteria are based on relatively high-speed, deep-water maneuvers such as turning circles and zig-zags, where $u \gg v$ and drift angles remain relatively low. For more general maneuvering performance prediction, knowledge of the forces and moments is required over the full range of possible drift angles. This paper will review selected maneuvering literature, summarize recent research by the USCG, and propose a maneuvering simulation model capable of predicting arbitrary ship maneuvers.

The modular approach attempts to separate the forces and moments experienced by the hull, rudder, and propeller, and to predict these separate forces from basic physical principles. With such a model, a different hull form, rudder shape or propeller design could be accounted for separately to allow the designer to predict the performance of various configurations in the preliminary design stage. Note that "modular" in this context has nothing to do with software design, although use of separate subroutines (or procedures) is always good programming practice. The main requirement is to be able to separate the forces imposed on the hull, from those on the propeller, and from those on the rudder.

Naturally, there are important interactions between these components. Even in straight ahead motion, it is well known that the hull form affects the velocity of flow into the propeller, and that propeller suction increases the resistance of the hull over that predicted from a towed model (the so-called thrust deduction effect). During maneuvering, the hull also affects the inflow angles to the propeller, producing a flow straightening effect which makes the actual inflow angle less than the geometric angle. The propeller also induces velocities downstream which increase the velocities experienced by the part of the rudder which is in the propeller race, and produce

additional flow straightening. These interactions, and others, will be discussed in more detail later.

Thus, we seek to develop a "modular" model which correctly accounts for the fluid physics, isolates the forces exerted on each of the separate components, accounts for interactions between the components, and allows different configurations to be studied without performing additional model tests on each configuration.

Equations of Motion

The basis of any maneuvering simulation is to express Newton's second law using equations of the type $F = m\ddot{x}$ (or the rotational analog, $M = I\ddot{\alpha}$). Virtually all simulators have such equations for sway, surge and yaw. Some also include equations for roll and propeller rotation. The basic coordinate system and sign conventions used in this paper are illustrated in Figure 1.

Assuming that the vessel is symmetric about the centerplane, does not roll significantly, and is travelling sufficiently slowly that it does not make appreciable waves ($Fr < 0.25$), it can be shown [e.g. Fedyayevskiy and Sobolev] that the 3 degree-of-freedom equations of motion are:

$$\text{Surge: } m(\dot{u} - vr) = -m_{11}\dot{u} + m_{22}vr + m_{26}r^2 + X_H + X_P + X_R$$

$$\text{Sway : } m(\dot{v} + ur) = -m_{22}\dot{v} - m_{11}ur - m_{26}\dot{r} + Y_H + Y_P + Y_R$$

$$\text{Yaw : } I_z\dot{r} = -m_{66}\dot{r} - m_{26}\dot{v} - m_{26}ur - (m_{22}-m_{11})uv + N_H + N_P + N_R$$

Inertial forces on the left-hand side consist of the usual mass times acceleration term, and in the surge and sway equations, a

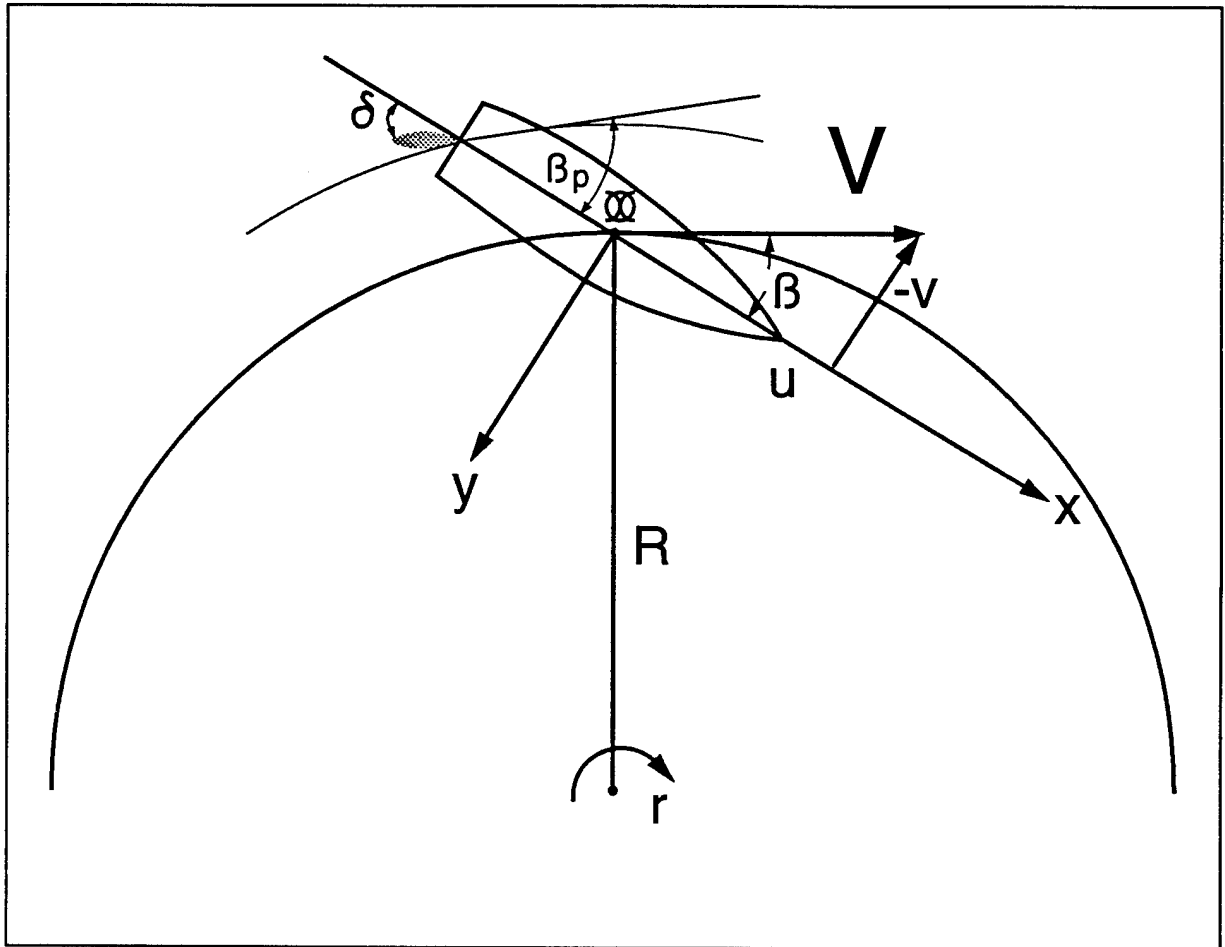


Figure 1. Coordinate System & Sign Conventions
(Also see Figure 59)

second term that results from the fact that the equations of motion are written in a moving co-ordinate system. (Alternatively, these additional terms may be transferred to the right-hand side and considered as centrifugal force terms). The right-hand sides contain all of the hydrodynamic force terms. Those expressions containing added mass terms are forces which result from motion in an ideal (inviscid) fluid. An excellent theoretical derivation of these equations is given in [Newman], whose generalized expressions for forces and moments in inviscid flow with all six degrees of freedom are given in Chapter 4, eqns. 115 and 116. These equations reduce, in three degrees of freedom, for a ship symmetrical about the centerplane, to the same equations given by [Fedyayevskiy and Sobolev]. The added masses can be computed theoretically, or derived from planar motion mechanism tests. Specific values for these m_{ij} terms are discussed further in Appendix B.

The last three right-hand terms in each of the above equations represent forces of a viscous nature acting on the hull, propeller and rudder, respectively, including interaction effects. These include frictional drag, bilge vortex shedding, and lift and drag forces from the propeller and rudder. (Recall that it is viscosity which imposes the Kutta condition and enables surfaces such as the rudder and propeller to develop lift). These viscous forces are subject to Reynolds number scale effects.

Figure 1 shows that a maneuvering vessel has an instantaneous speed, radius of curvature, drift angle, and yaw rate. Using a quasi-steady hypothesis, the forces and moments acting on the hull at that instant can be obtained from a bare hull rotating arm test. Note that un-corrected rotating arm measurements include centrifugal forces, all terms on the right-hand sides of the equations of motion which do not include derivatives with respect to time, and aerodynamic forces (which are generally negligible). If the low frequency added masses are

available from calculation or planar motion mechanism tests, the viscous forces acting on the hull can be obtained by subtracting all steady-state forces (including centrifugal) from the measured forces. When predicting full scale performance, the effect of Reynolds number on the viscous forces should be accounted for. In particular, X_H should be multiplied by C_{FS}/C_{FM} . Viscous corrections for Y_H and N_H are not well known and are often ignored. The total hydrodynamic forces (and moment) can then be non-dimensionalised against $\rho/2 L^2 V^2$ (and $\rho/2 L^3 V^2$), and used to calculate the full scale forces and moment acting on the bare hull. Additionally, when the hydrodynamic moment has been measured about amidships, transferring it to the LCG requires addition of the additional moment, $Y (-LCG)$.

On an operating ship, the ahead resistance is increased due to interaction with the propeller. Thus, the bare hull hydrodynamic surge force should be multiplied by $1/(1-t) = 1+a$ to account for this resistance augmentation, where t for steady ahead operation may be obtained from model tests or regression analyses. When the vessel is accelerating or decelerating however, this resistance augmentation changes with the instantaneous propeller loading coefficient, C_T , as shown in Figure 2. (See also [Harvaldt]). There is a further interaction effect due to pressure modification on the hull caused by a deflected rudder [Martinussen and Linnerud], [Kijima and Nakiri]. This effect is small and often neglected, but will be discussed further later in this paper. Thus, basic hull forces are subject to several interaction effects. If the viscous forces on the rudder and propeller (including interaction effects) can also be accounted for, the equations above can be integrated from their initial conditions to obtain velocity and position at a subsequent time step. By repeating this process, any arbitrary maneuver can be simulated.

In realistic maneuvering conditions, other forces may also arise due to bank suction, shallow water effects, inter-ship

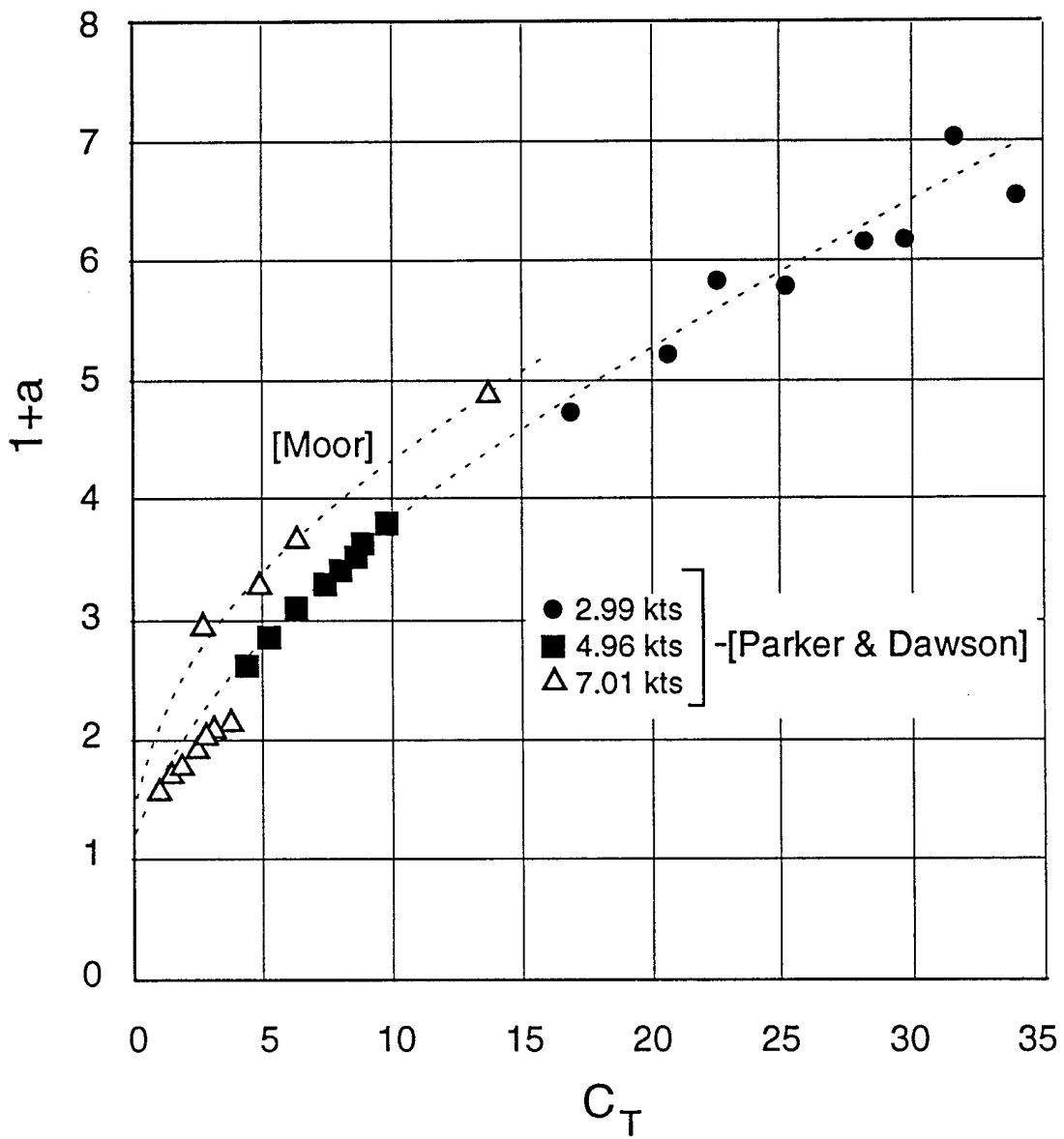


Figure 2. Increase of Resistance Augmentation with Propeller Load

interactions, currents, wind, tugs or lateral thrusters. Such effects could be incorporated into the maneuvering equations, but are not the primary focus of this paper, and will be omitted for simplicity.

During an unsteady maneuver, the propulsive thrust is generally not in equilibrium with the vessel's resistance. Since the propeller operating conditions play an important role in certain interaction effects, as previously discussed, it is necessary to include an additional equation for the rotational accelerations of the engine, gearing, shafting and propeller system. The following equation, combining those used in references [Inoue et al., 1981 (b)] and [Dand], is suggested.

$$\text{Propeller RPM: } 2\pi I_{pp} \dot{n} = -2\pi J_{pp} \dot{n} + Q_d - Q_f - \rho n^2 D^5 K_q$$

where Q_d is the developed engine torque times the gear reduction ratio, Q_f is the torque due to shaft friction, and the final term on the right hand side is the propeller torque. For a diesel powered vessel, the assumption of constant engine torque is reasonable. For a steam plant, the RPM from the previous time step and the constant power assumption can be used to determine the instantaneous engine torque. Additional formulae for engine models are given by [Inoue et al., 1981 (b)], and by [Goodwin et al.]. Added propeller inertia, J_{pp} , can be calculated from the data given in [Norrie]. There is no convenient way to determine damping forces in the gears and bearings, but it is suggested that approximate values can be derived by comparing full scale data from accelerating and decelerating trials to simulations using different assumed damping values. (Such data is available for a steam powered Mariner class ship, for example, [Morse and Price]).

Ship maneuvering generally induces roll, which in turn effects the underwater shape of the hull and the hydrodynamic forces acting on it. [Inoue et al., 1981 (b)], therefore

includes a degree of freedom for roll,

$$\text{Roll: } I_{xx} \ddot{\phi} = -m_{44} \ddot{\phi} + \Delta GM \sin \phi + N_r + Q$$

Where I_{xx} is the roll moment of inertia, and the first term on the right is the added hydrodynamic inertia. The next term is the hydrostatic righting moment. N_r is the rudder induced roll moment, and Q is the propeller torque. Strictly speaking, roll produces additional terms in the surge, sway and yaw equations. [Inoue et al., 1981 (b)] do not include all these coupled terms, but do include a term for yaw moment due to roll.

The Japanese Mathematical Modeling Group (MMG)

In the late 1970's, Japanese researchers began to develop a practical maneuvering simulator which incorporated all the above degrees of freedom, and also accounted for the effect of constant trim on the forces in the surge, sway and yaw equations. Much of the basic work is available only in Japanese, but summary papers [Inoue et al., 1981 (a) and 1981 (b)] and [Hirano et al., 1987] provide valuable insight into their model. Other references pertaining to the MMG model are given in the translation by [Chislett]. Also, an excellent summary of the Japanese model has been compiled by [Lantos and Kendrick]. The Japanese model has proven effective at predicting high-speed maneuvering characteristics, such as those required by the IMO, for a wide variety of ships, but contains no algorithms for computing hull forces at the large drift angles which occur during low speed maneuvering.

Coast Guard Experimental Program

In order to obtain better data on the hydrodynamic forces and moments, the U.S. Coast Guard sponsored a number of rotating arm and towing tank tests. One part of this program, performed

at Stevens Institute of Technology (SIT) involved measuring forces and moments on a systematic series of bare hull forms, and relating them to basic hull form parameters which are generally known during preliminary design. Another part of this program, performed at the David Taylor Research Center (DTRC), involved investigating the interactions between hull, propeller and rudder on a large MARINER model. The Coast Guard program also included full-scale maneuvering trials, conducted by DTRC, on a MARINER hull presently operated by the Navy. Finally, the Coast Guard compared this trials data to simulation results. These various phases of the Coast Guard study are discussed in detail in the following sections.

Stevens Institute of Technology Test Program

For the bare hull tests, the Coast Guard developed lines plans for a series of vessels, called the Asinovsky Maneuvering Series, on which hull form parameters known to effect a vessel's maneuvering characteristics were systematically varied. The parent model is very close in form to the well known MARINER class ship. This series is generally applicable to high-speed fine-form vessels such as commercial cargo ships. The characteristics of the series are given in Table 1, and body plans are shown in [Klosinski and Lewandowski]. (Note that the variations of lateral area coefficients essentially represent different amounts of deadwood and forefoot area).

This series of models was designed to have identical displacements and midship sections, ($C_M = 0.93$), and waterline lengths of approximately six feet each. Scale effects for bare hull tests of fine form ships have been shown to be negligible [Strumpf, 1982], so relatively small models and a less expensive rotating arm were used for these tests. Tests were conducted by Stevens Institute of Technology's Davidson Laboratories, at a Froude number of 0.22, in order to develop forces as large as

Table 1
USCG SERIES - HULL CHARACTERISTICS

HULL	L ft	MODEL		DRAFT in	WEIGHT lb	SHIP WEIGHT 1-TONS	L/B	L/H	C _p	C _{fca}	C _{aca}
		LOA in	BEAM in								
MARINER	5.032	64.00	8.77	3.120	36.1	18640	6.9	19.4	---	---	---
PARENT	5.816	74.89	9.80	3.125	51.6	20930	7.1	22.3	0.70	0.95	0.90
A1	5.814	74.88	9.80	3.819	62.1	25190	7.1	18.3	0.70	0.95	0.90
A2	5.814	74.88	9.80	2.644	43.9	17790	7.1	26.4	0.70	0.95	0.90
B1	5.817	74.87	9.80	3.125	57.0	23120	7.1	22.3	0.75	0.95	0.90
B2	5.817	74.88	9.80	3.125	48.2	19550	7.1	22.3	0.65	0.95	0.90
C1	5.817	74.88	9.15	3.125	47.7	19350	7.6	22.3	0.70	0.95	0.90
C2	5.817	74.89	10.57	3.125	55.6	22550	6.6	22.3	0.70	0.95	0.90
C3	5.817	74.88	11.45	3.125	60.8	24660	6.1	22.3	0.70	0.95	0.90
D1	5.725	75.03	9.80	3.125	51.8	21010	7.0	22.0	0.70	0.95	0.80
D2	5.725	74.97	9.80	3.125	52.0	21100	7.0	22.0	0.70	0.95	0.85
D3	5.725	74.92	9.80	3.125	51.6	20940	7.0	22.0	0.70	0.95	0.95
E1	5.805	74.89	9.80	3.125	52.2	21180	7.1	22.3	0.70	0.85	0.90
E2	5.805	74.89	9.80	3.125	51.8	21040	7.1	22.3	0.70	0.90	0.90
E3	5.781	74.22	9.80	3.125	51.9	21050	7.1	22.2	0.70	1.00	0.90

possible without generating wavemaking forces. A rake of vertical rods was towed ahead of the model to stimulate turbulence. Each model was fully fixed by the dynamometer and tested without trim in calm water. Each was tested at various drift angles (-30° to $+30^\circ$ in 10° increments) and five non-dimensional yaw rates ($r' = 0$ to 0.65). Tests for $r' = 0$ were conducted in the linear towing tank, while the rotating arm tank was used for all other tests. Centrifugal force effects were measured by rotating the model in air, and considering aerodynamic forces negligible. The measured forces in air were then deducted from the measured results in water. The remaining forces and moments were non-dimensionalized by dividing by $(\rho/2) L^2 V^2$ and $(\rho/2) L^3 V^2$, respectively. Thus, non-dimensional steady-state hydrodynamic forces, and the moment about amidships were determined. These results are plotted in Figures 3-47.

An additional series of tests was run on the MARINER model at the same speed and yaw rates, but with β ranging from -180° to $+180^\circ$ in 30° increments. These results are shown in Figures 48-50, but may contain wavemaking effects at $|\beta|$ near 90° due to the relatively high test speed. Additional details of the calibration, testing procedure and data reduction used in these tests are given in [Klosinski and Lewandowski].

Comparison of Bare Hull Forces and Moment to Existing Data and Development of New Regression Equations

It is useful to compare the results of SIT's bare-hull tests to various predictive models which have been published previously. [Lantos and Kendrick] give the following expression for the x-force on a model:

$$X = X_0 (u/V)^2$$

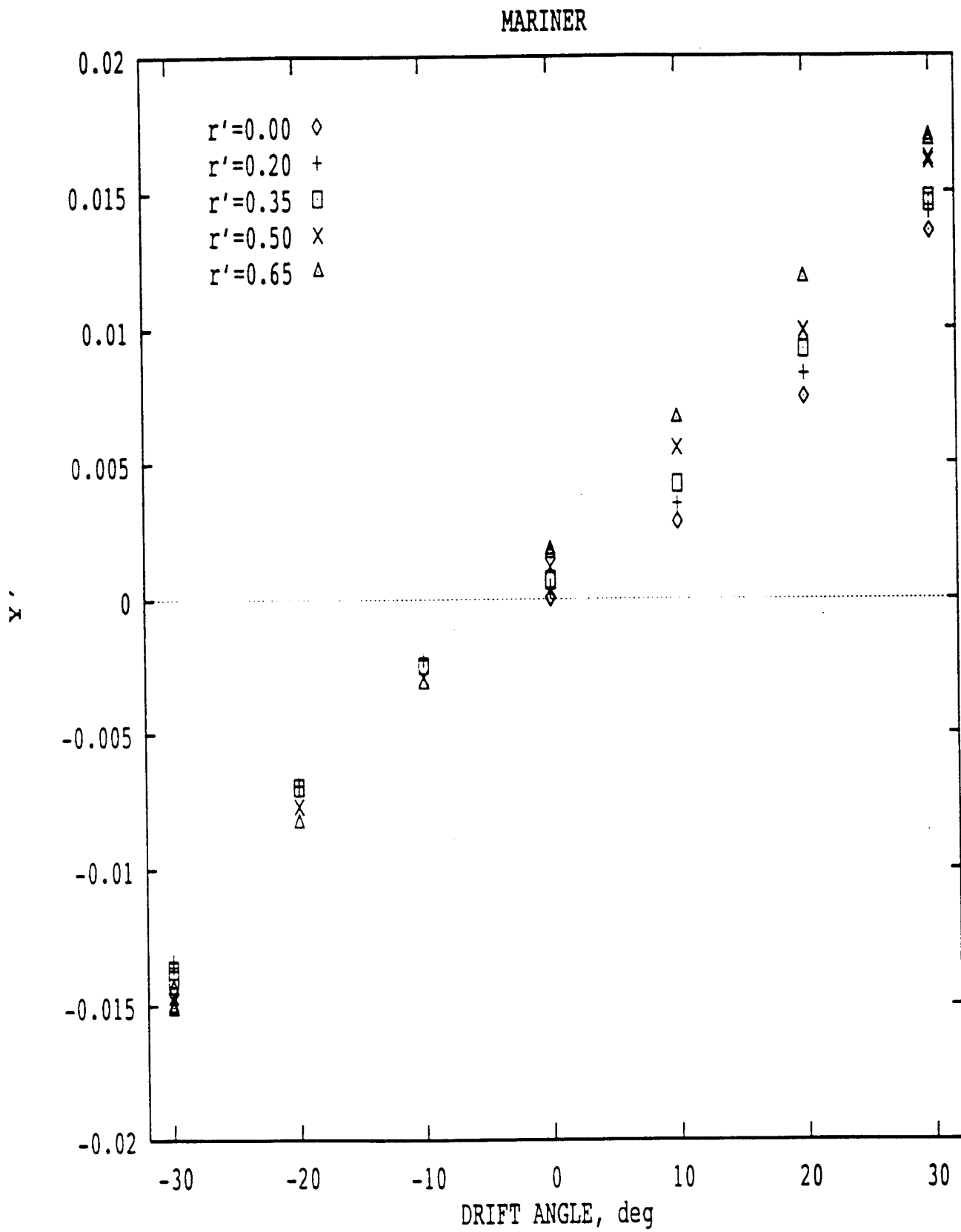


Figure 3. Non-Dimensional Side Force on MARINER Model,
from [Klosinski and Lewandowski]

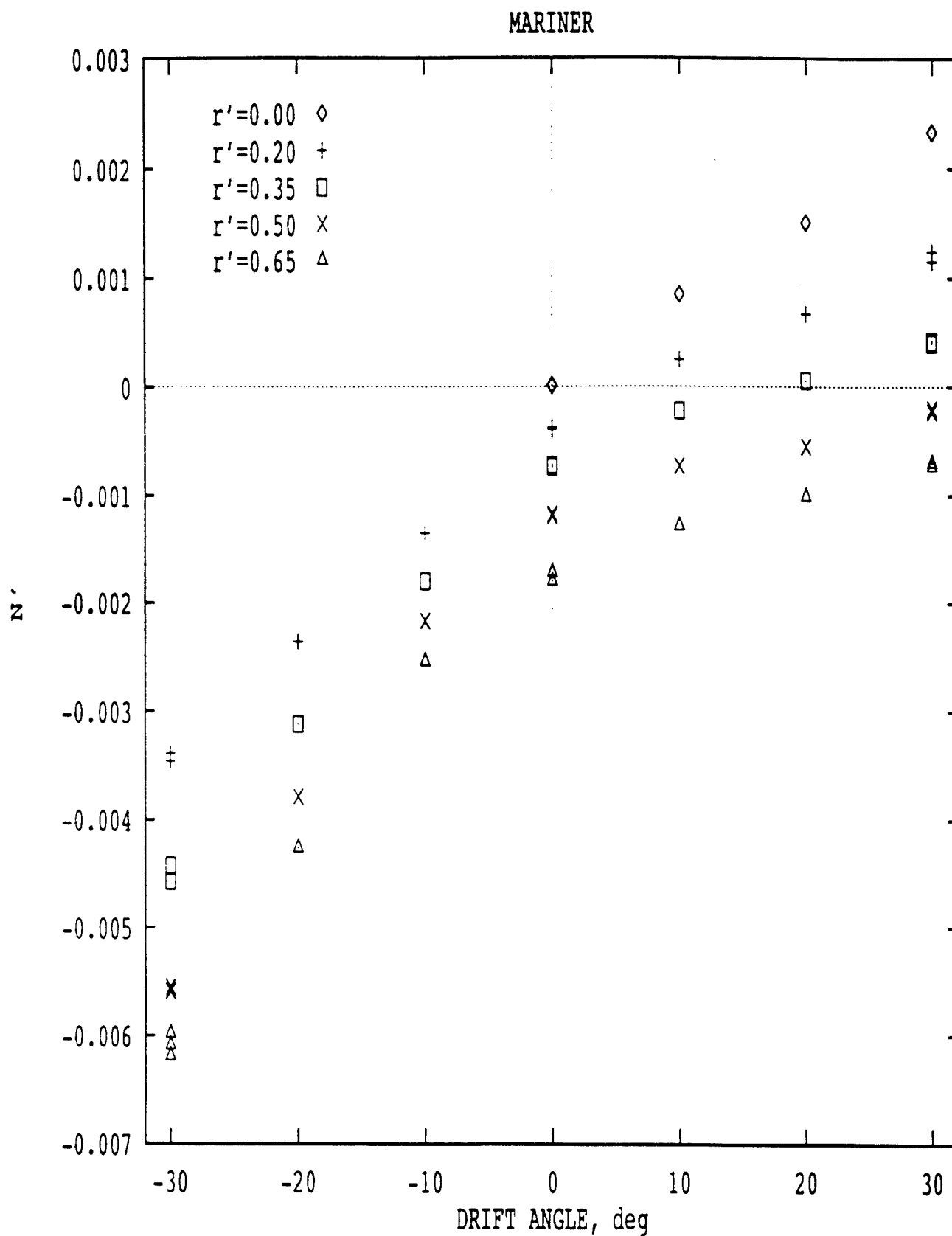


Figure 4. Non-Dimensional Yaw Moment on MARINER Model,
from [Klosinski and Lewandowski]

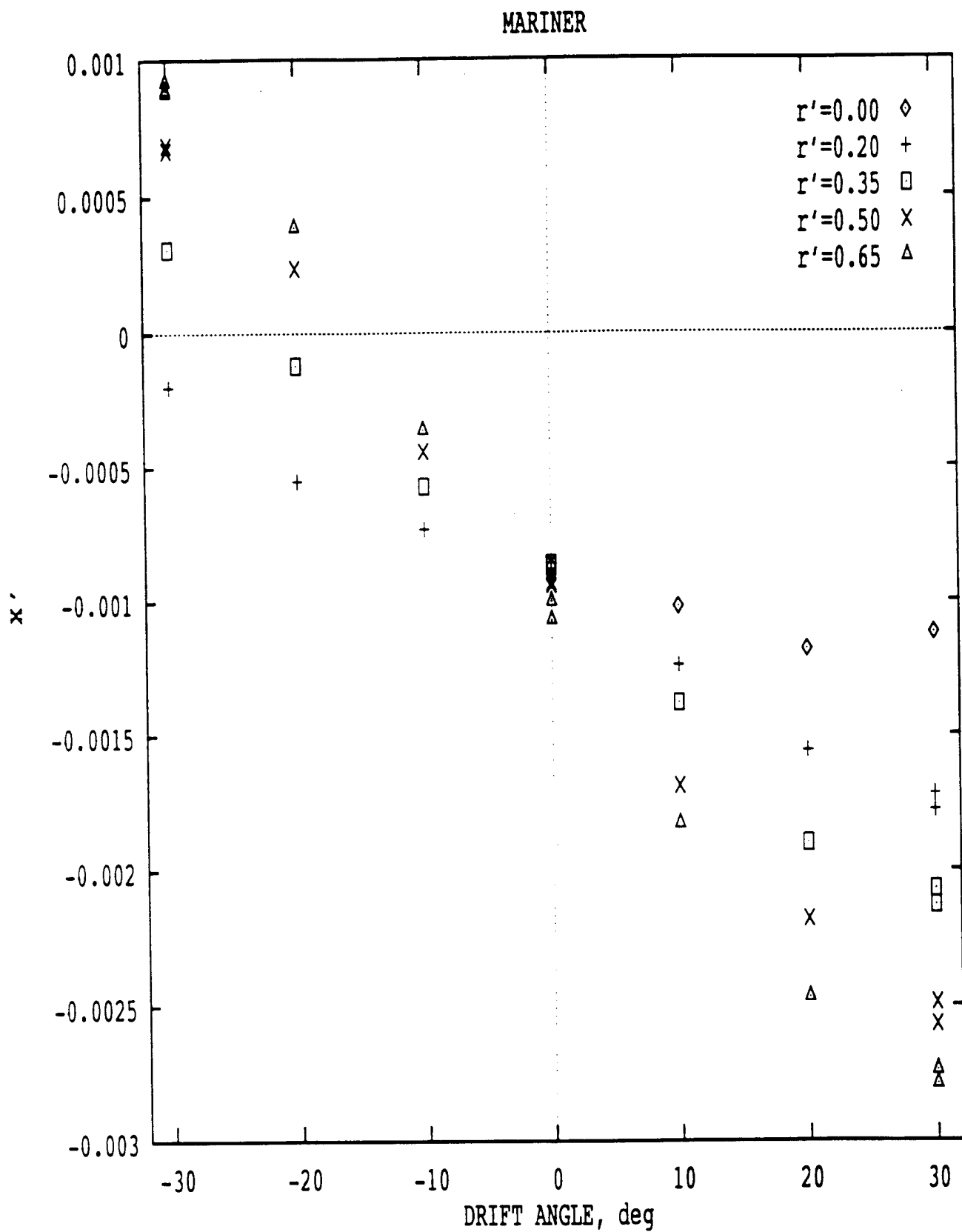


Figure 5. Non-Dimensional Axial Force on MARINER Model,
from [Klosinski and Lewandowski]

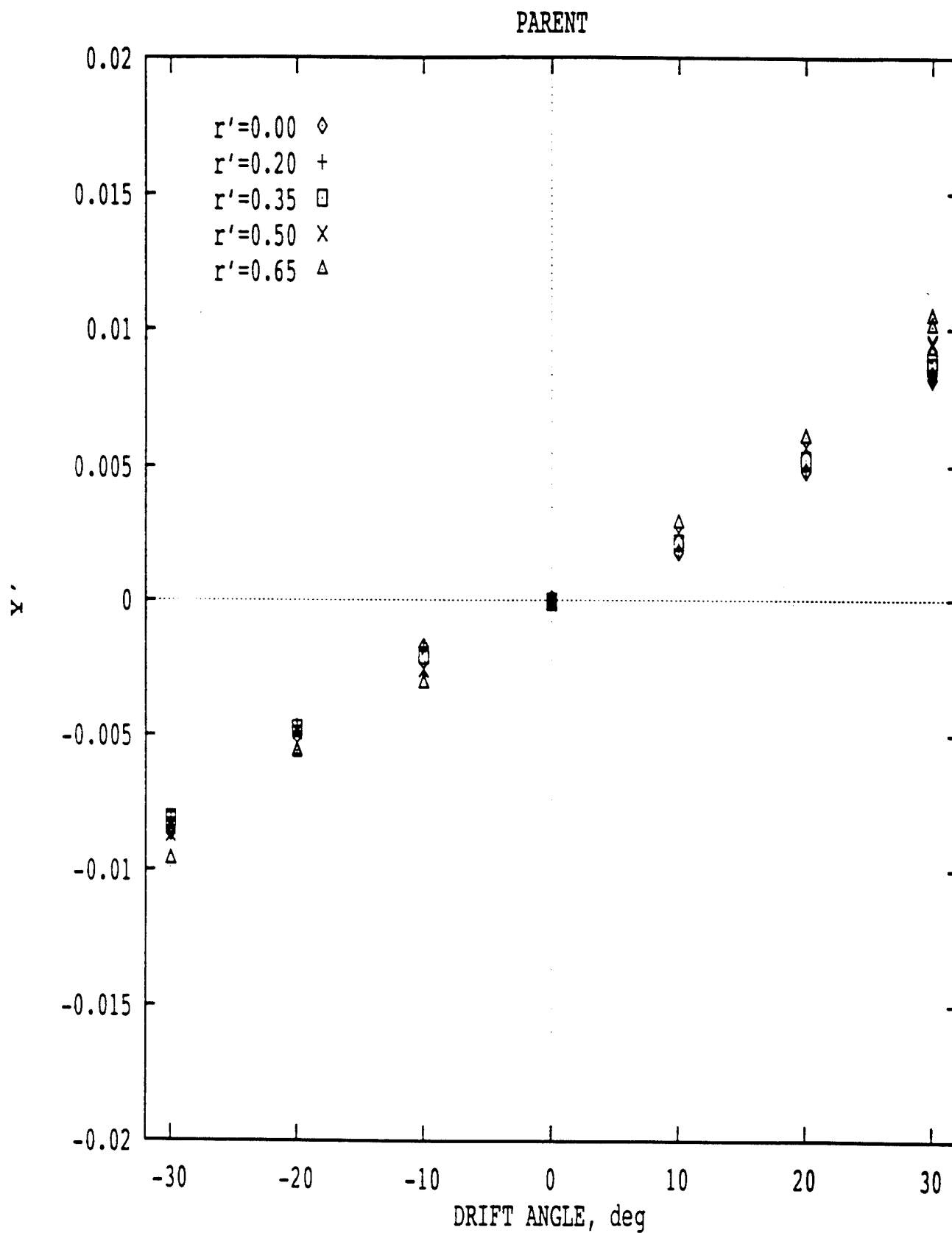


Figure 6. Non-Dimensional Side Force on Parent Model, from [Klosinski and Lewandowski]

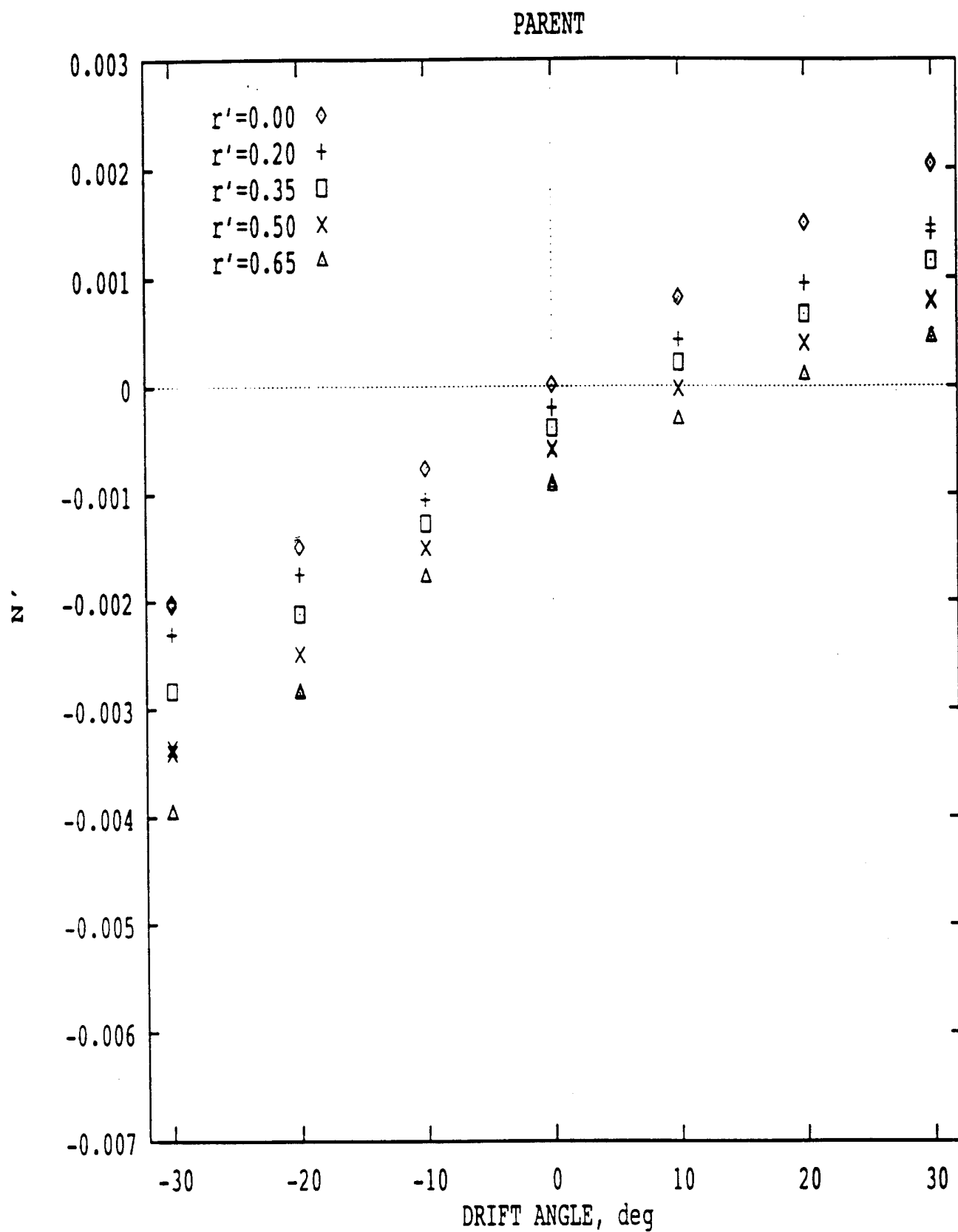


Figure 7. Non-Dimensional Yaw Moment on Parent Model, from [Klosinski and Lewandowski]

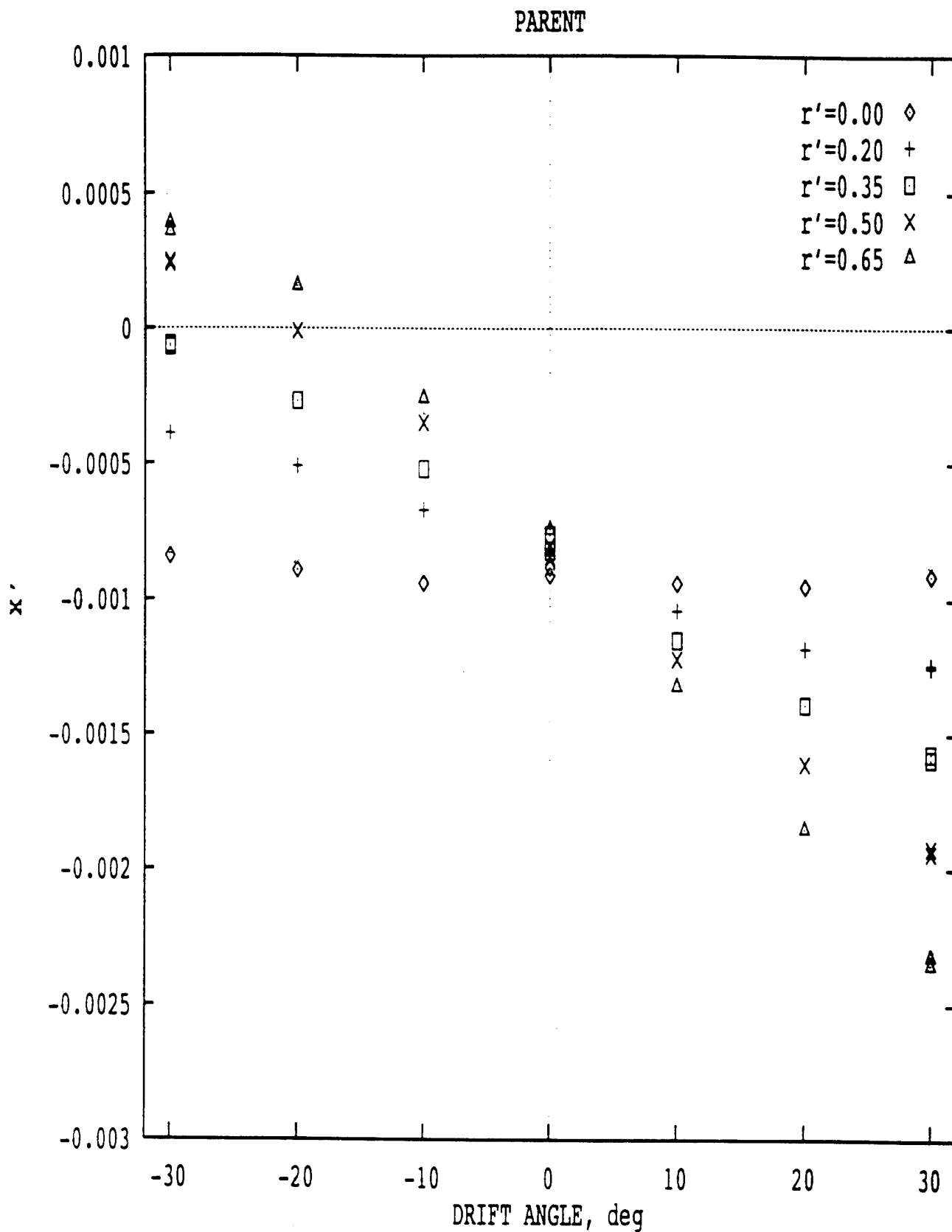


Figure 8. Non-Dimensional Axial Force on Parent Model, from [Klosinski and Lewandowski]

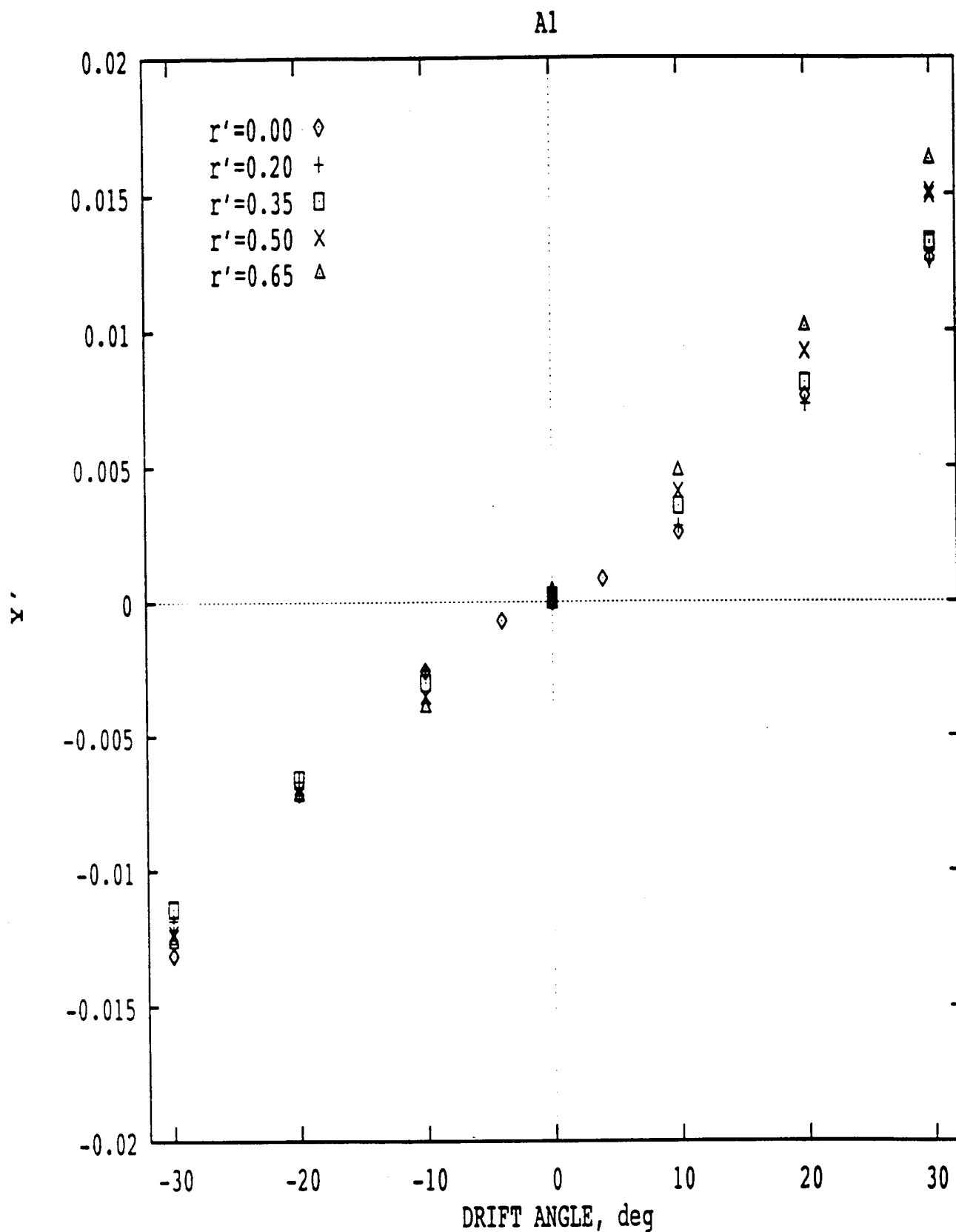


Figure 9. Non-Dimensional Side Force on Model A1, from [Klosinski and Lewandowski]

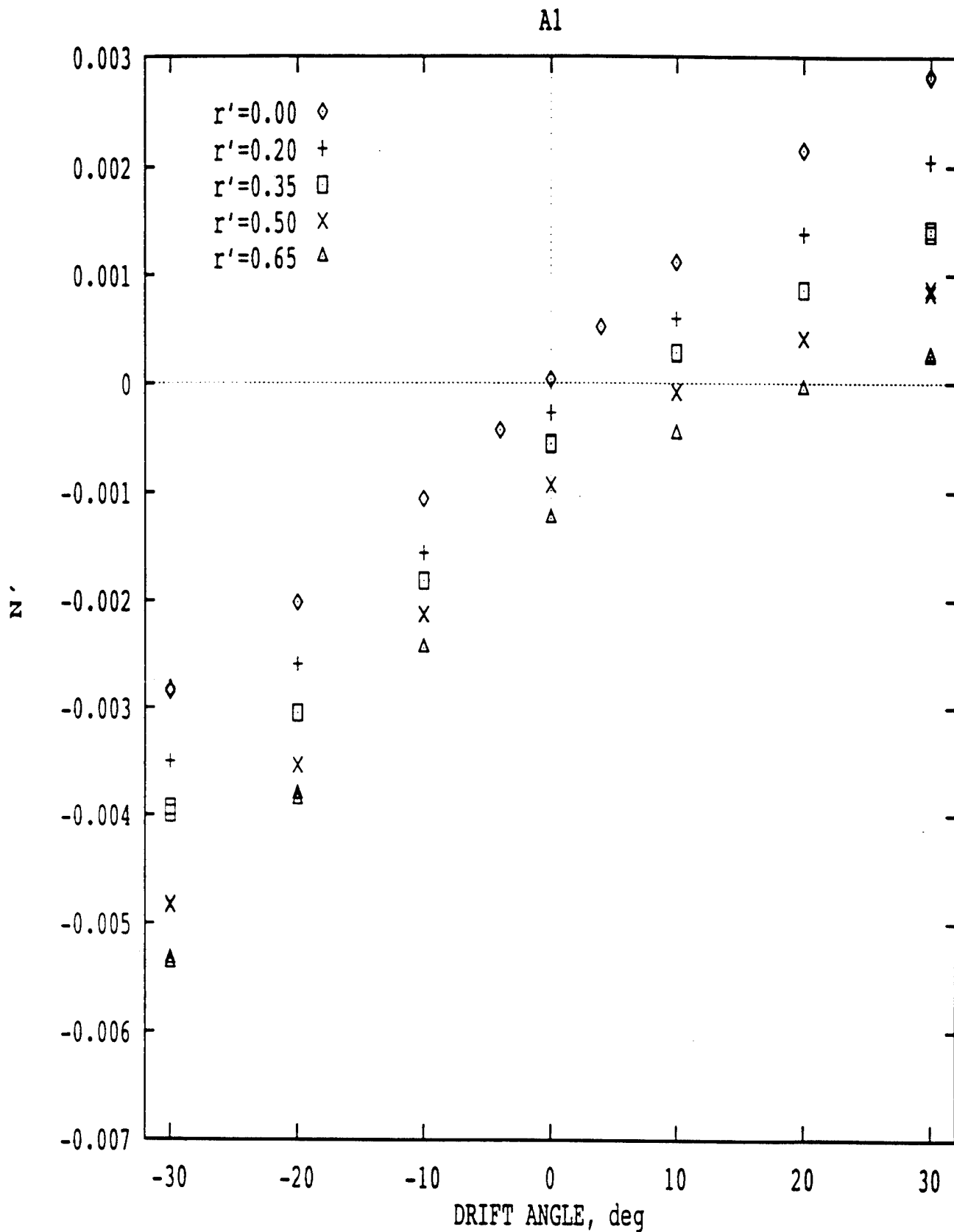


Figure 10. Non-Dimensional Yaw Moment on Model A1, from [Klosinski and Lewandowski]

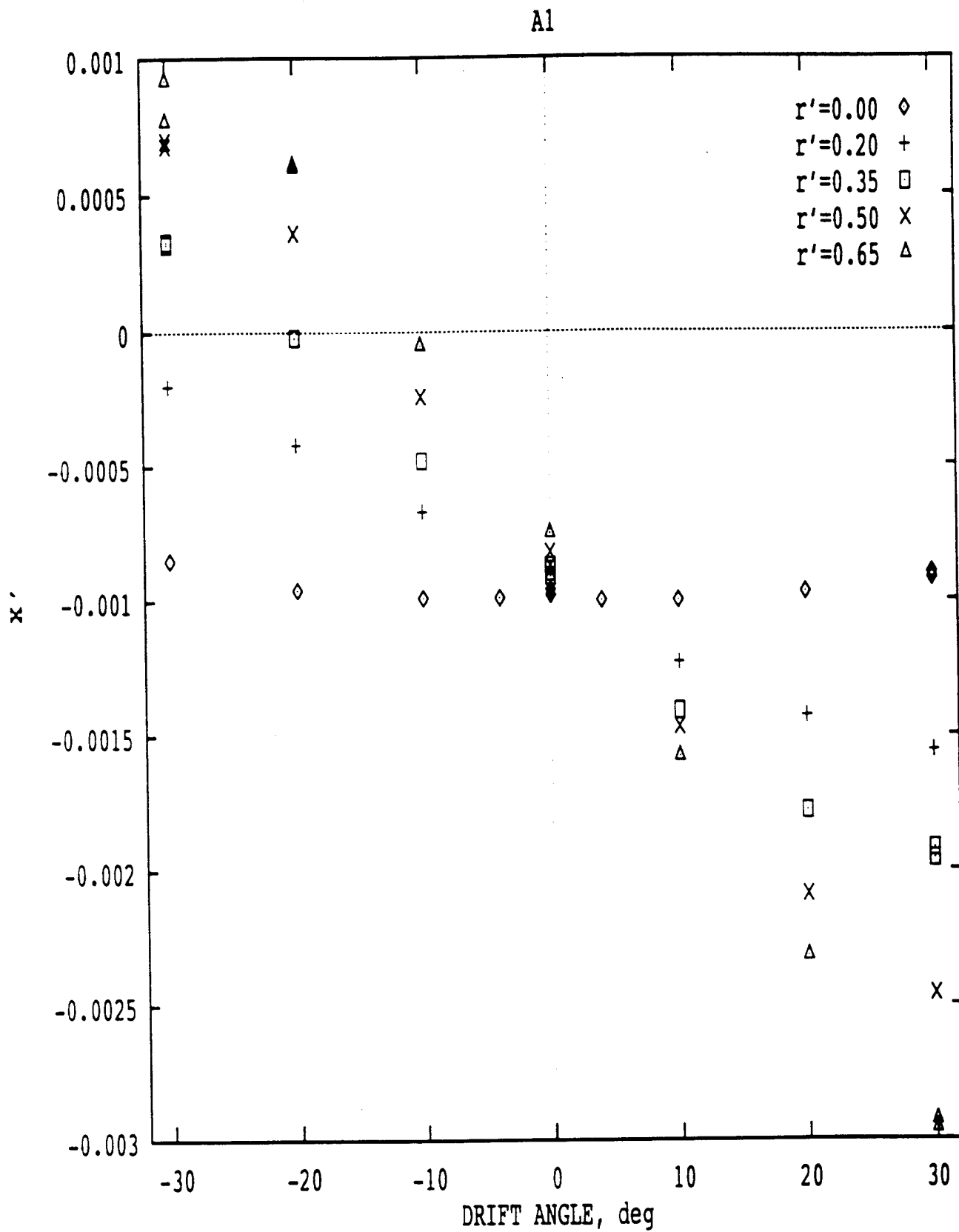


Figure 11. Non-Dimensional Axial Force on Model A1, from [Klosinski and Lewandowski]

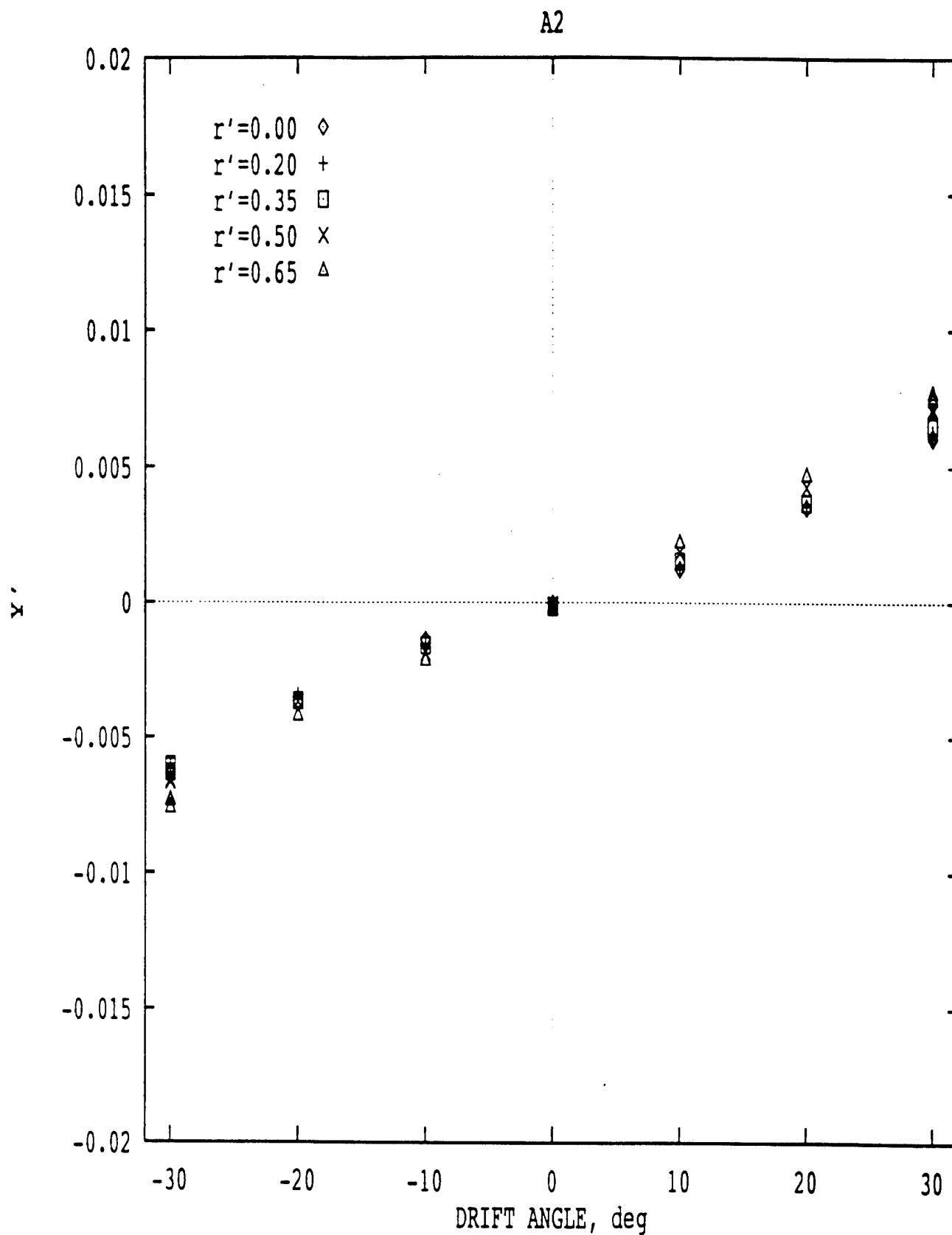


Figure 12. Non-Dimensional Side Force on Model A2, from [Klosinski and Lewandowski]

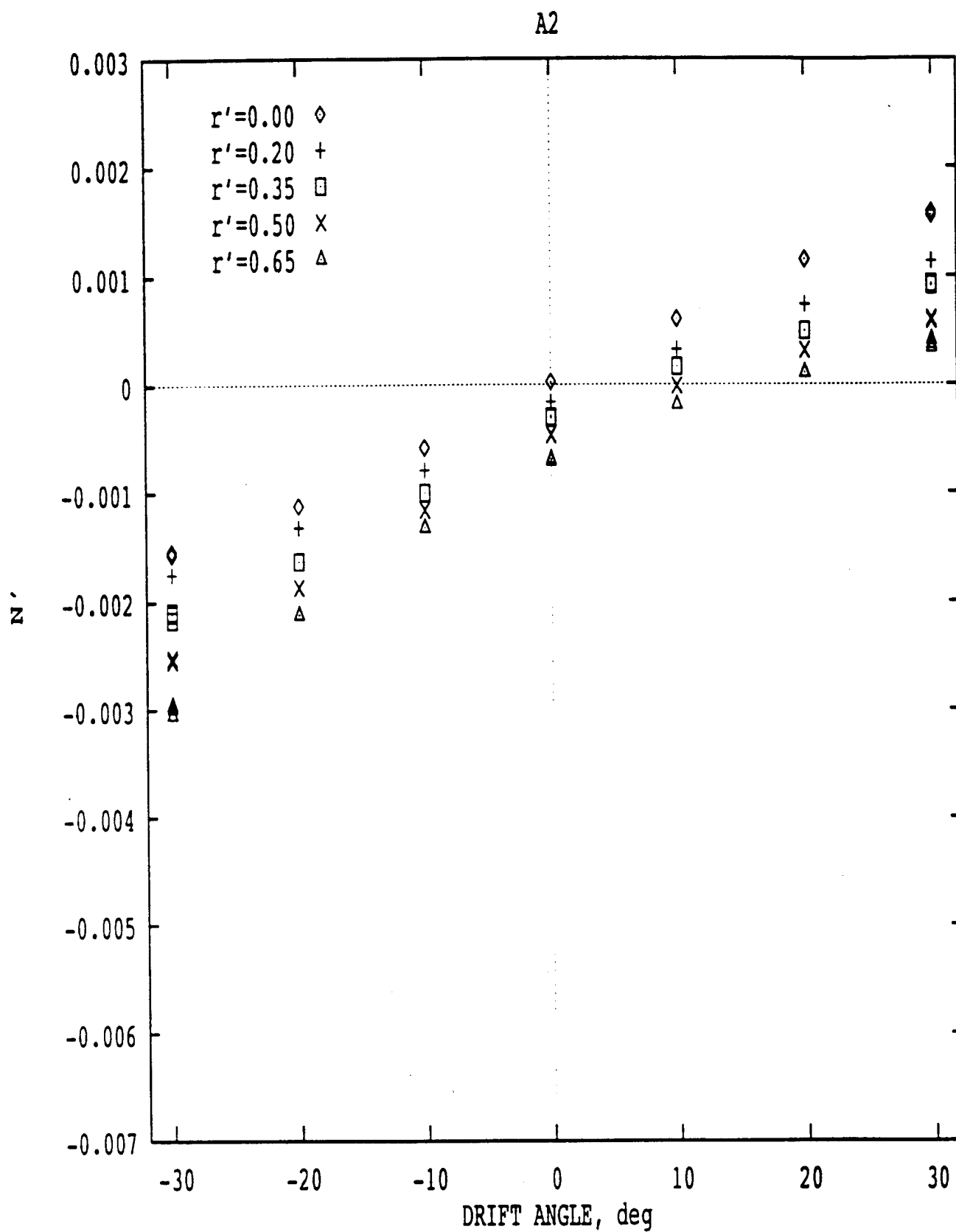


Figure 13. Non-Dimensional Yaw Moment on Model A2, from [Klosinski and Lewandowski]

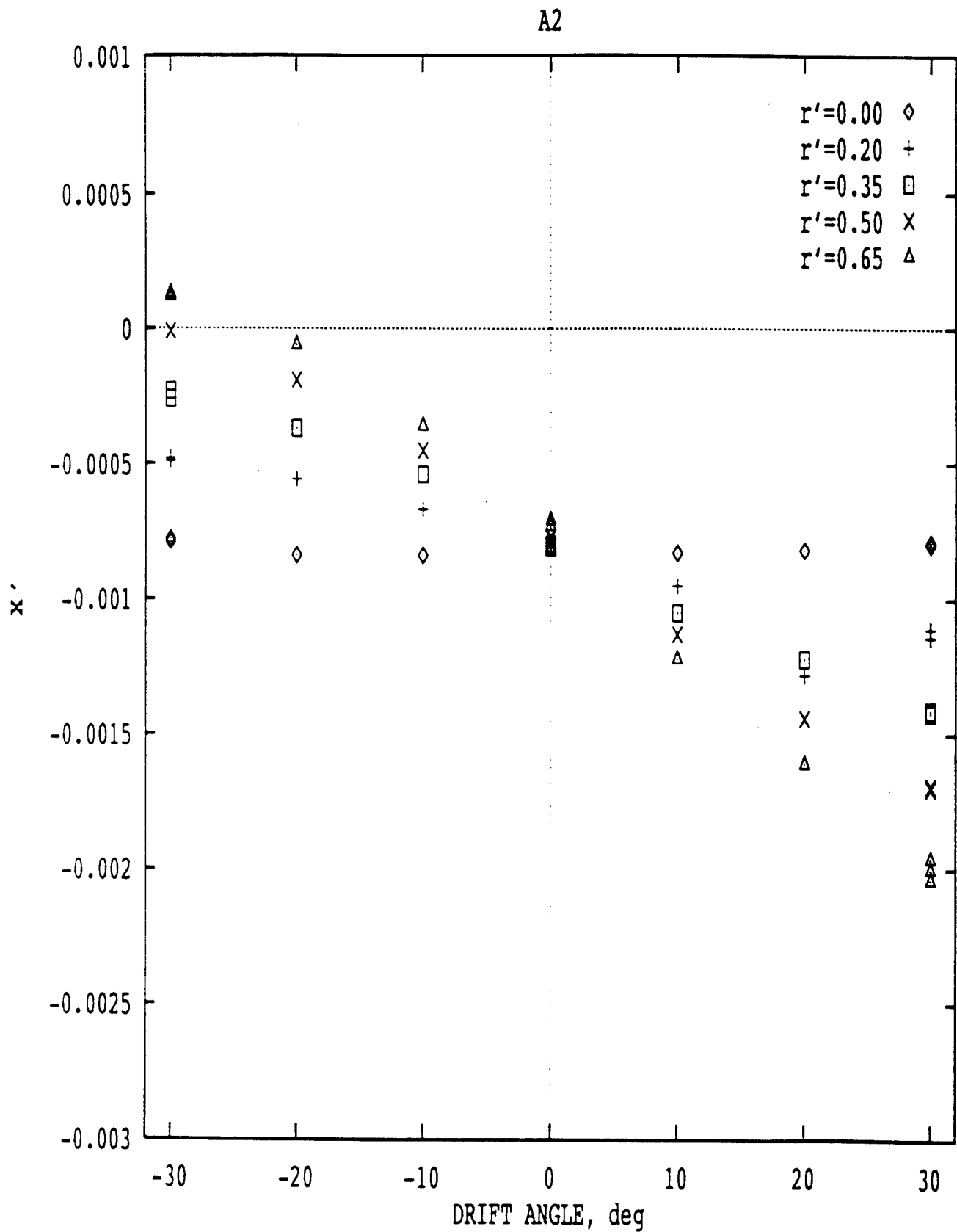


Figure 14. Non-Dimensional Axial Force on Model A2, from [Klosinski and Lewandowski]

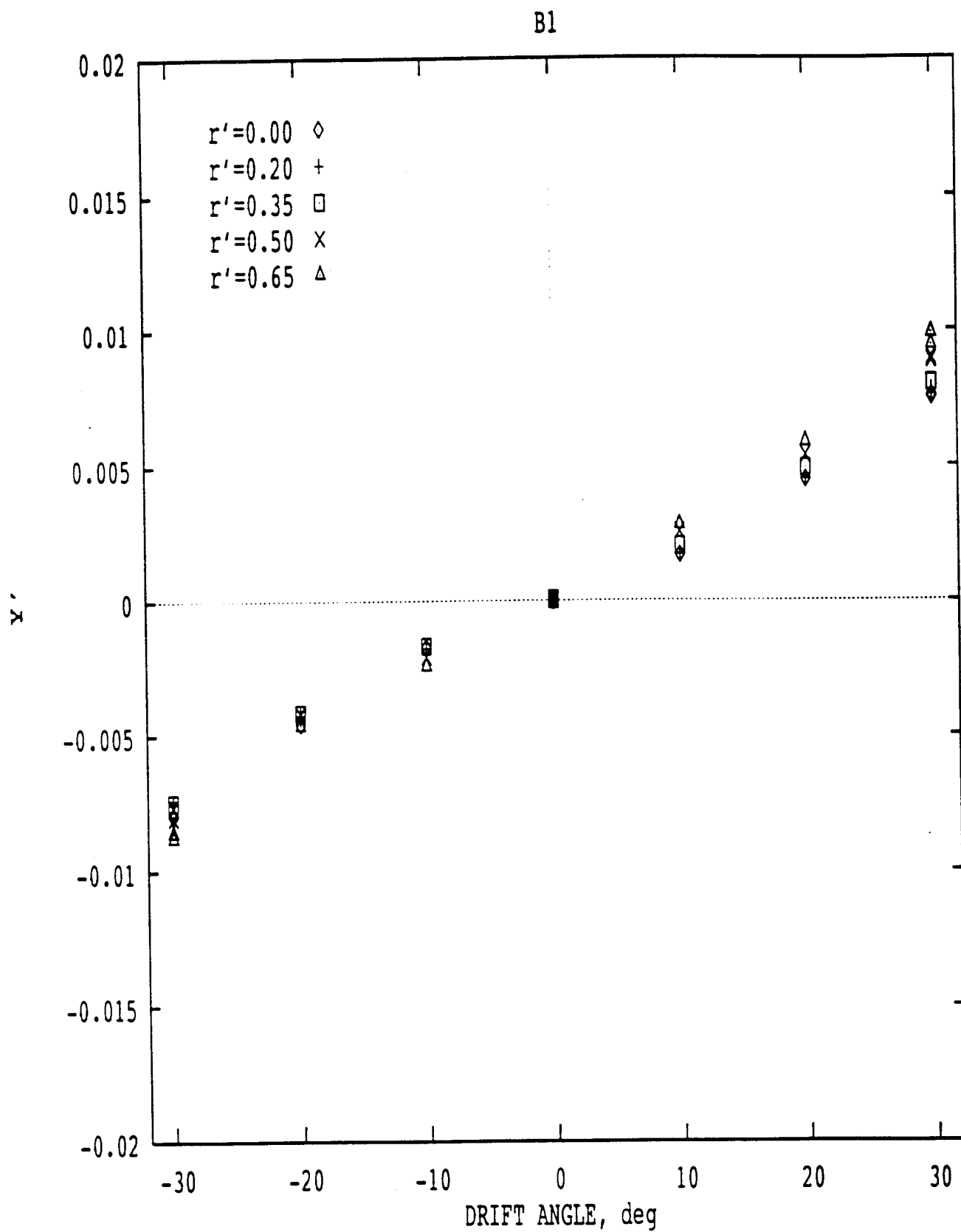


Figure 15. Non-Dimensional Side Force on Model B1, from [Klosinski and Lewandowski]

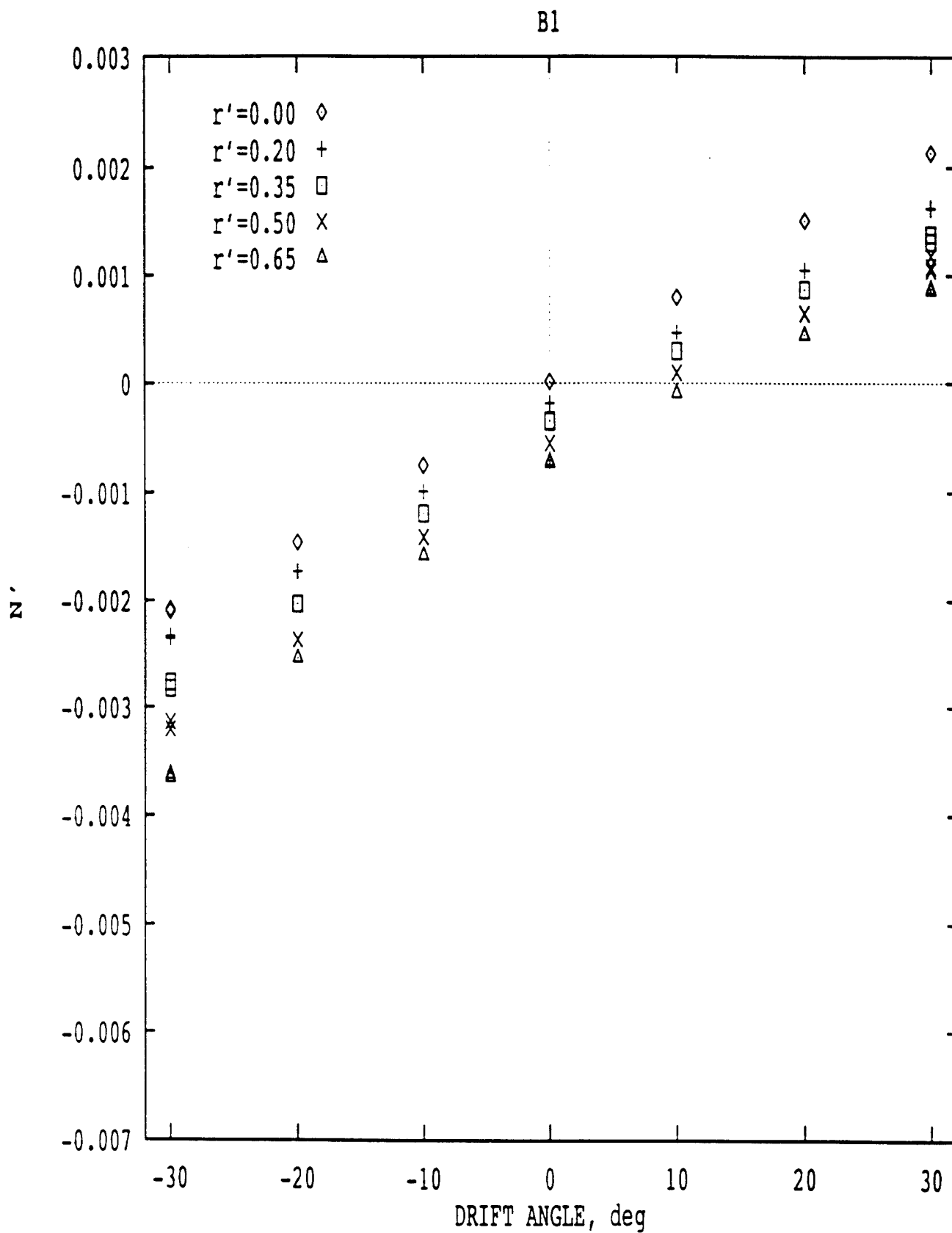


Figure 16. Non-Dimensional Yaw Moment on Model B1, from [Klosinski and Lewandowski]

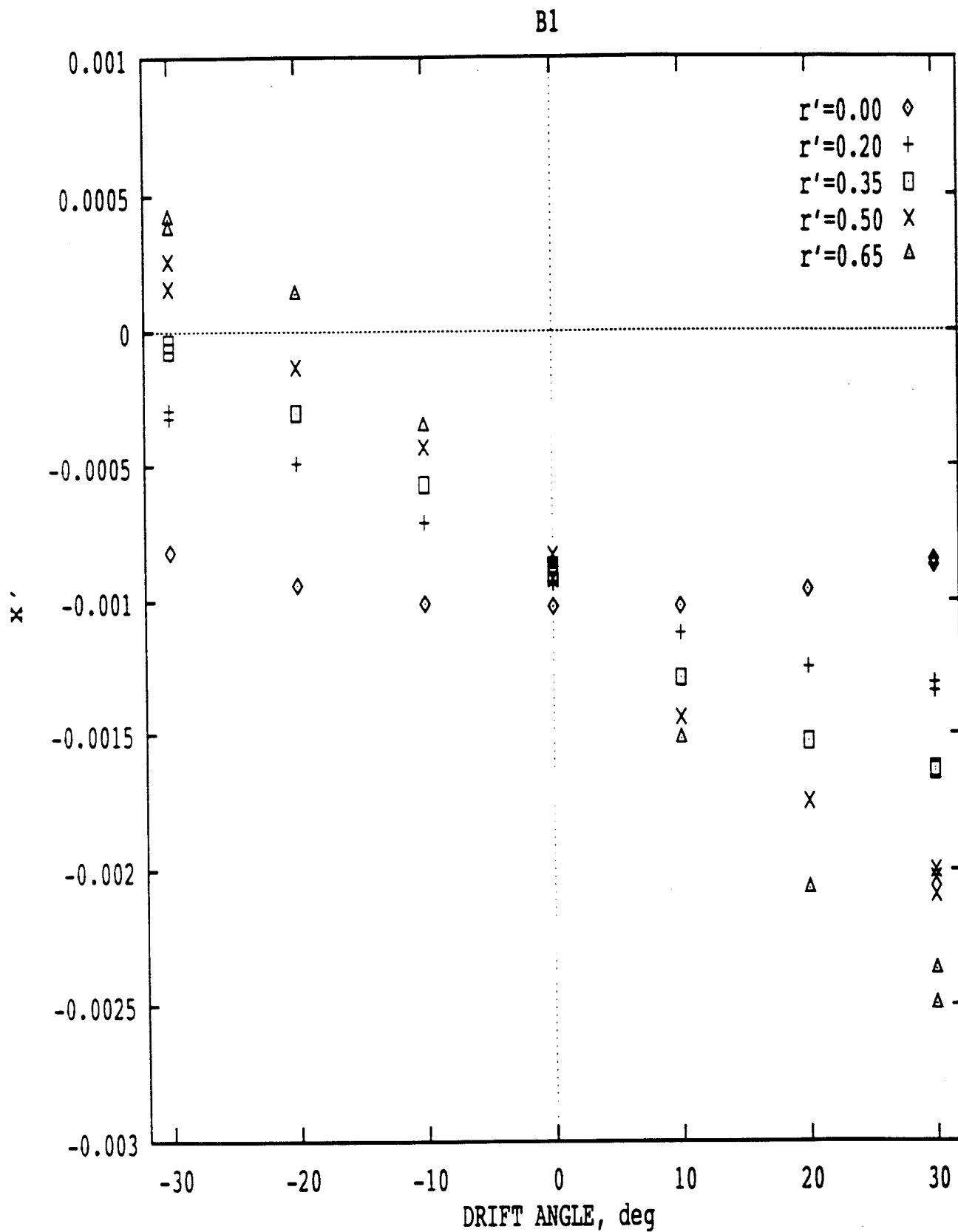


Figure 17. Non-Dimensional Axial Force on Model B1, from [Klosinski and Lewandowski]

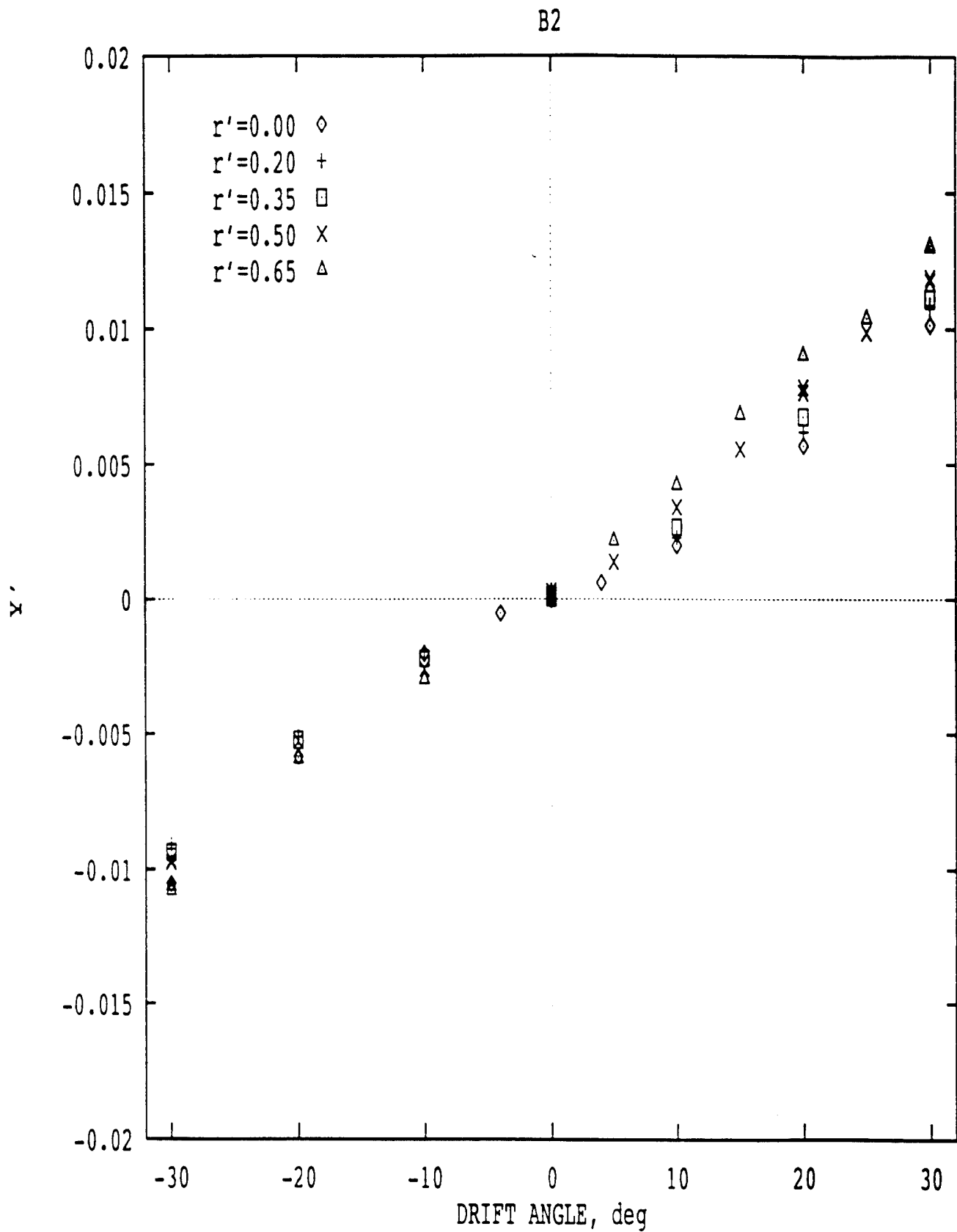


Figure 18. Non-Dimensional Side Force on Model B2, from [Klosinski and Lewandowski]

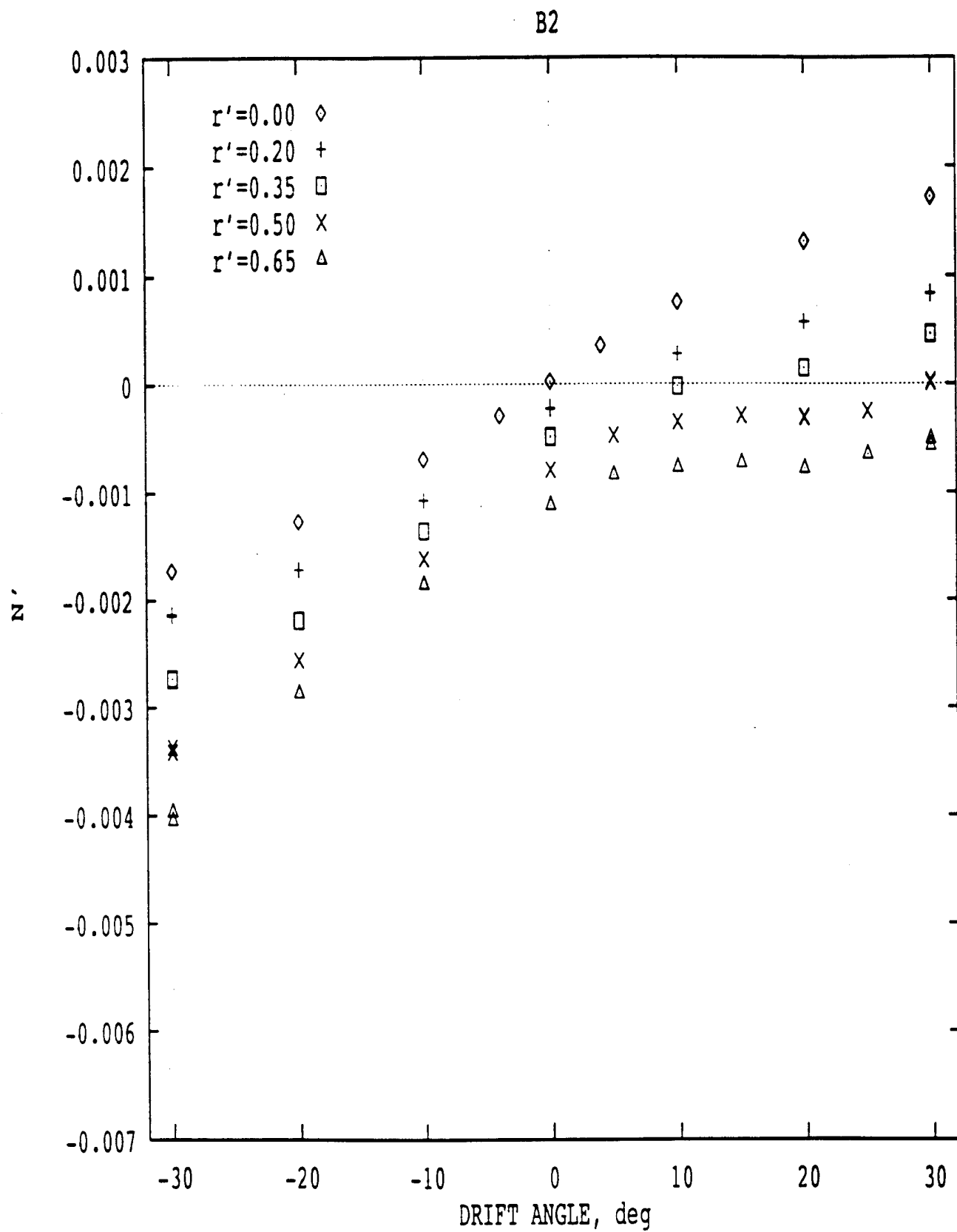


Figure 19. Non-Dimensional Yaw Moment on Model B2, from [Klosinski and Lewandowski]

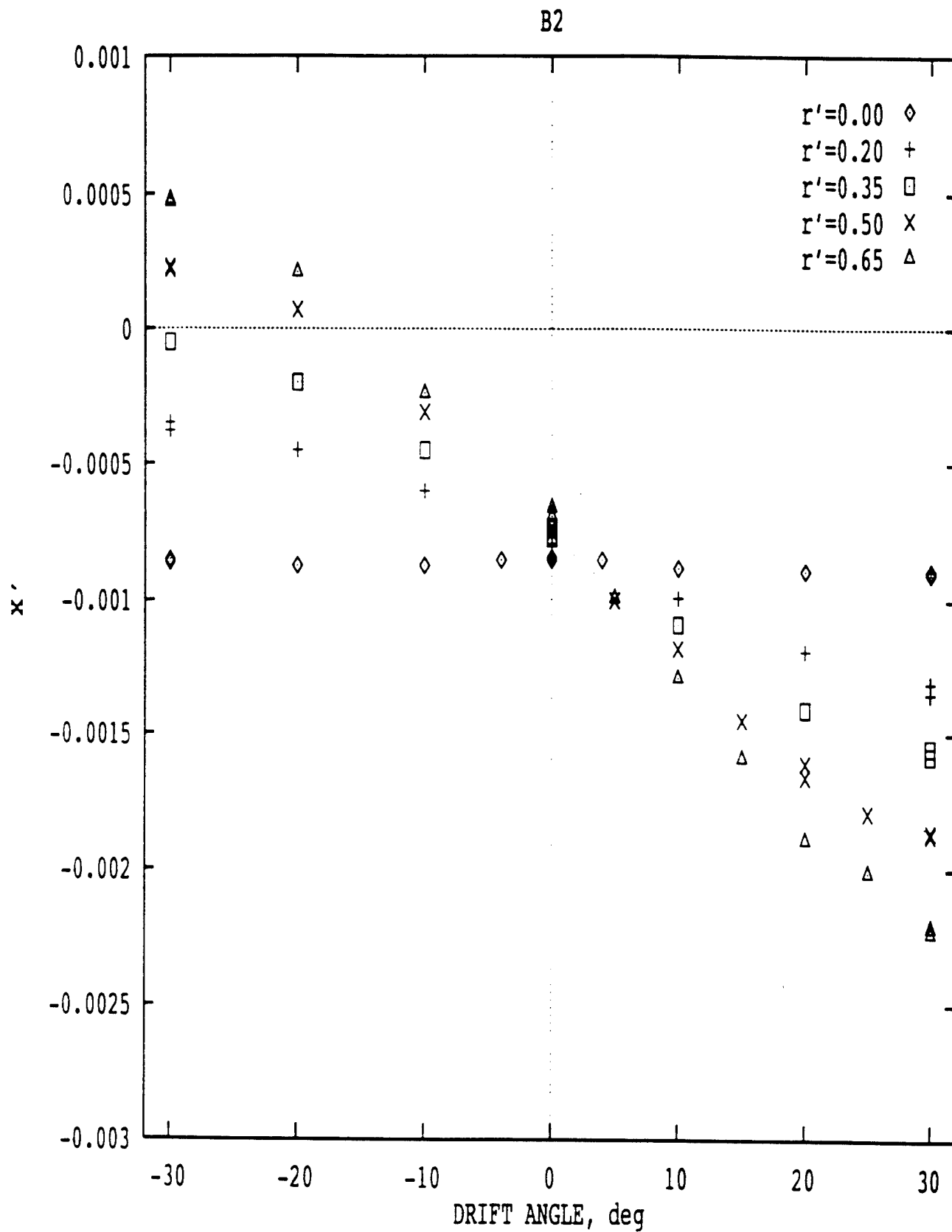


Figure 20. Non-Dimensional Axial Force on Model B2, from [Klosinski and Lewandowski]

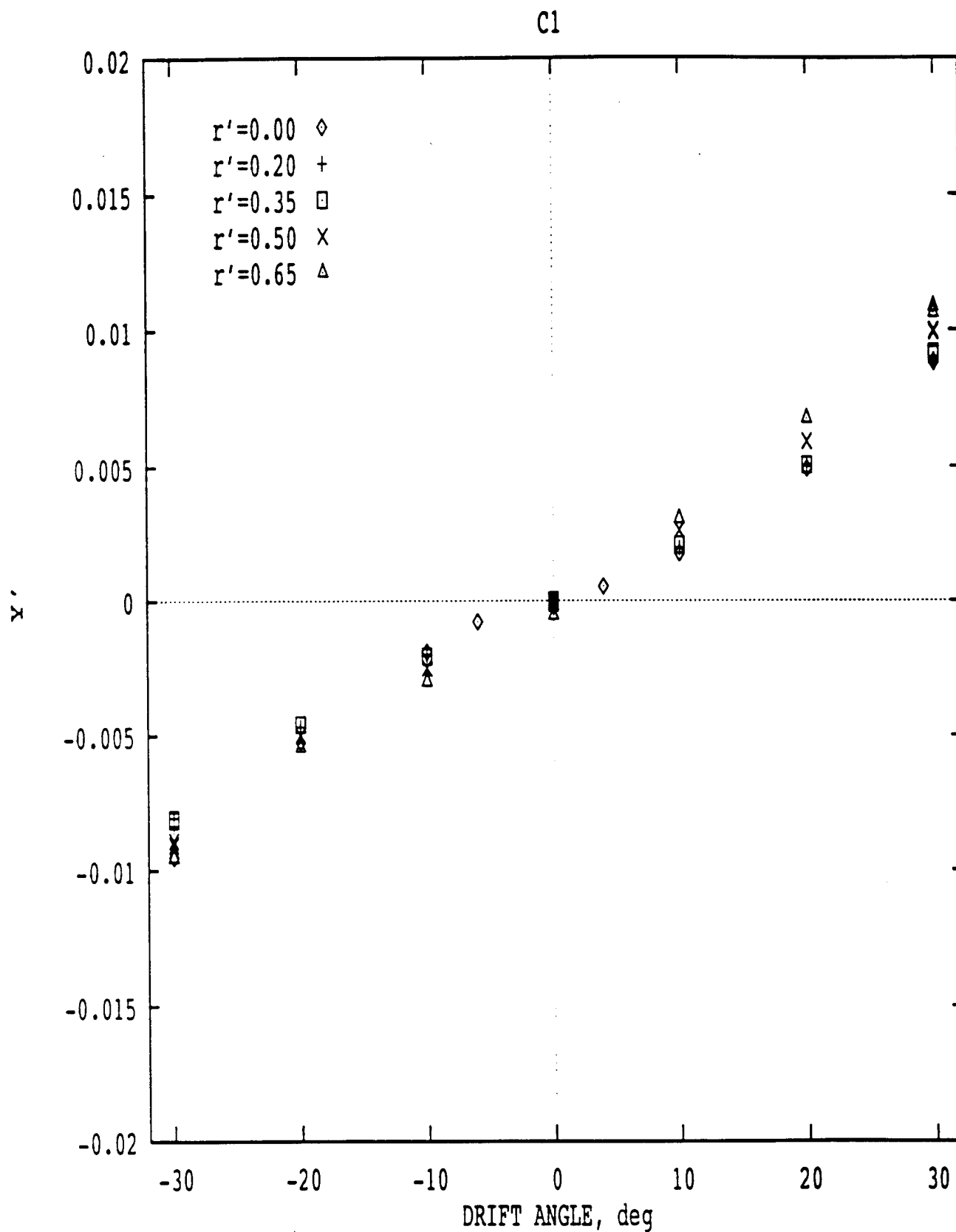


Figure 21. Non-Dimensional Side Force on Model C1, from [Klosinski and Lewandowski]

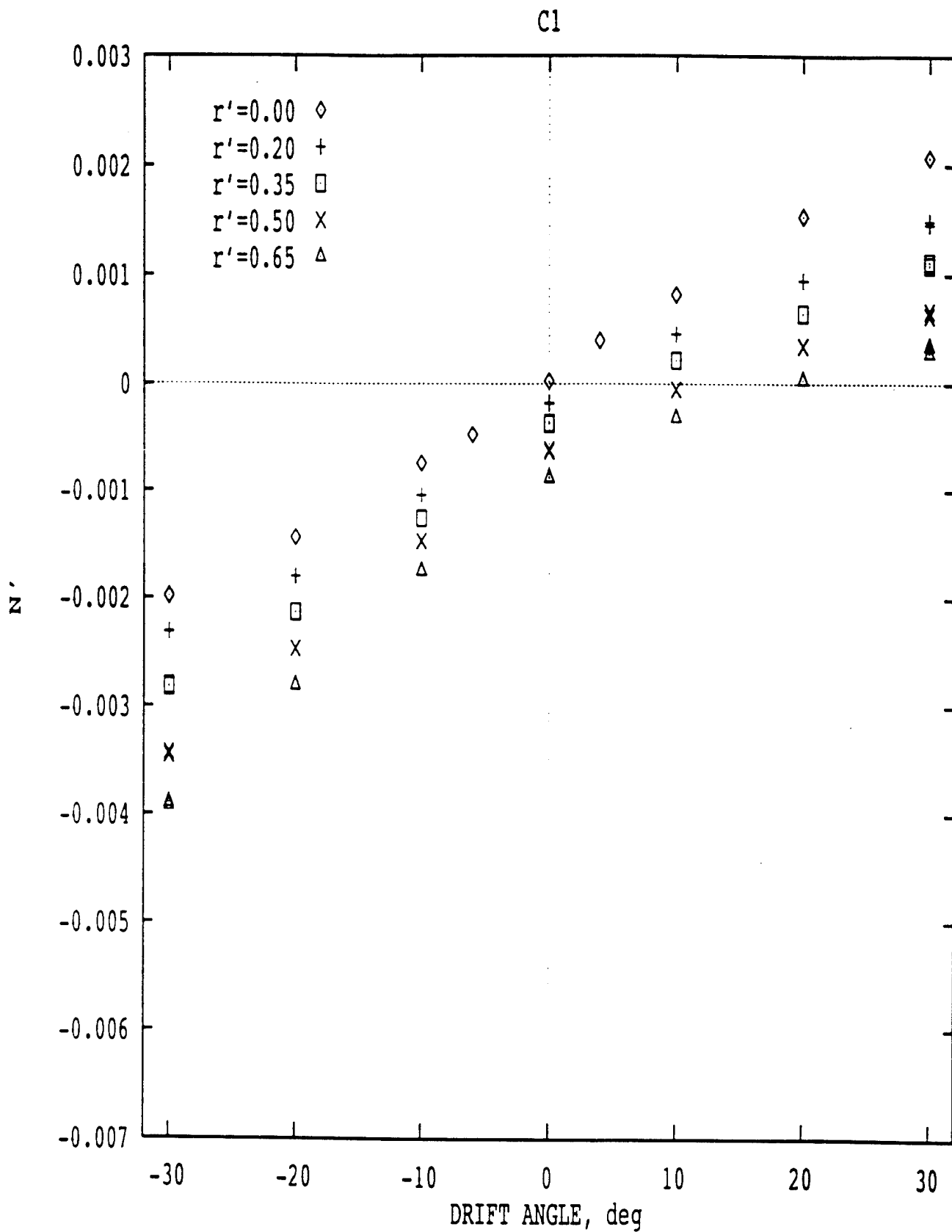


Figure 22. Non-Dimensional Yaw Moment on Model C1, from [Klosinski and Lewandowski]

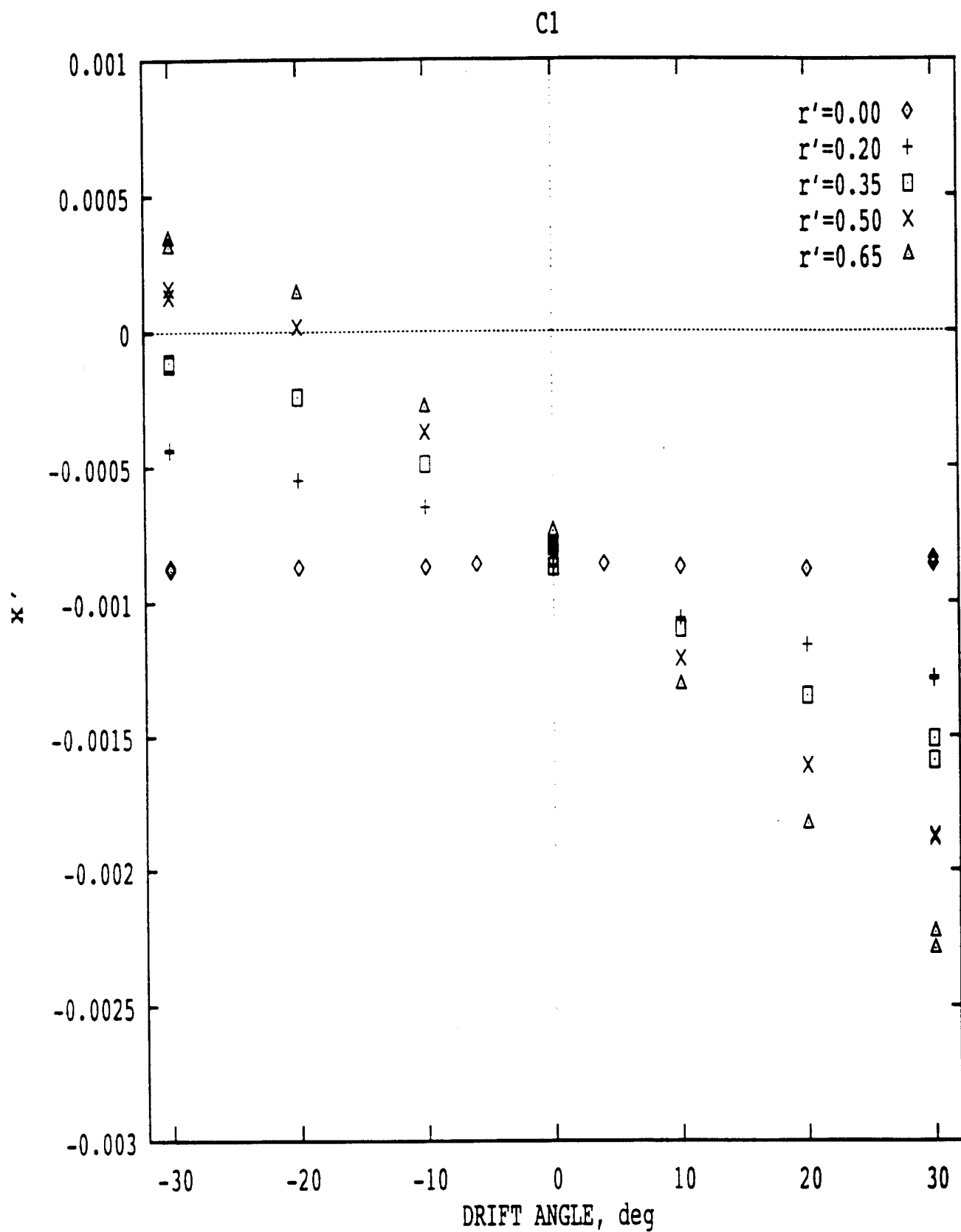


Figure 23. Non-Dimensional Axial Force on Model C1, from [Klosinski and Lewandowski]

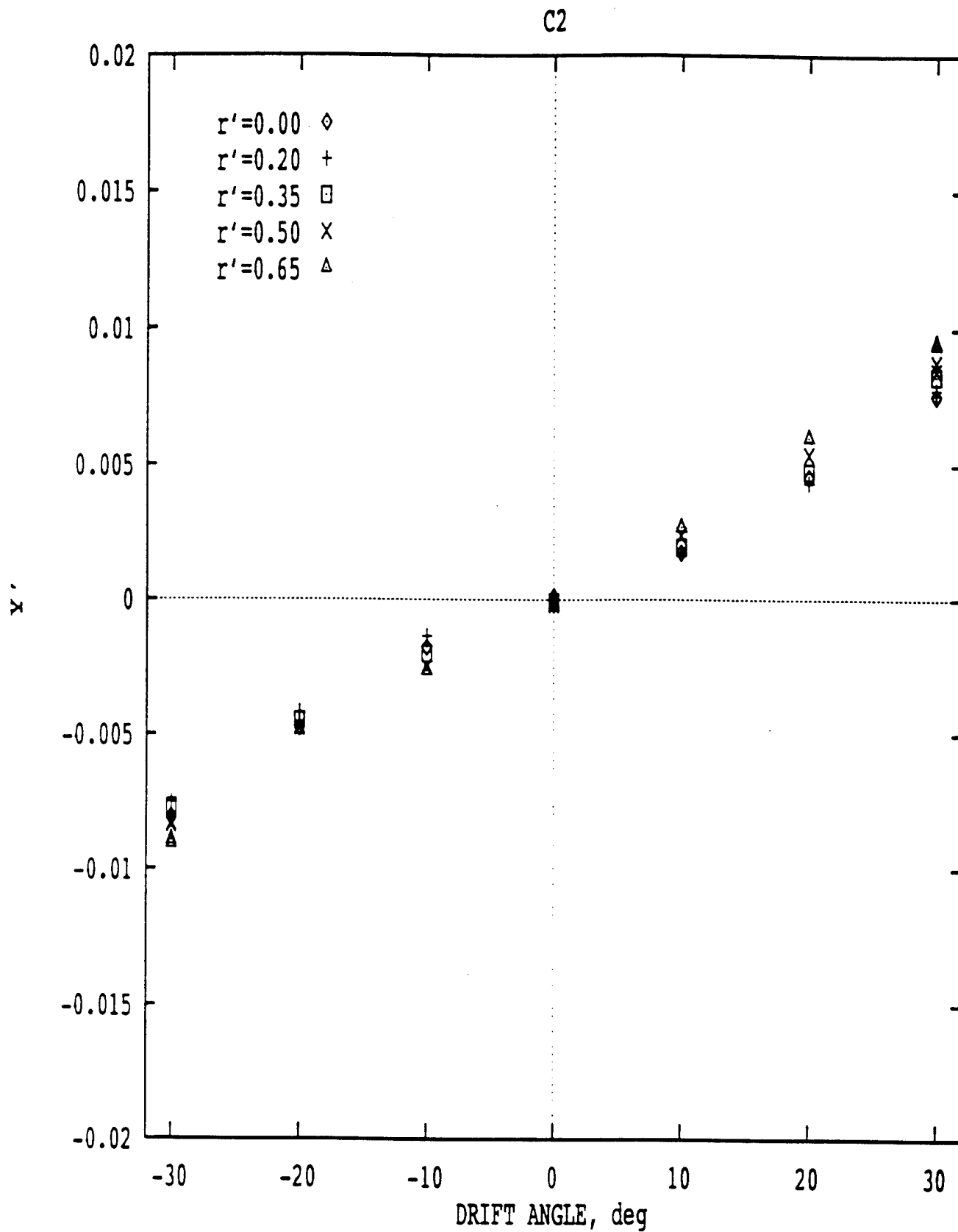


Figure 24. Non-Dimensional Side Force on Model C2, from [Klosinski and Lewandowski]

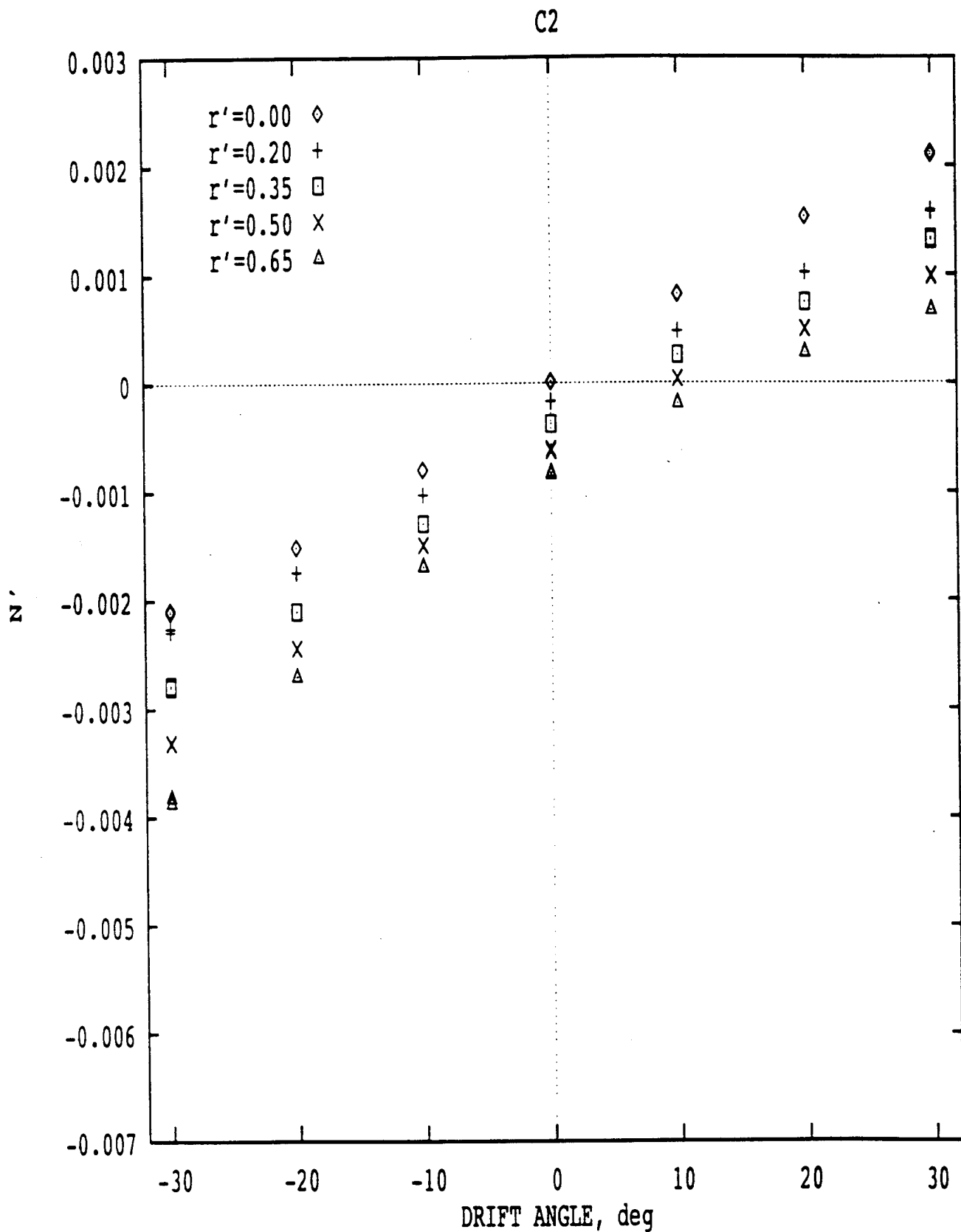


Figure 25. Non-Dimensional Yaw Moment on Model C2, from [Klosinski and Lewandowski]

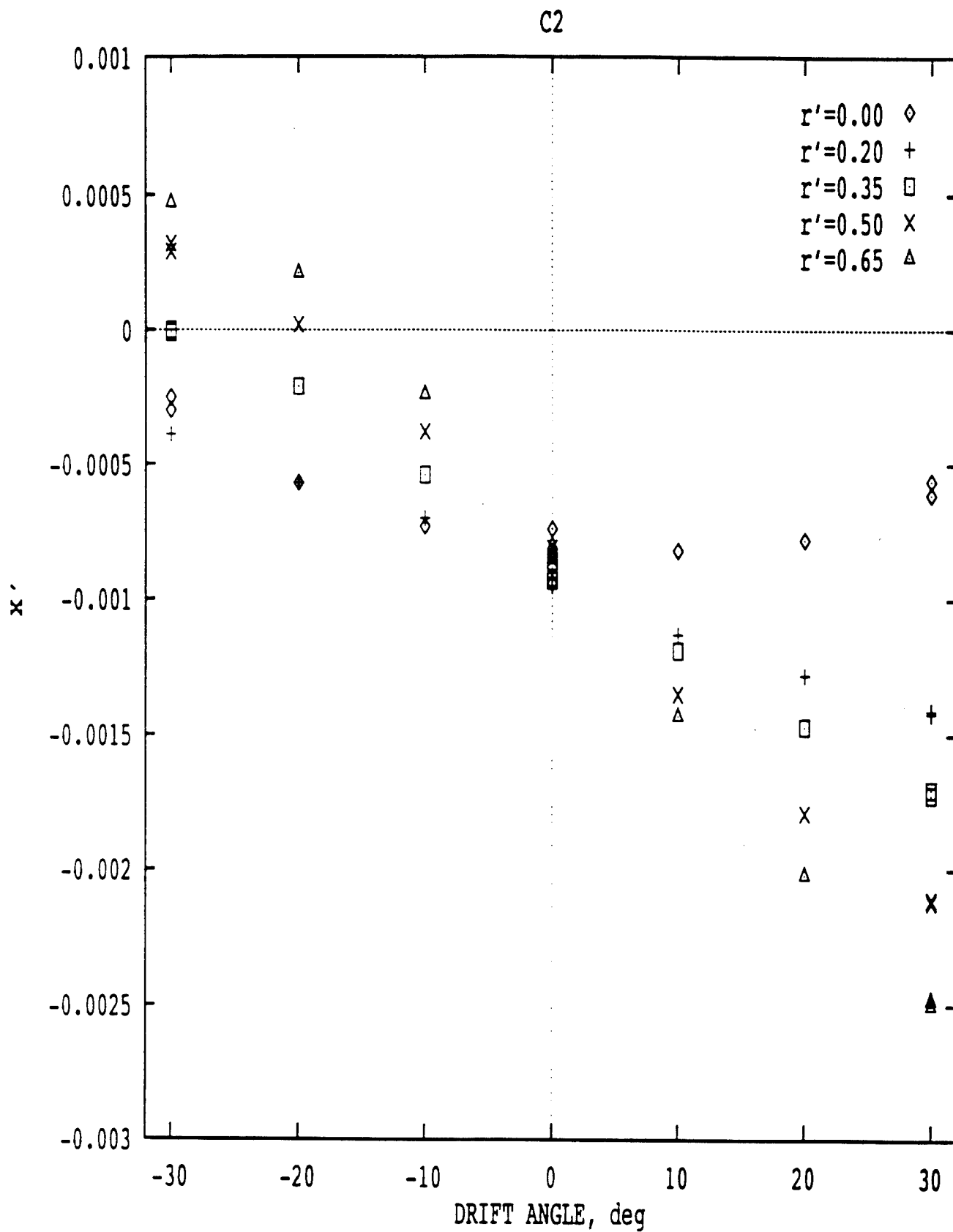


Figure 26. Non-Dimensional Axial Force on Model C2, from [Klosinski and Lewandowski]

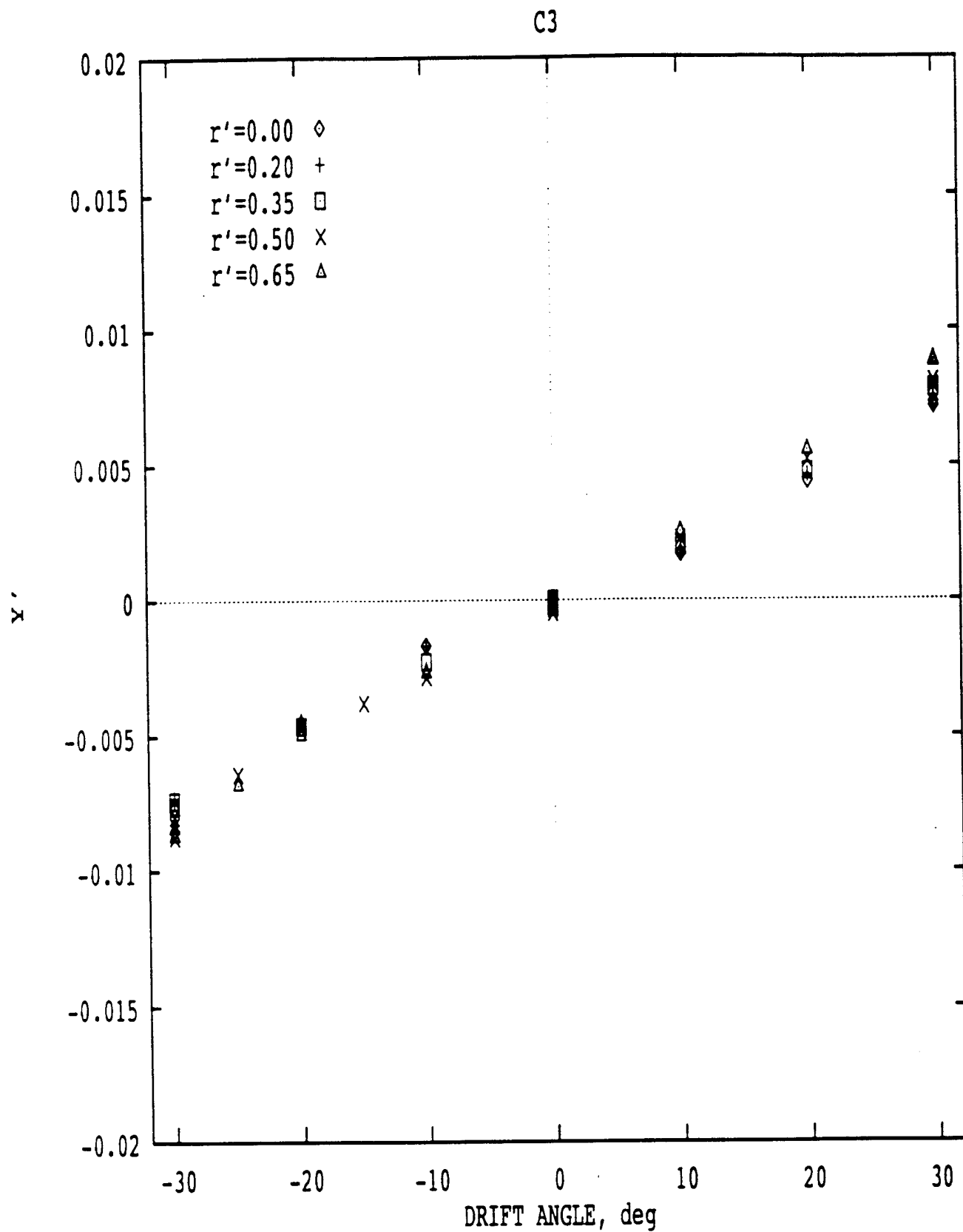


Figure 27. Non-Dimensional Side Force on Model C3, from [Klosinski and Lewandowski]

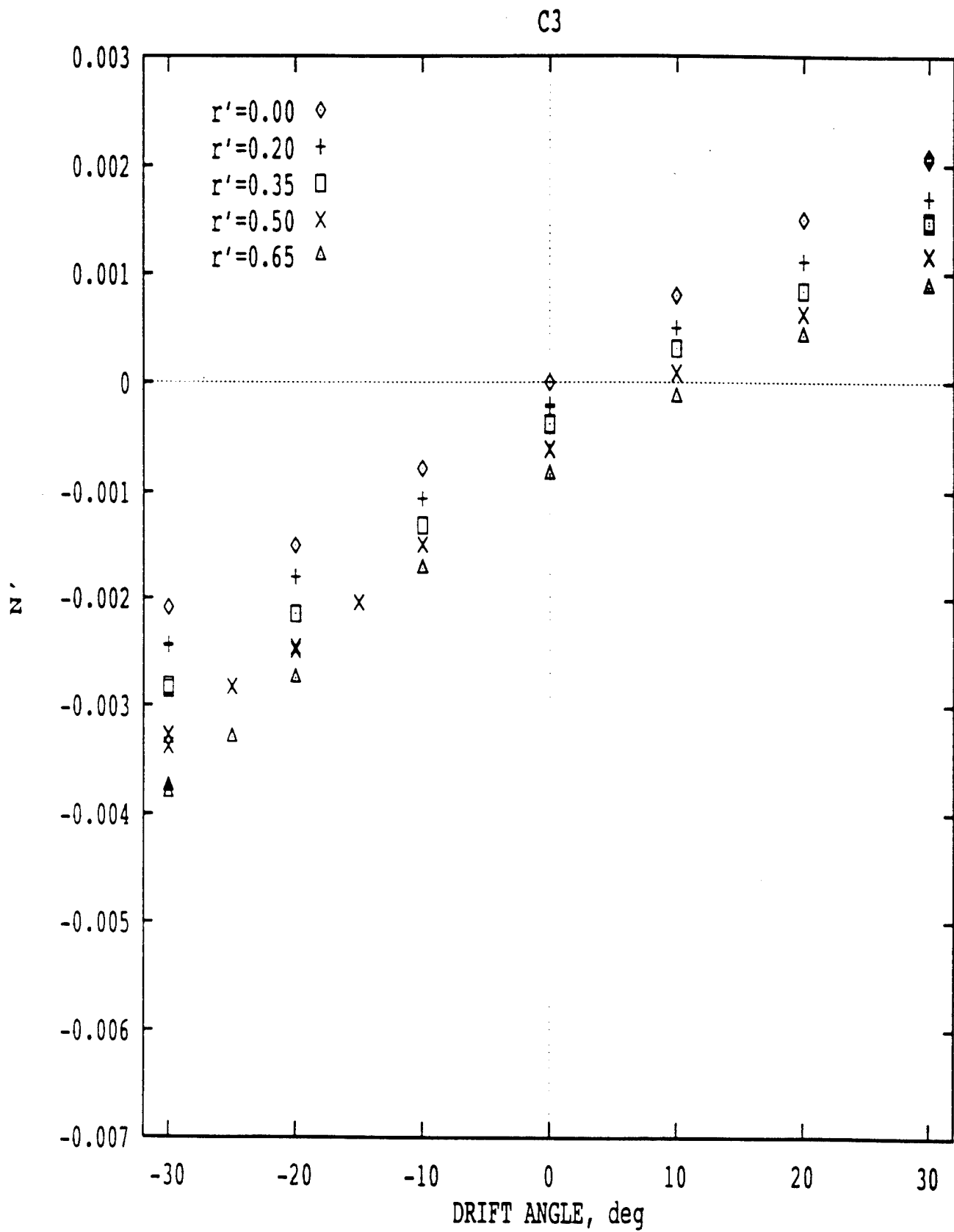


Figure 28. Non-Dimensional Yaw Moment on Model C3, from [Klosinski and Lewandowski]

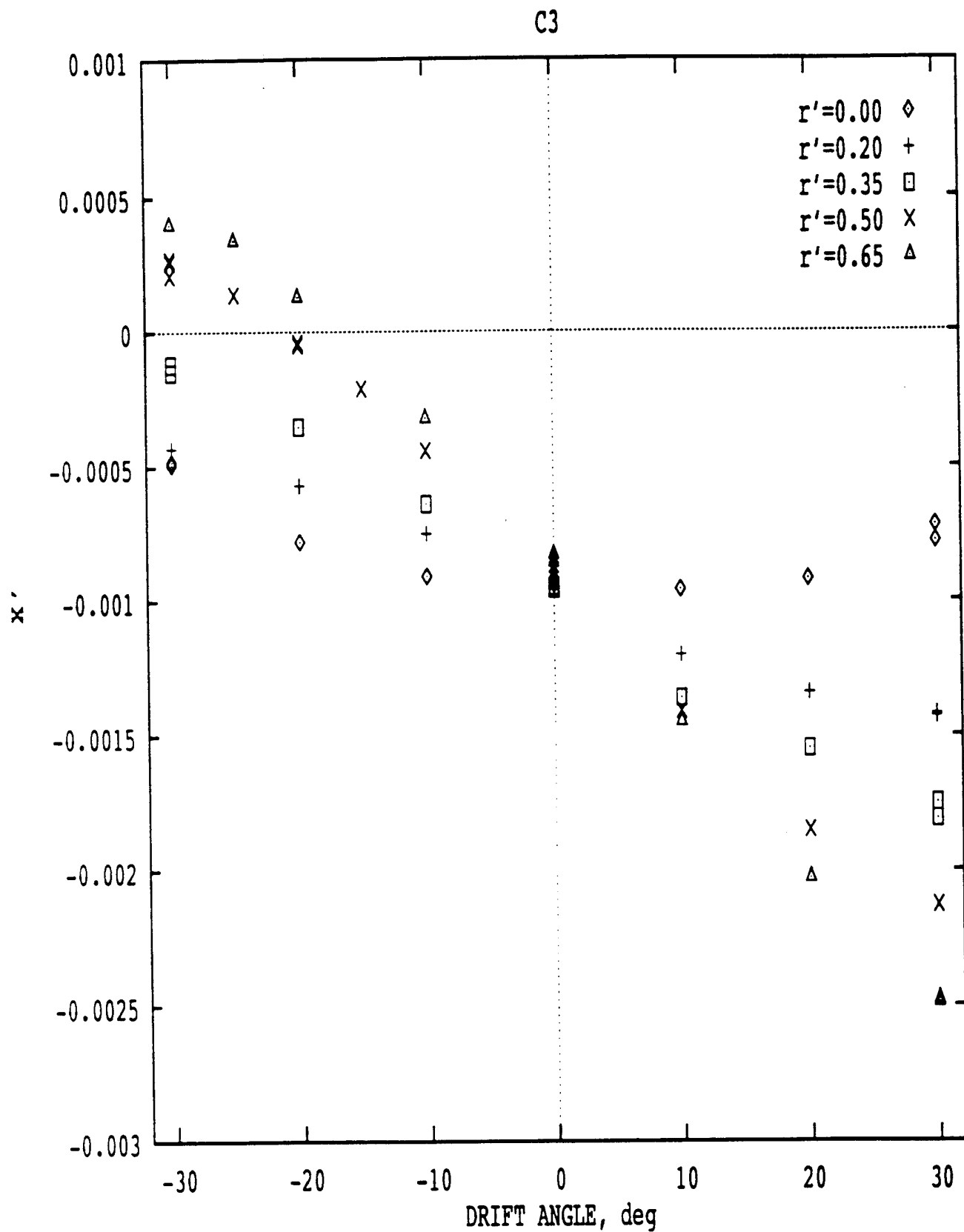


Figure 29. Non-Dimensional Axial Force on Model C3, from [Klosinski and Lewandowski]

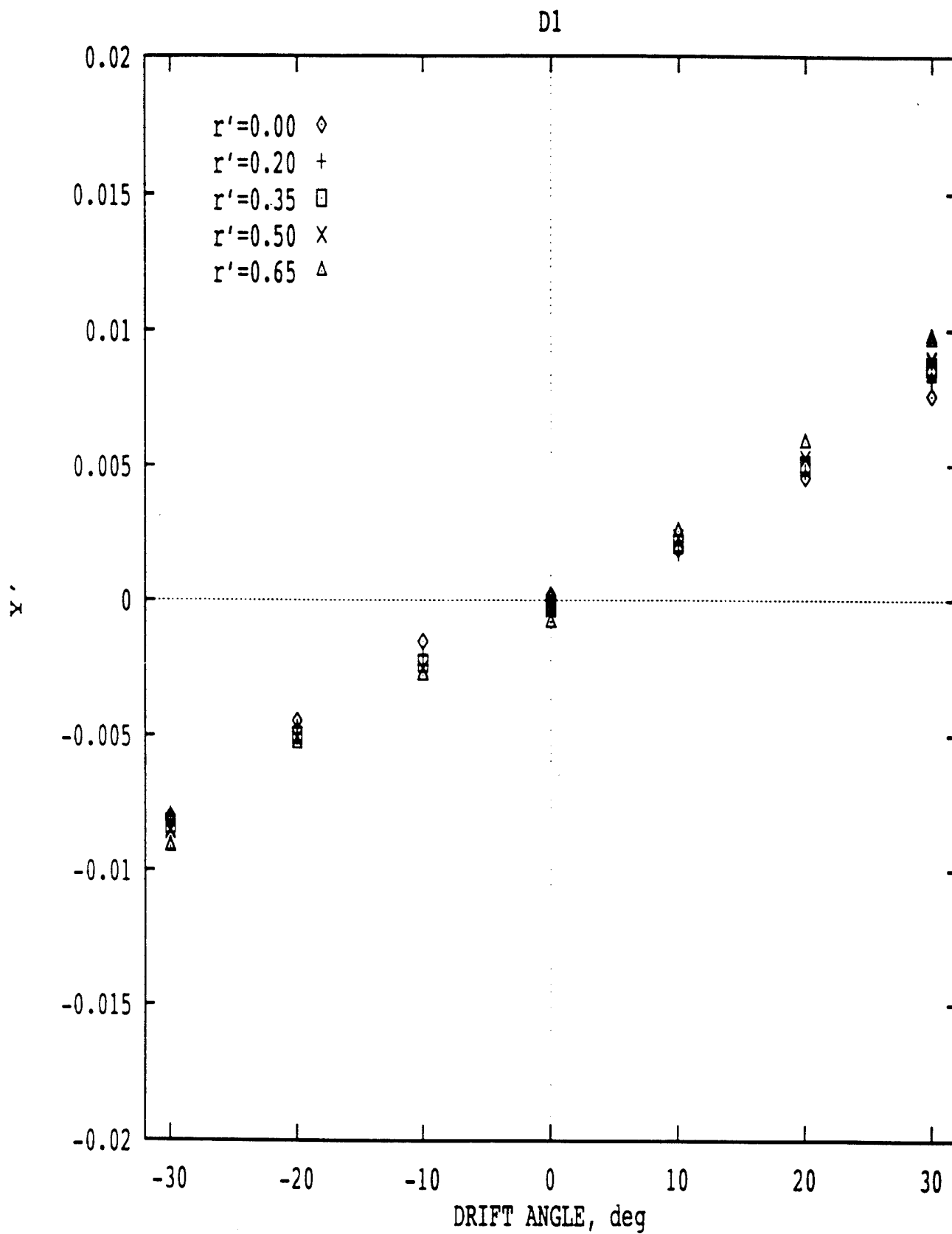


Figure 30. Non-Dimensional Side Force on Model D1, from [Klosinski and Lewandowski]

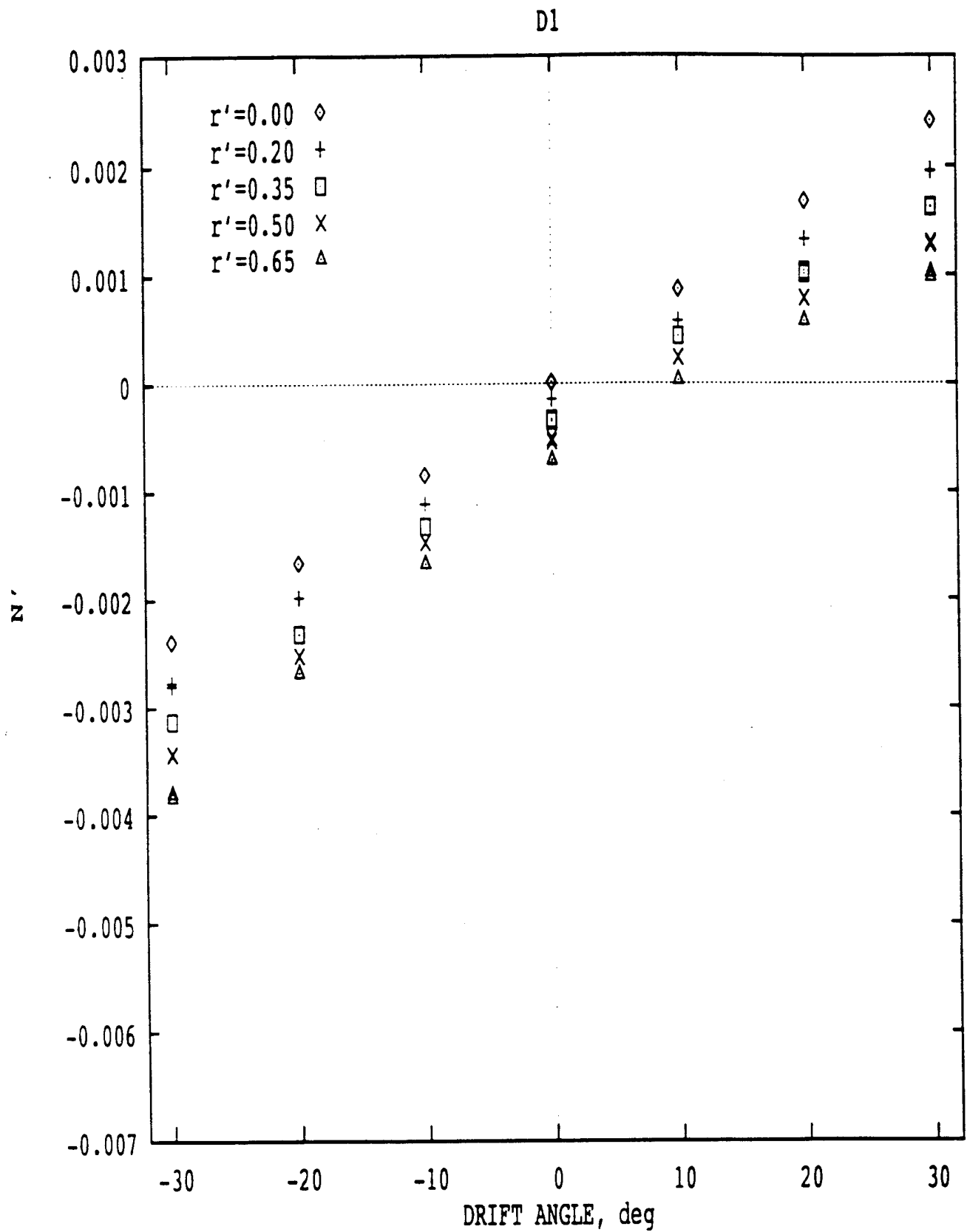


Figure 31. Non-Dimensional Yaw Moment on Model D1, from [Klosinski and Lewandowski]

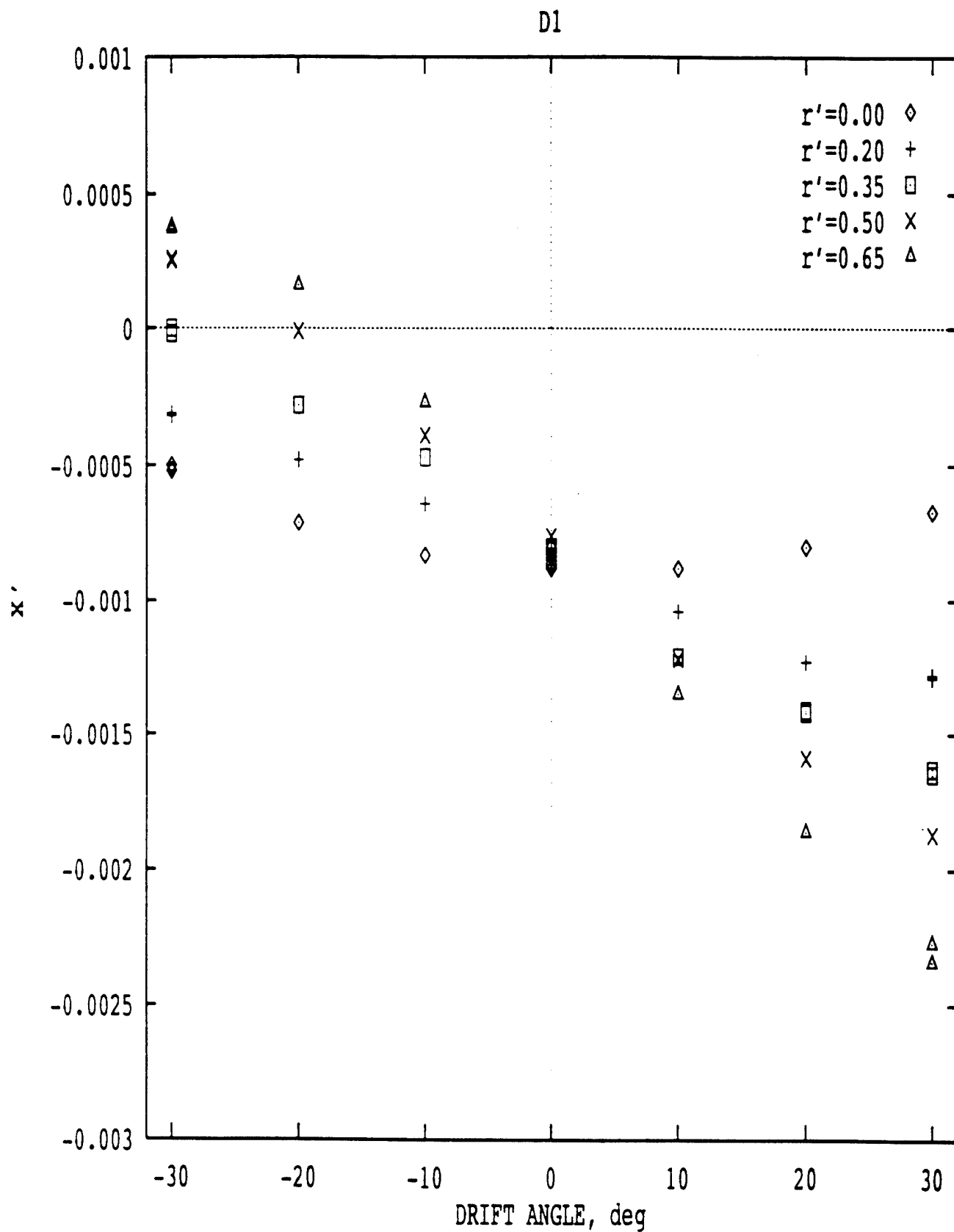


Figure 32. Non-Dimensional Axial Force on Model D1, from [Klosinski and Lewandowski]

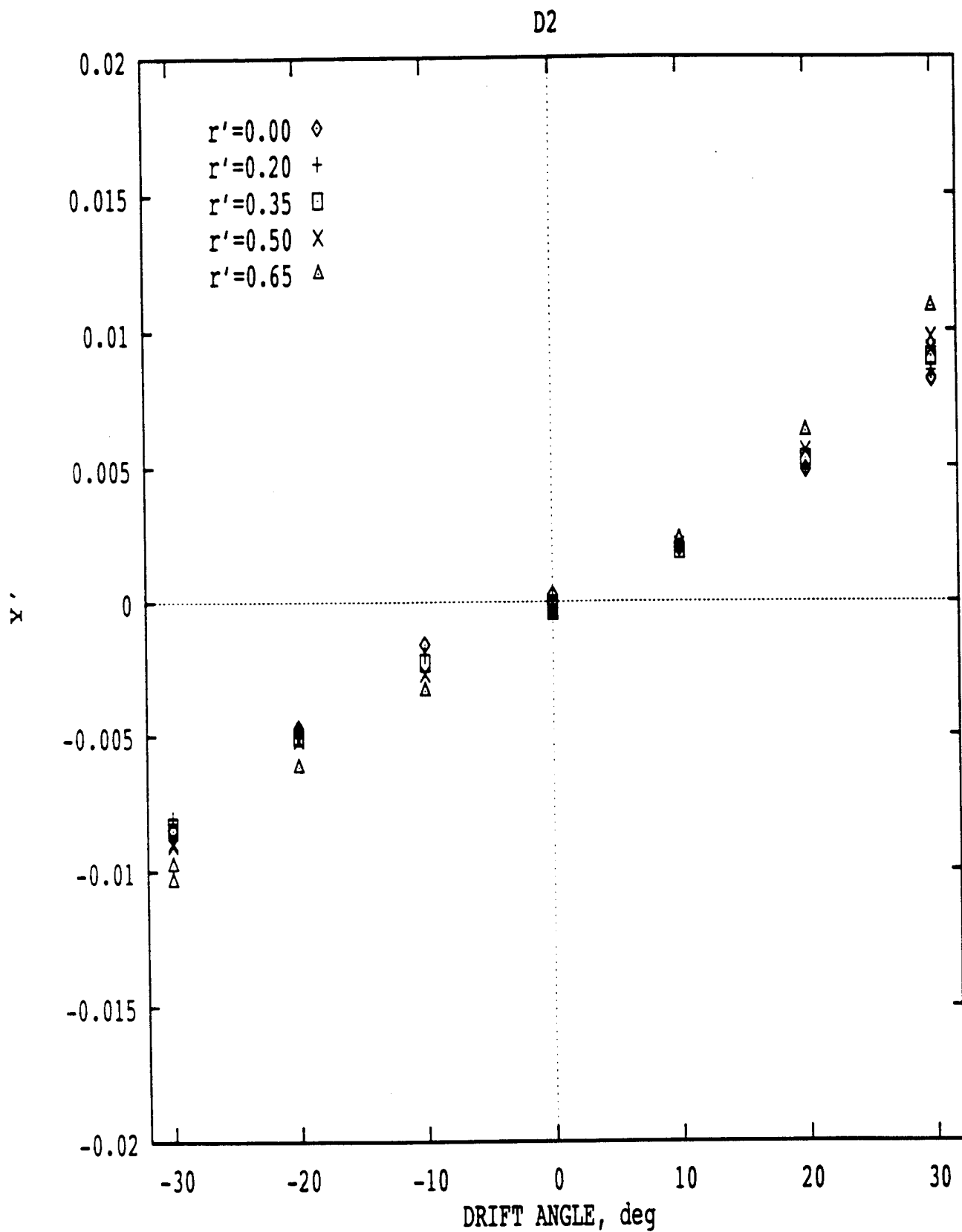


Figure 33. Non-Dimensional Side Force on Model D2, from [Klosinski and Lewandowski]

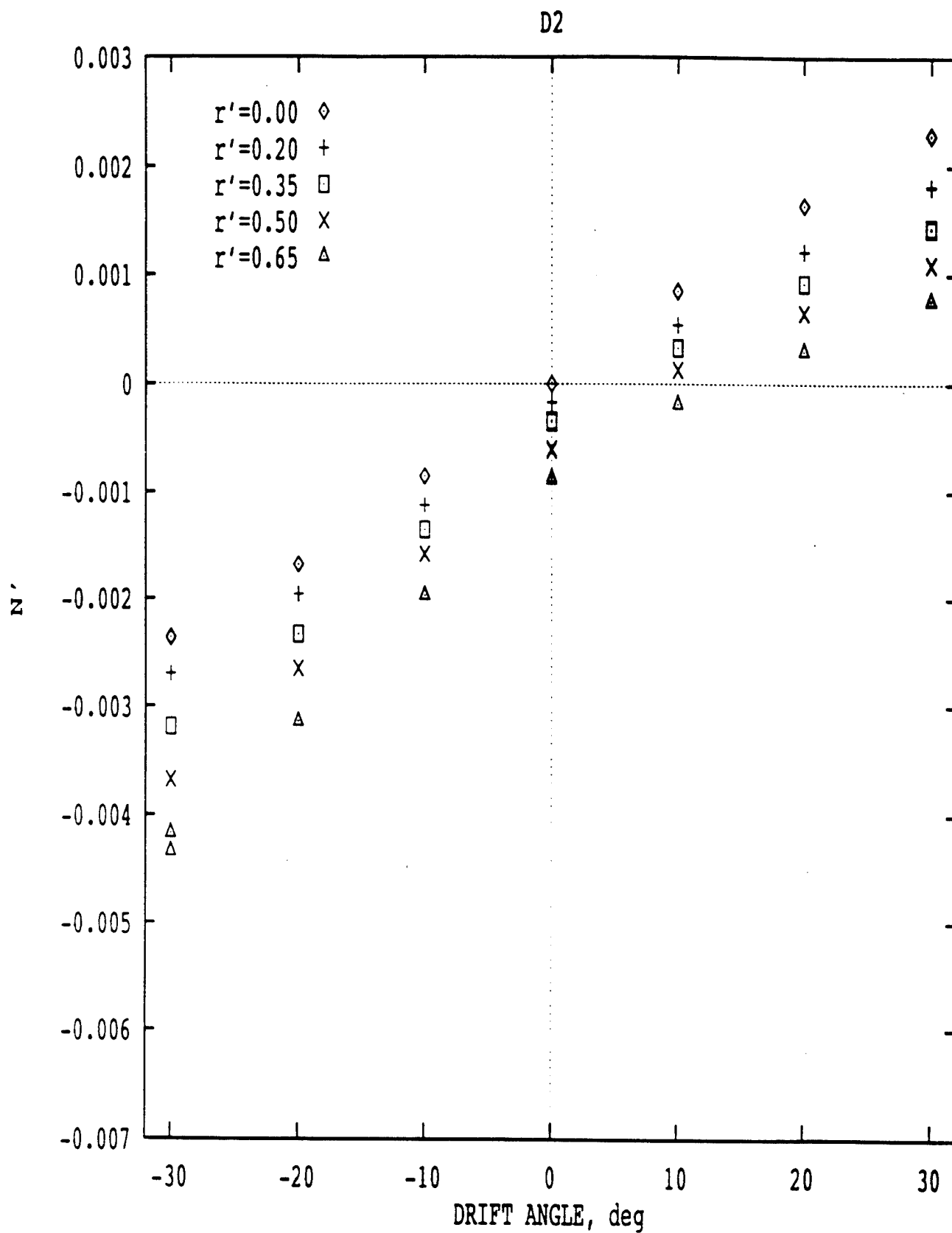


Figure 34. Non-Dimensional Yaw Moment on Model D2, from [Klosinski and Lewandowski]

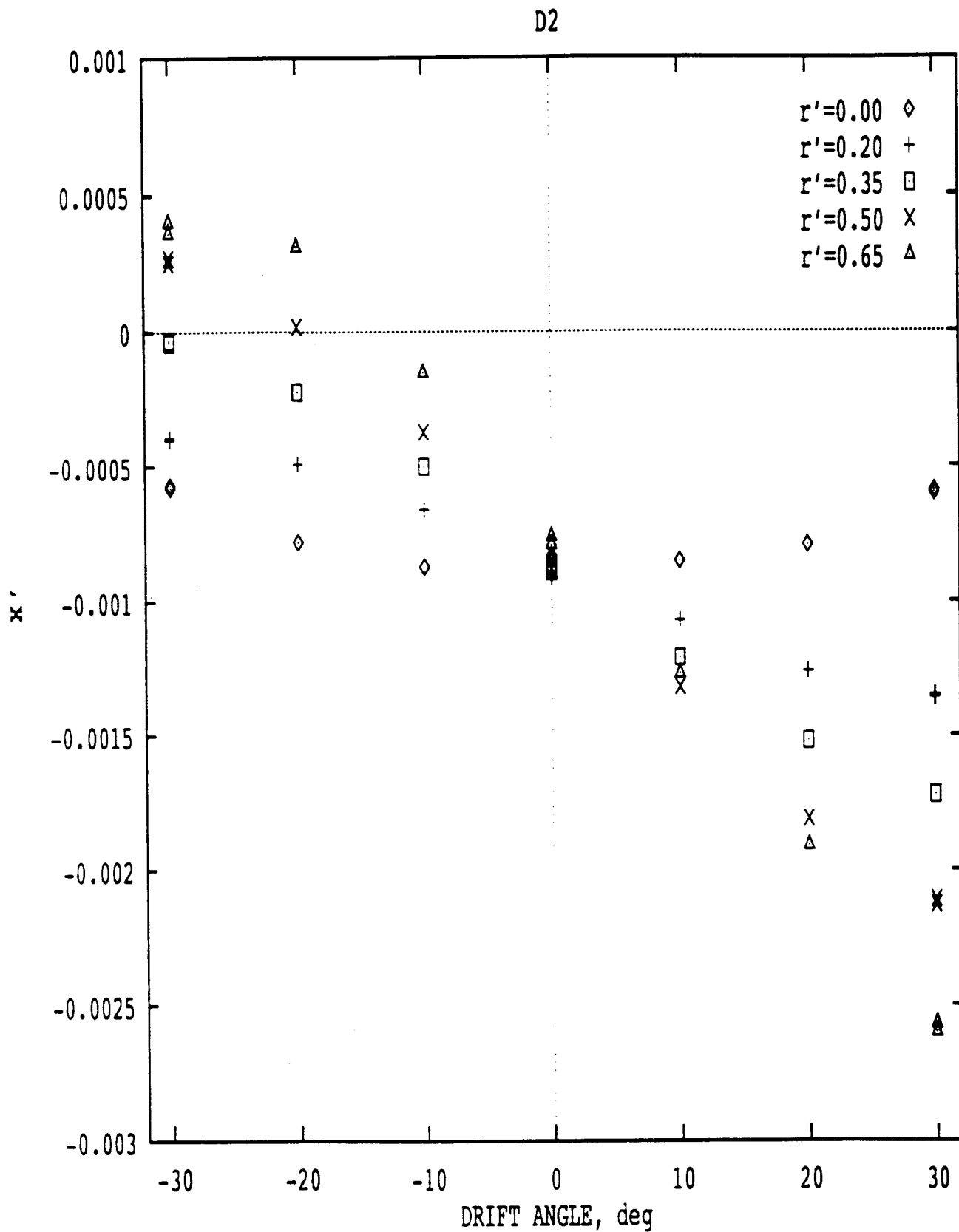


Figure 35. Non-Dimensional Axial Force on Model D2, from [Klosinski and Lewandowski]

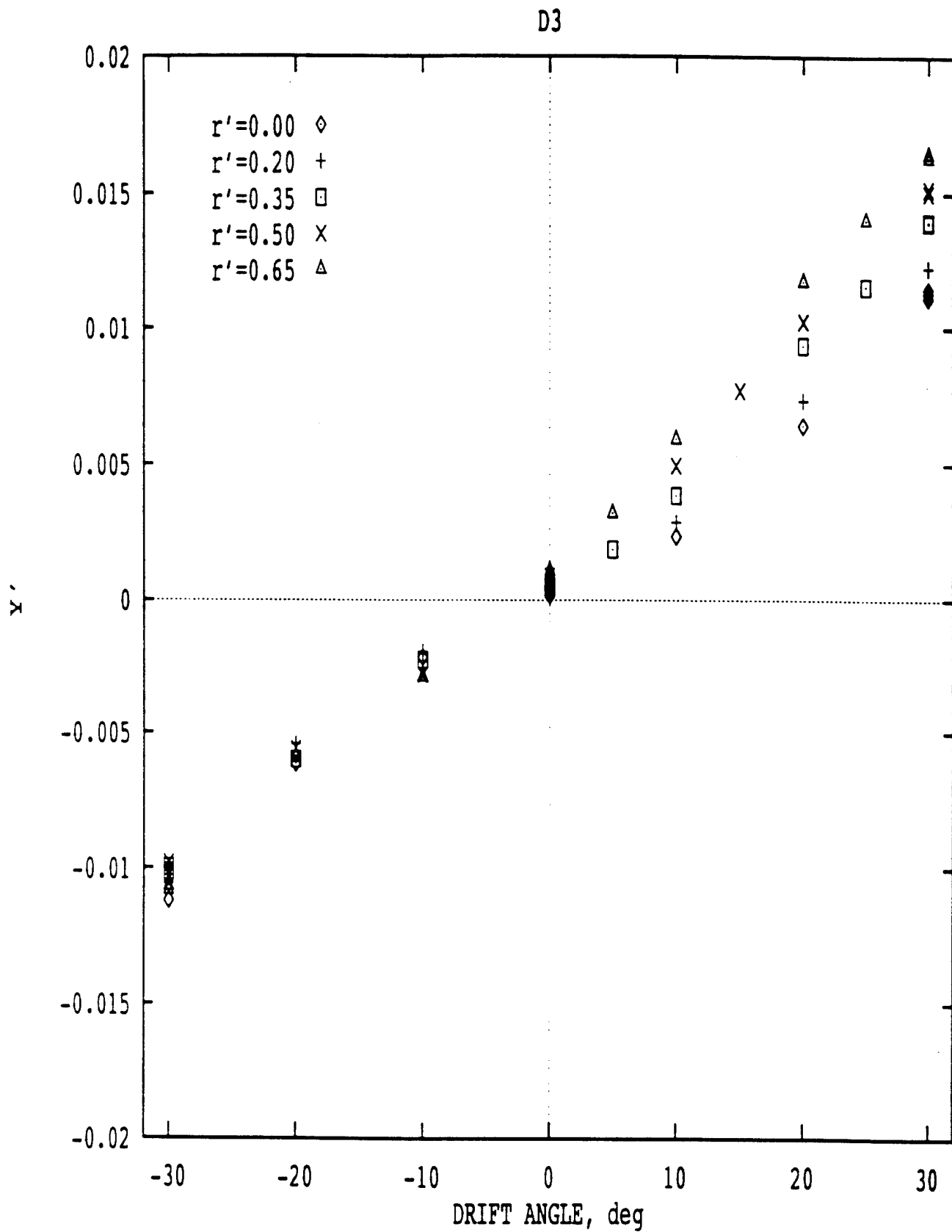


Figure 36. Non-Dimensional Side Force on Model D3, from [Klosinski and Lewandowski]

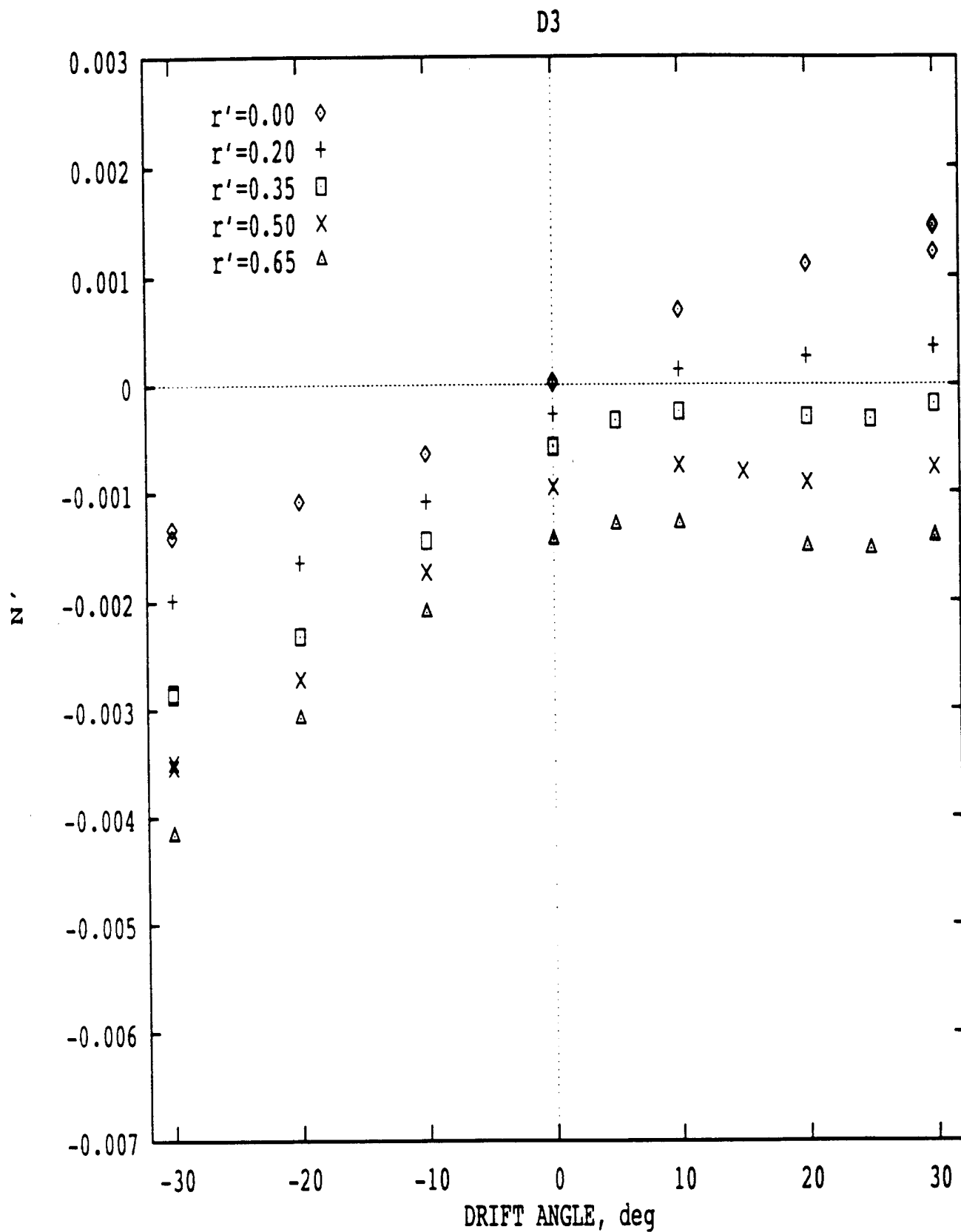


Figure 37. Non-Dimensional Yaw Moment on Model D3, from [Klosinski and Lewandowski]

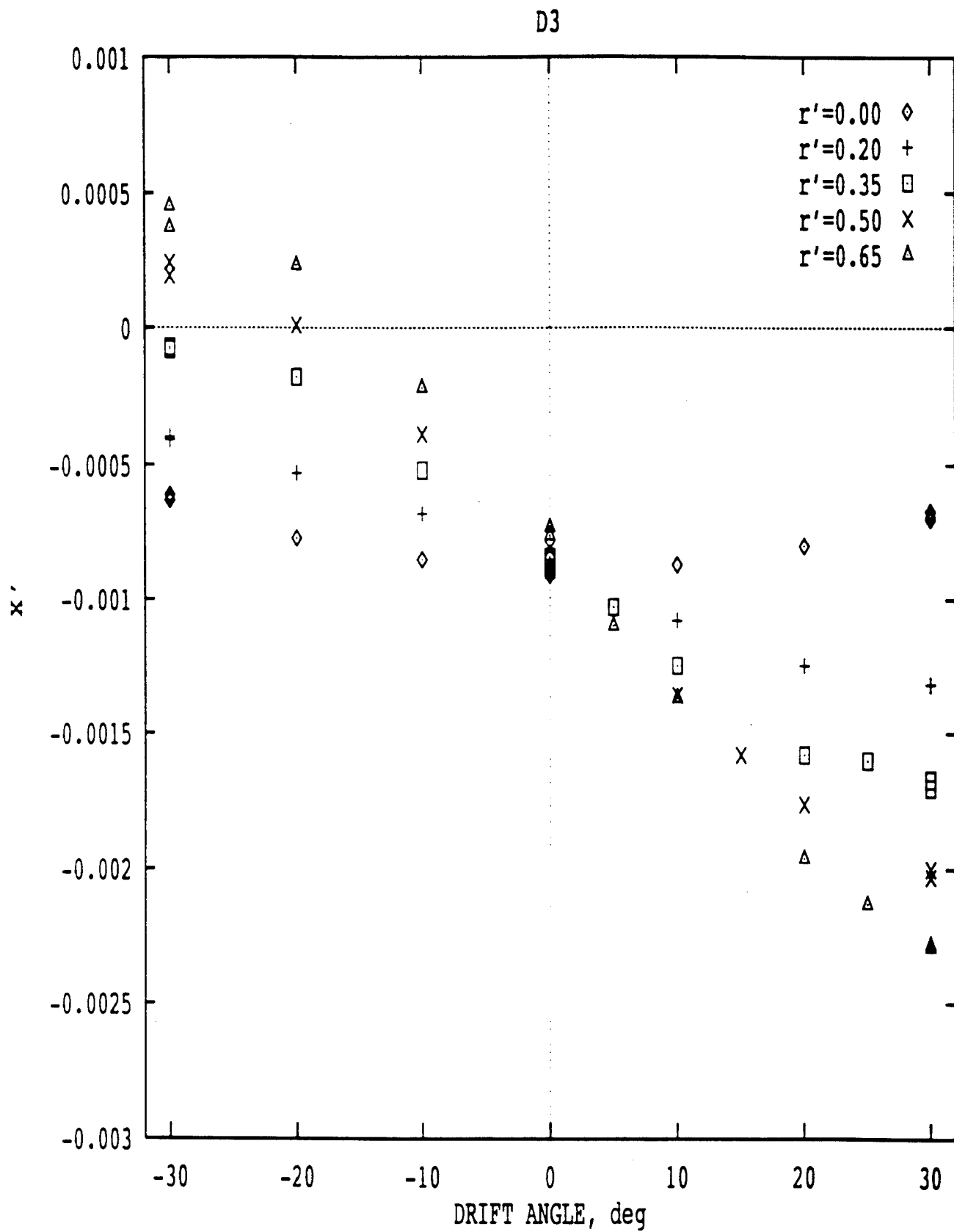


Figure 38. Non-Dimensional Axial Force on Model D3, from [Klosinski and Lewandowski]

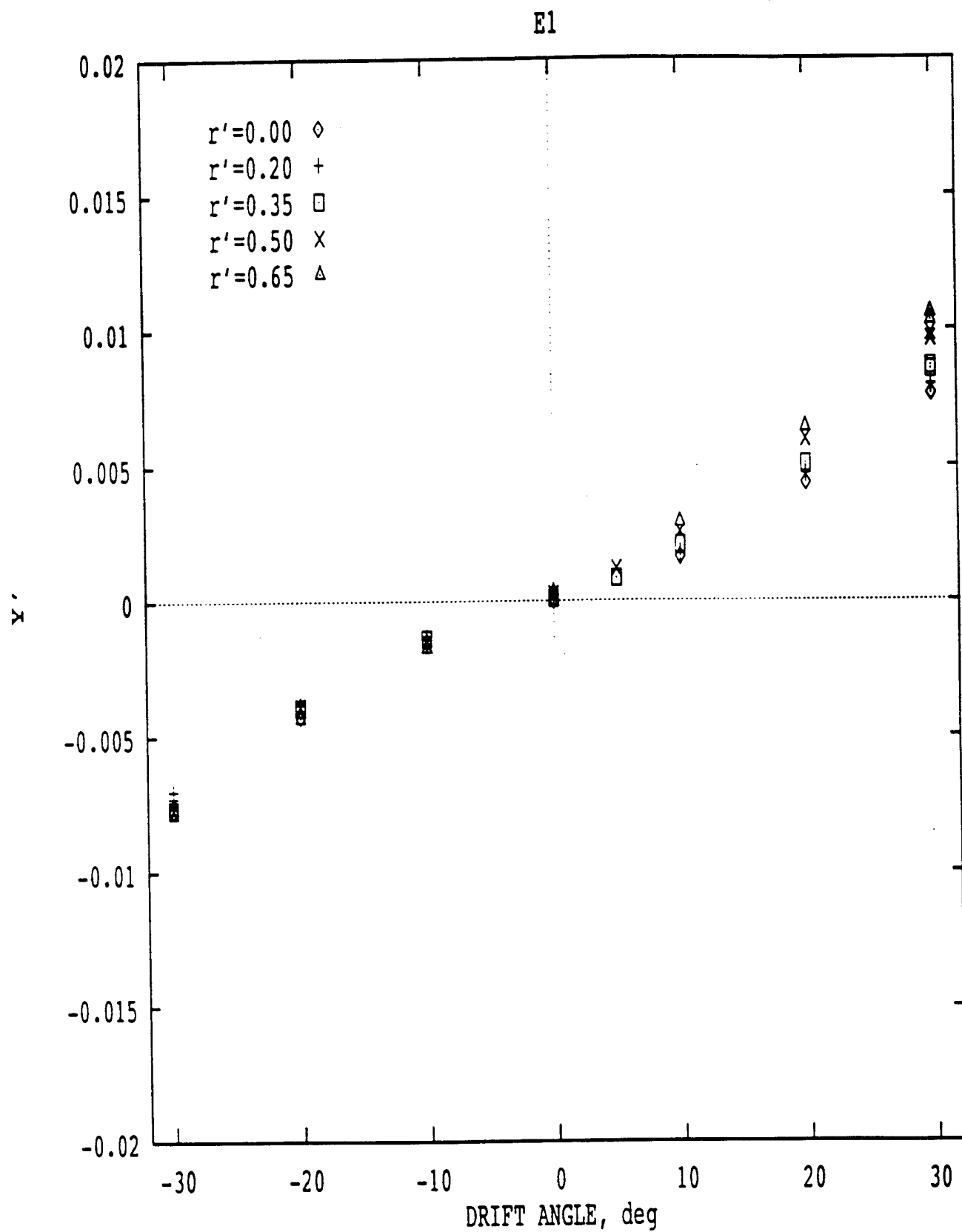


Figure 39. Non-Dimensional Side Force on Model E1, from [Klosinski and Lewandowski]

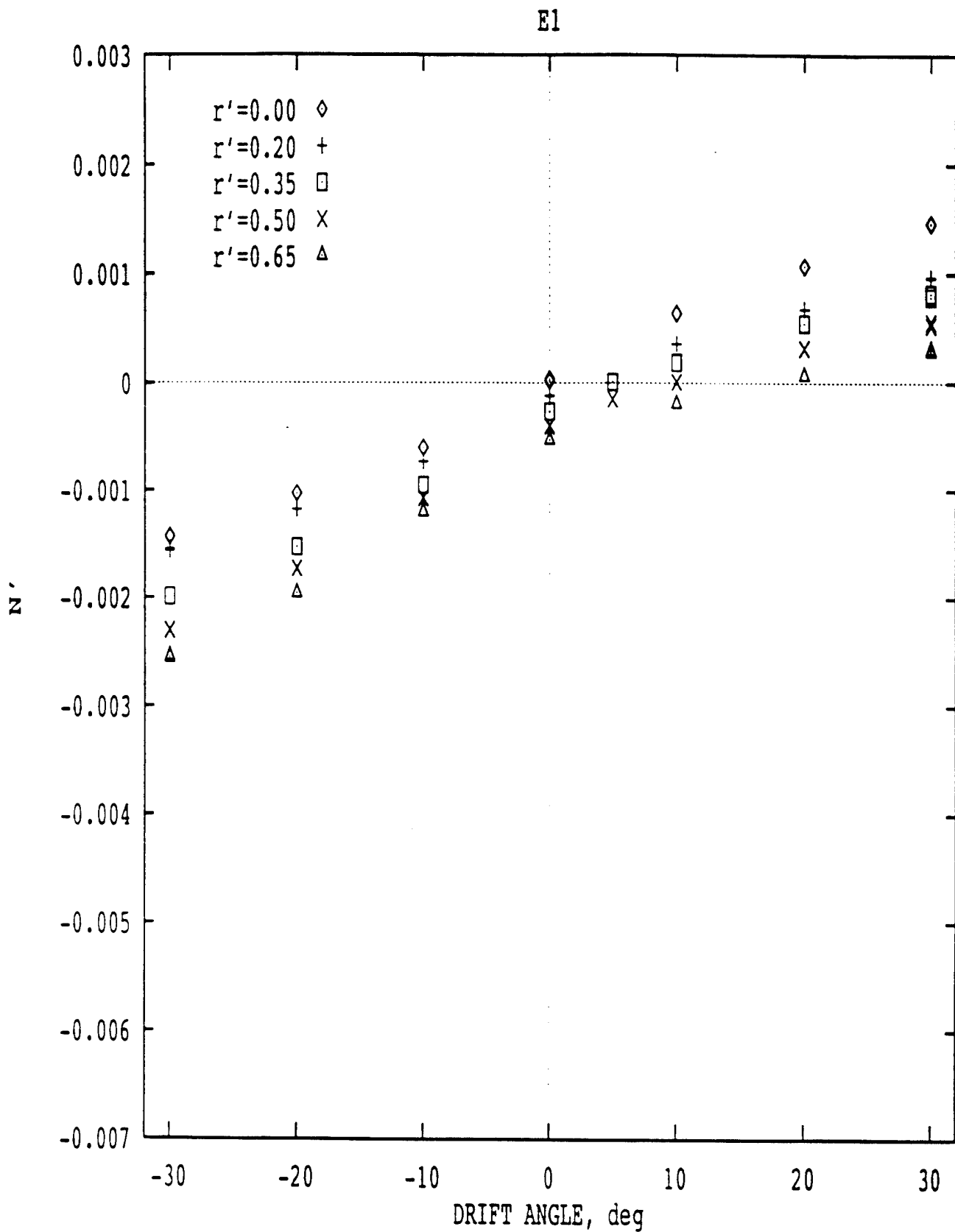


Figure 40. Non-Dimensional Yaw Moment on Model E1, from [Klosinski and Lewandowski]

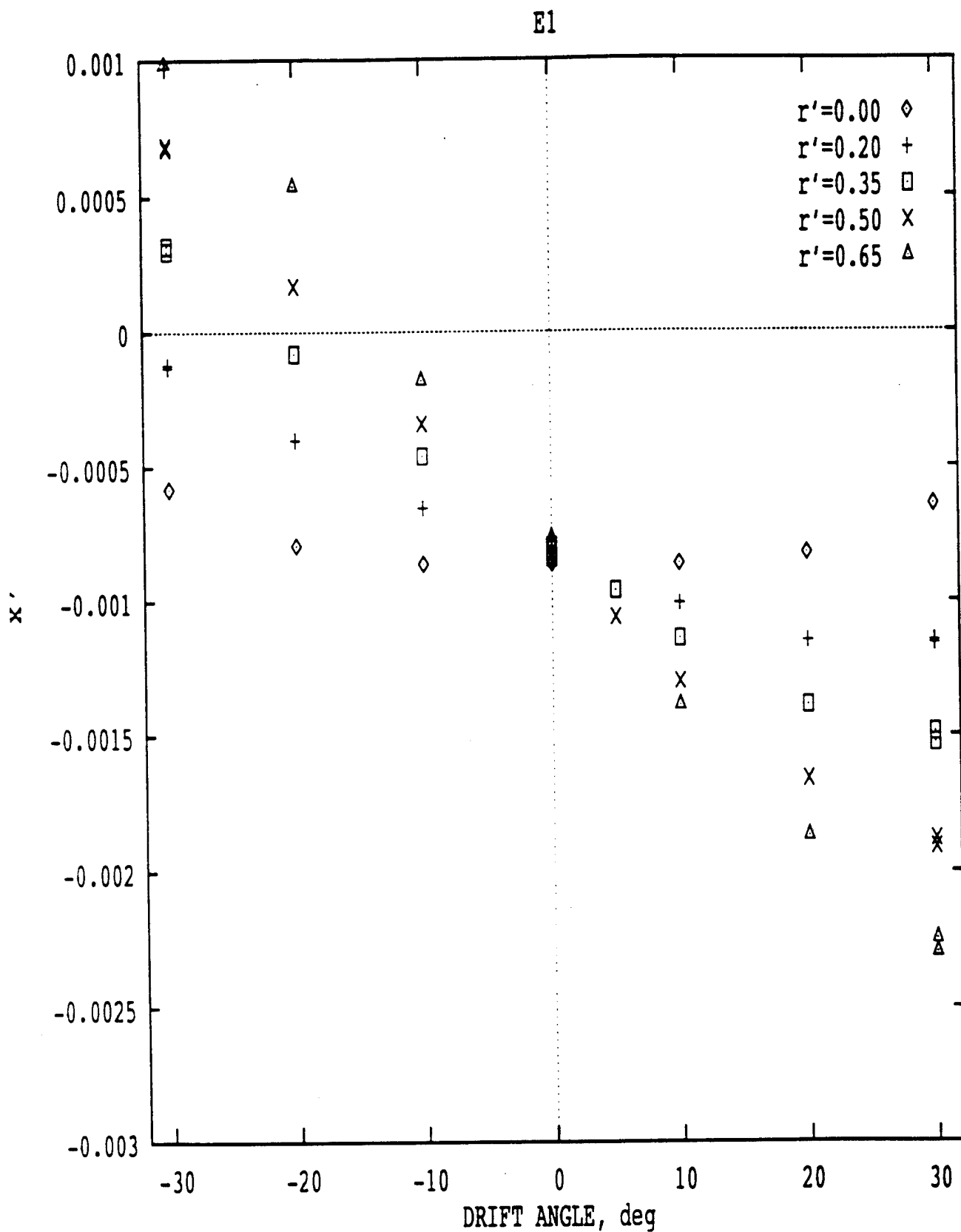


Figure 41. Non-Dimensional Axial Force on Model E1, from [Klosinski and Lewandowski]

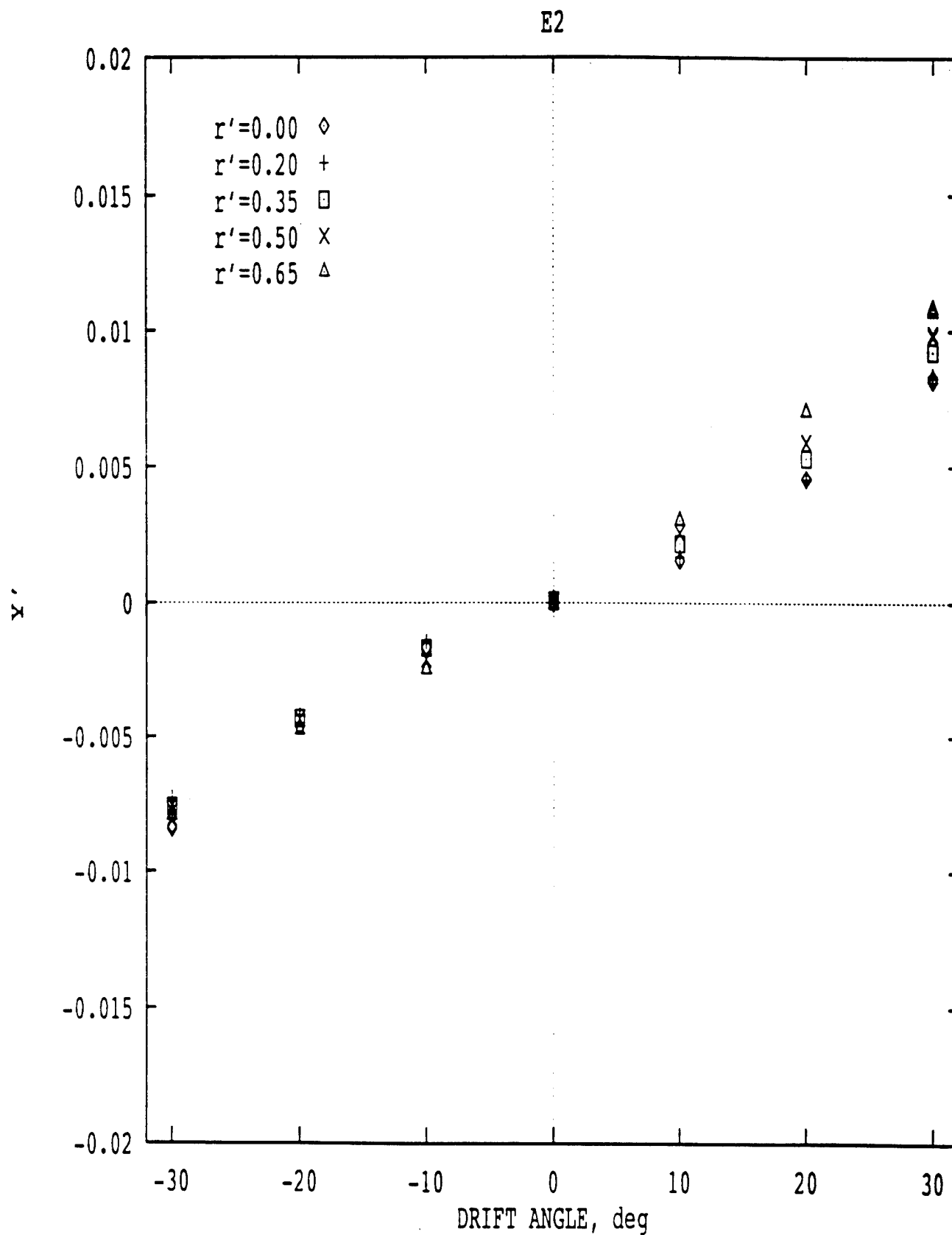


Figure 42. Non-Dimensional Side Force on Model E2, from [Klosinski and Lewandowski]

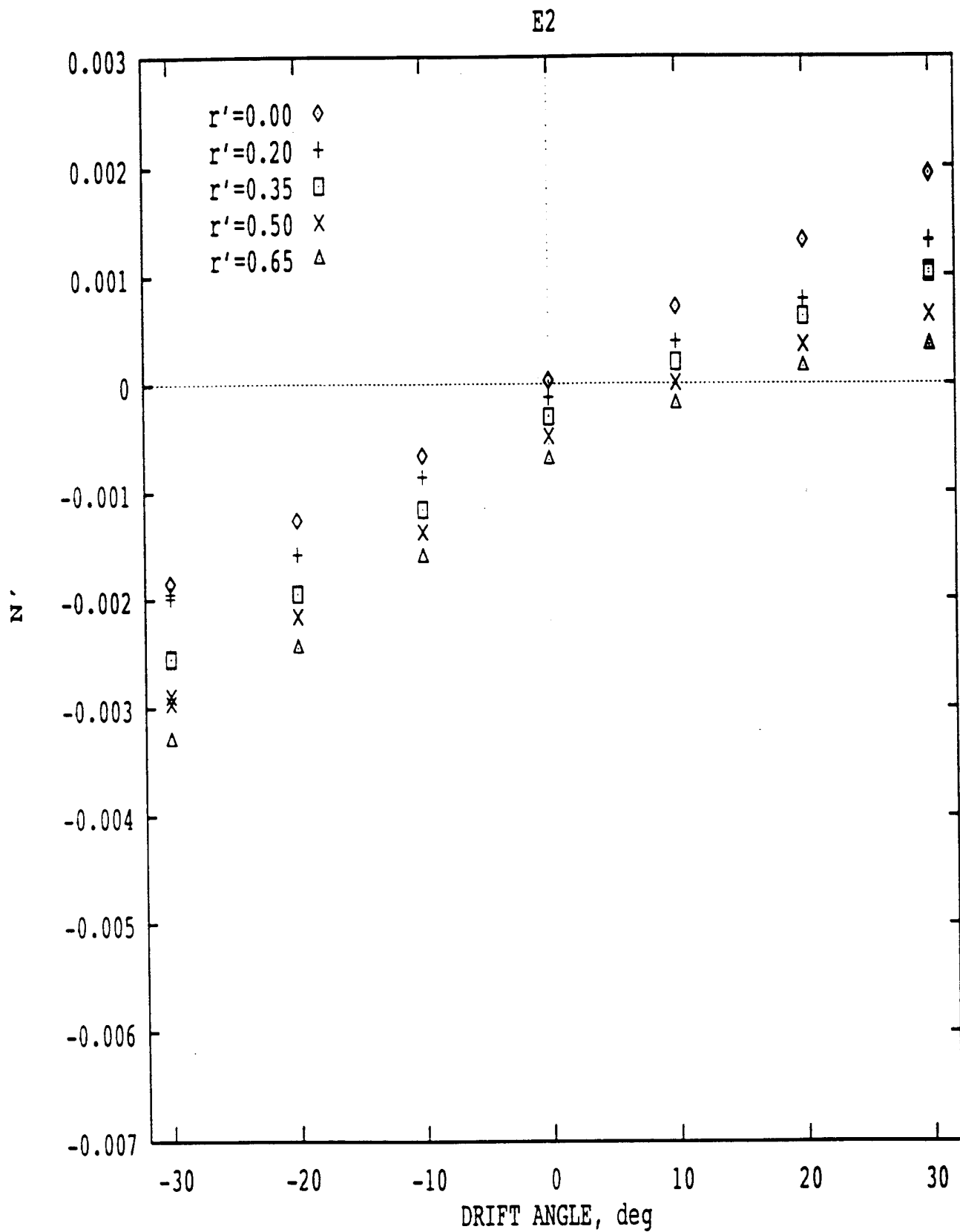


Figure 43. Non-Dimensional Yaw Moment on Model E2, from [Klosinski and Lewandowski]

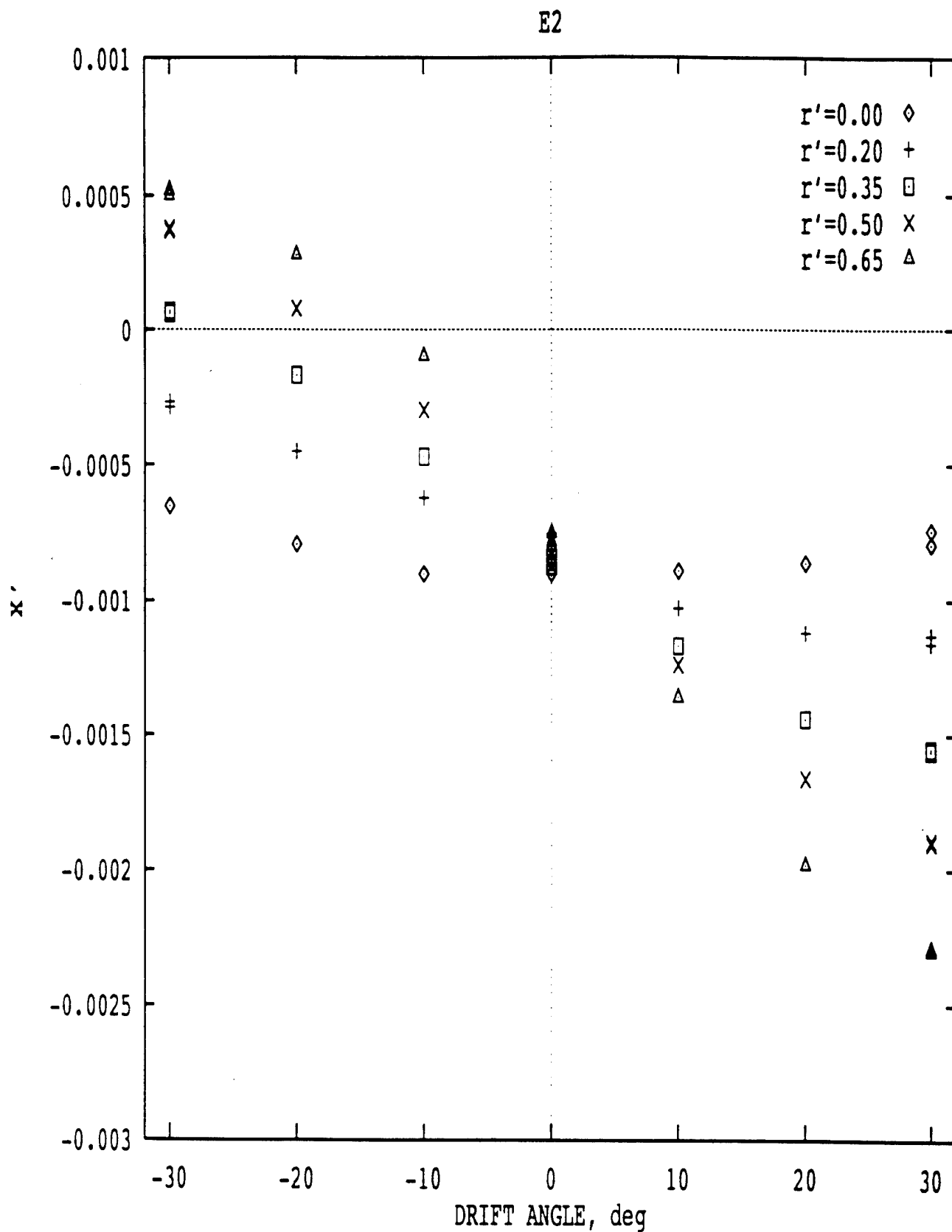


Figure 44. Non-Dimensional Axial Force on Model E2, from [Klosinski and Lewandowski]

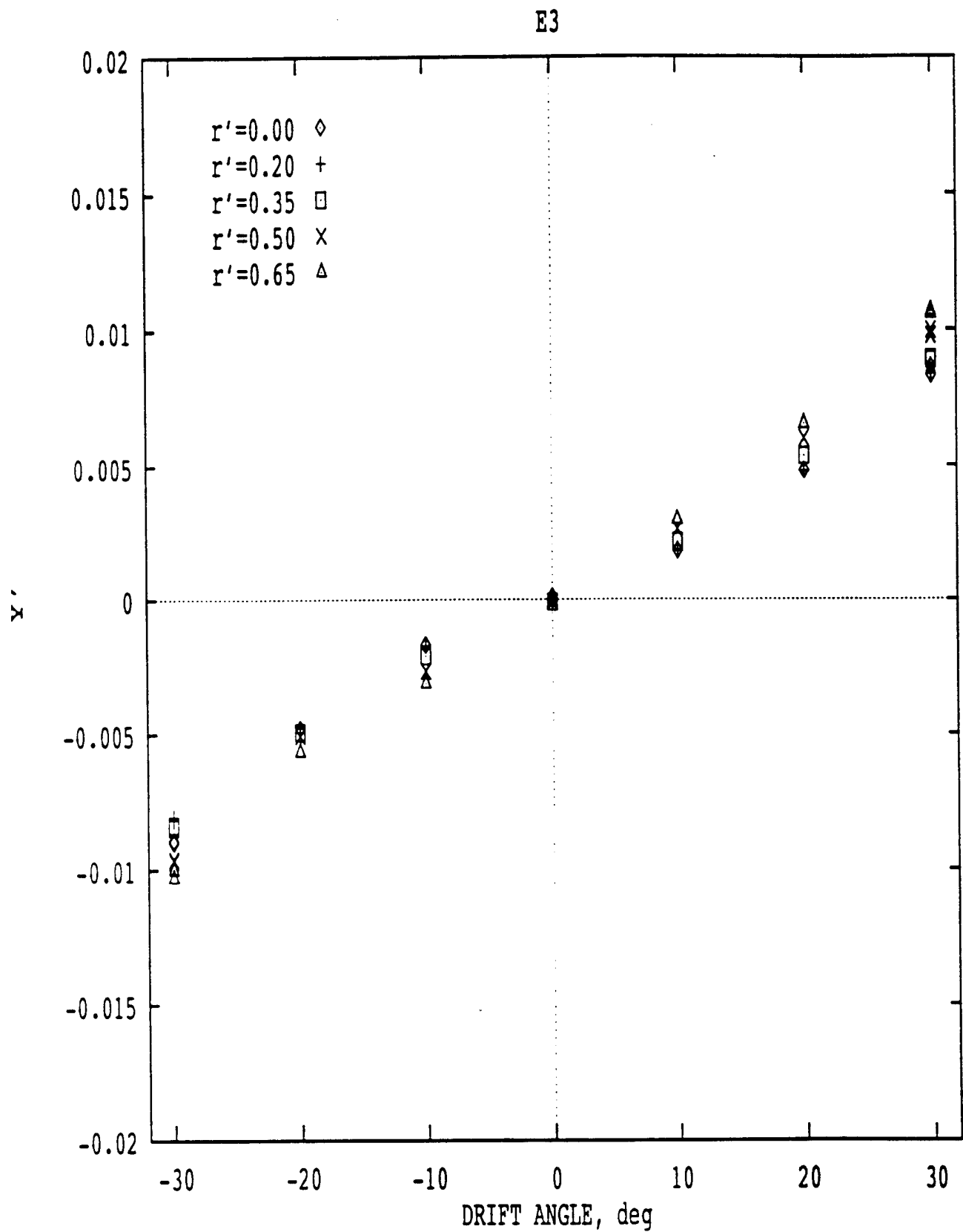


Figure 45. Non-Dimensional Side Force on Model E3, from [Klosinski and Lewandowski]

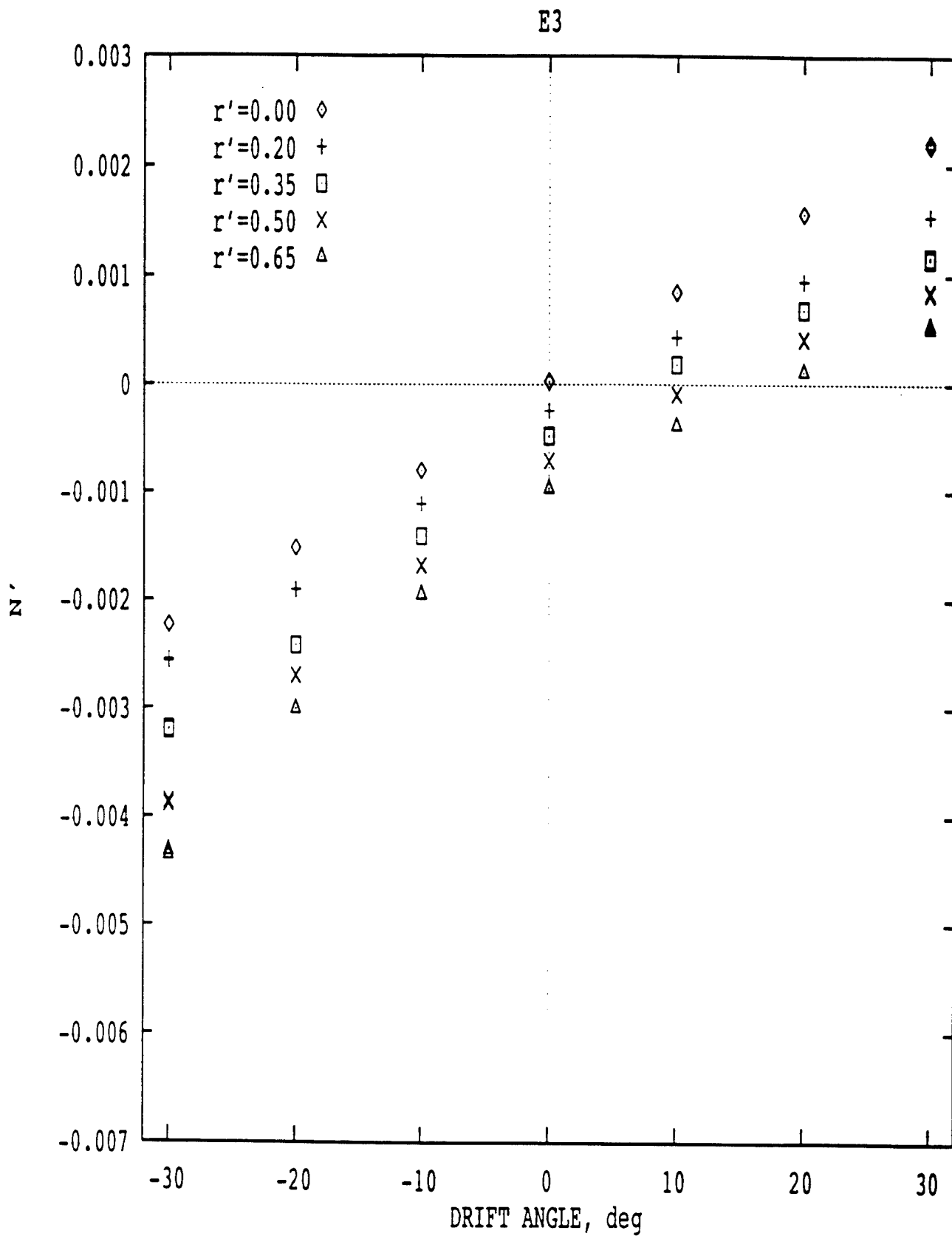


Figure 46. Non-Dimensional Yaw Moment on Model E3, from [Klosinski and Lewandowski]

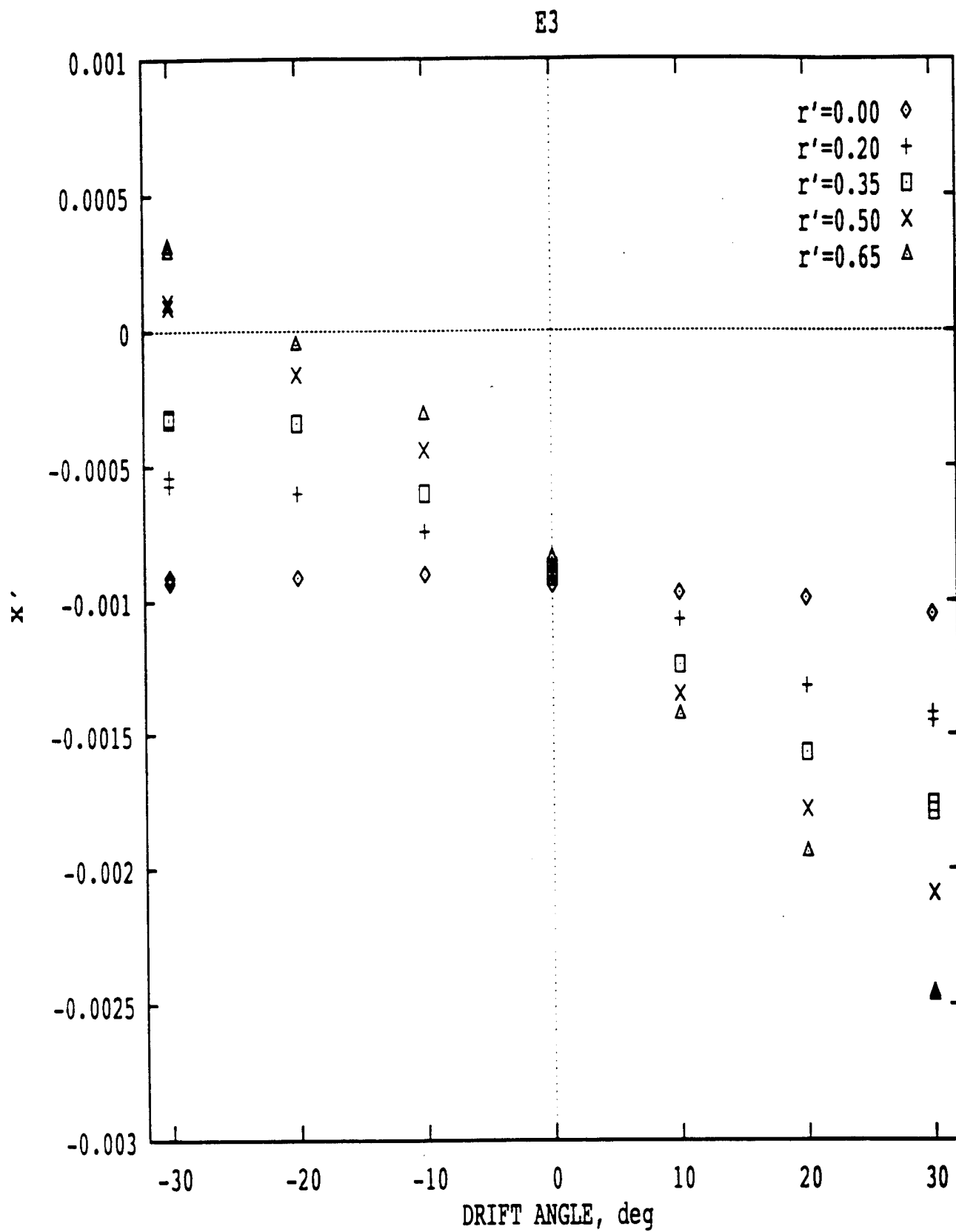


Figure 47. Non-Dimensional Axial Force on Model E3, from [Klosinski and Lewandowski]

MARINER

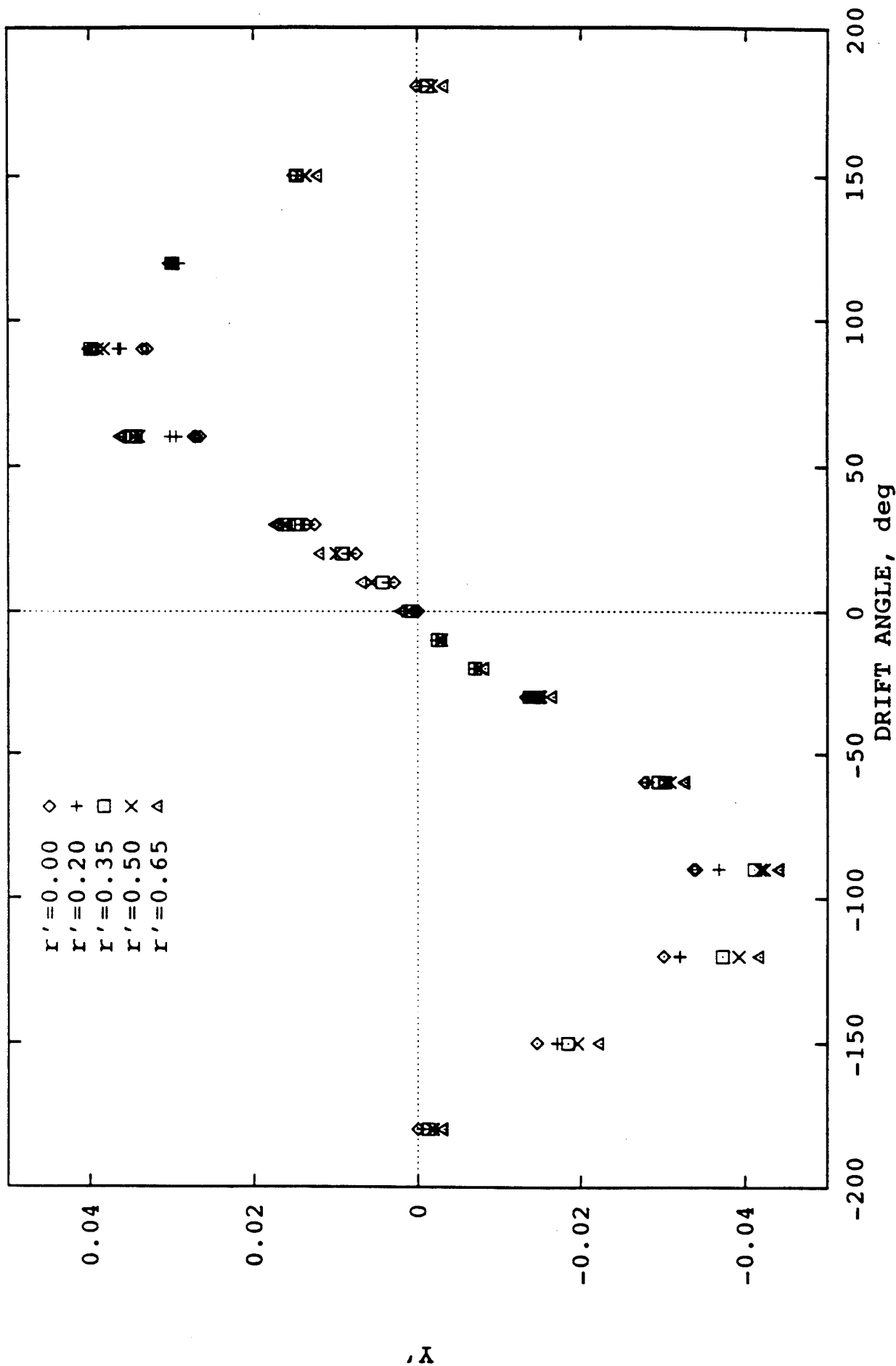


Figure 48. Non-Dimensional Side Force at Large Drift Angles for MARINER Model, from [Klosinski and Lewandowski]

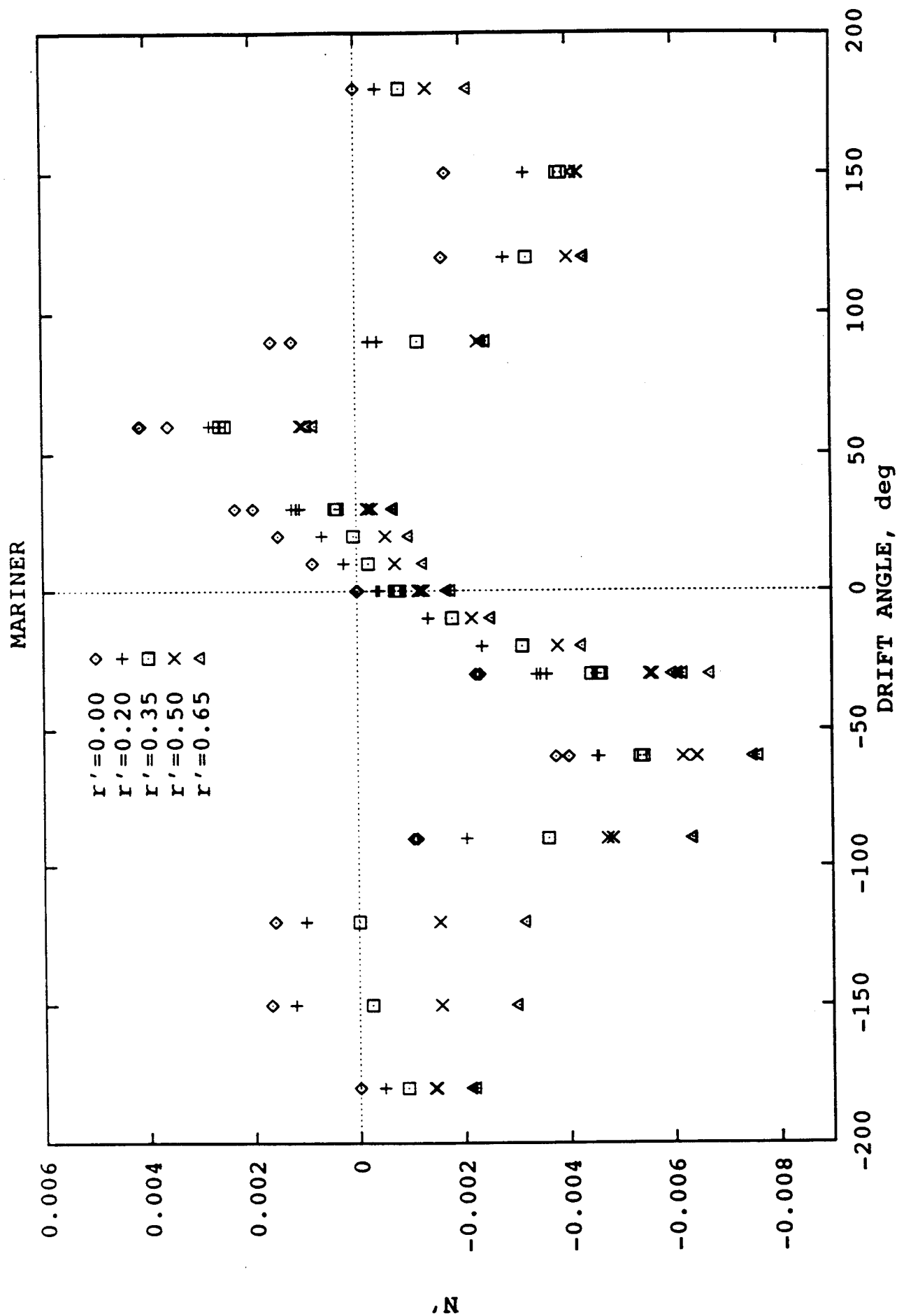


Figure 49. Non-Dimensional Yaw Moment at Large Drift Angles for MARINER Model, from [Klosinski and Lewandowski]

MARINER

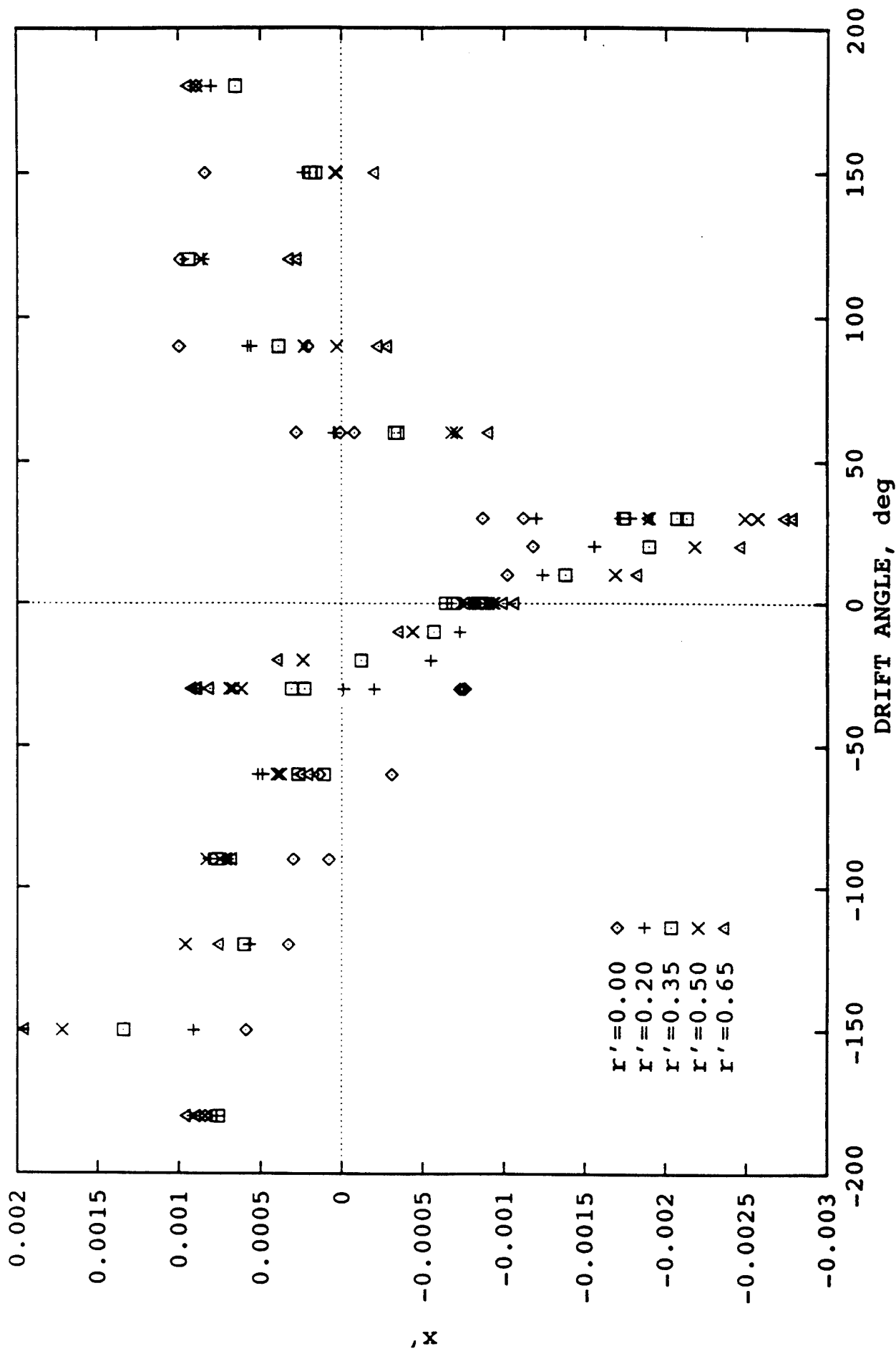


Figure 50. Non-Dimensional Axial Force at Large Drift Angles for MARINER Model, from [Klosinski and Lewandowski]

where X_0 is the axial force in steady straight ahead motion at speed V . This relationship is compared to data from the Parent model in Figure 51. While agreement is fair for zero yaw rate, it becomes increasingly poor at higher yaw rates.

[Inoue et al., 1981 (a)] conducted rotating arm tests on ten hull models, each 2.5 meters in length, at a Froude number of 0.06, over a range of yaw rates and drift angles. After deducting the centrifugal force components, the hydrodynamic sway force and moment were assumed to fit the following equations:

$$Y'' = c_1\beta + c_2r' + c_3\beta|\beta| + c_4\beta|r'| + c_5r'|r'|$$

$$N'' = c_6\beta - c_7r' + c_8r'|r'| + c_9r'^2\beta + c_{10}r'\beta^2$$

The coefficients $c_1 - c_{10}$ were found by regression analysis for each model, and plotted against various hull form parameters. This approach is attractive since it is possible to determine the hydrodynamic coefficients for an arbitrary hull form prior to a simulation. During the simulation, only the equations above need be evaluated at each time step. Since Y'' and N'' differ from Y' and N' only by a factor of L/H , it is possible to compare the Japanese regression equations directly to the SIT rotating arm data. This comparison is illustrated by the dashed lines in Figures 52-53. Agreement is seen to be fair, but substantial differences are present. (Whether these differences are due to test speed, hull form or other factors is not presently known). Using Inoue's model and the SIT data, new coefficients were obtained by regression, but the fit was not much improved. A new model was constructed with many more terms, and a backwards stepwise regression technique was used to eliminate least significant terms. The remaining terms were found to fit the data for each hull form reasonably well:

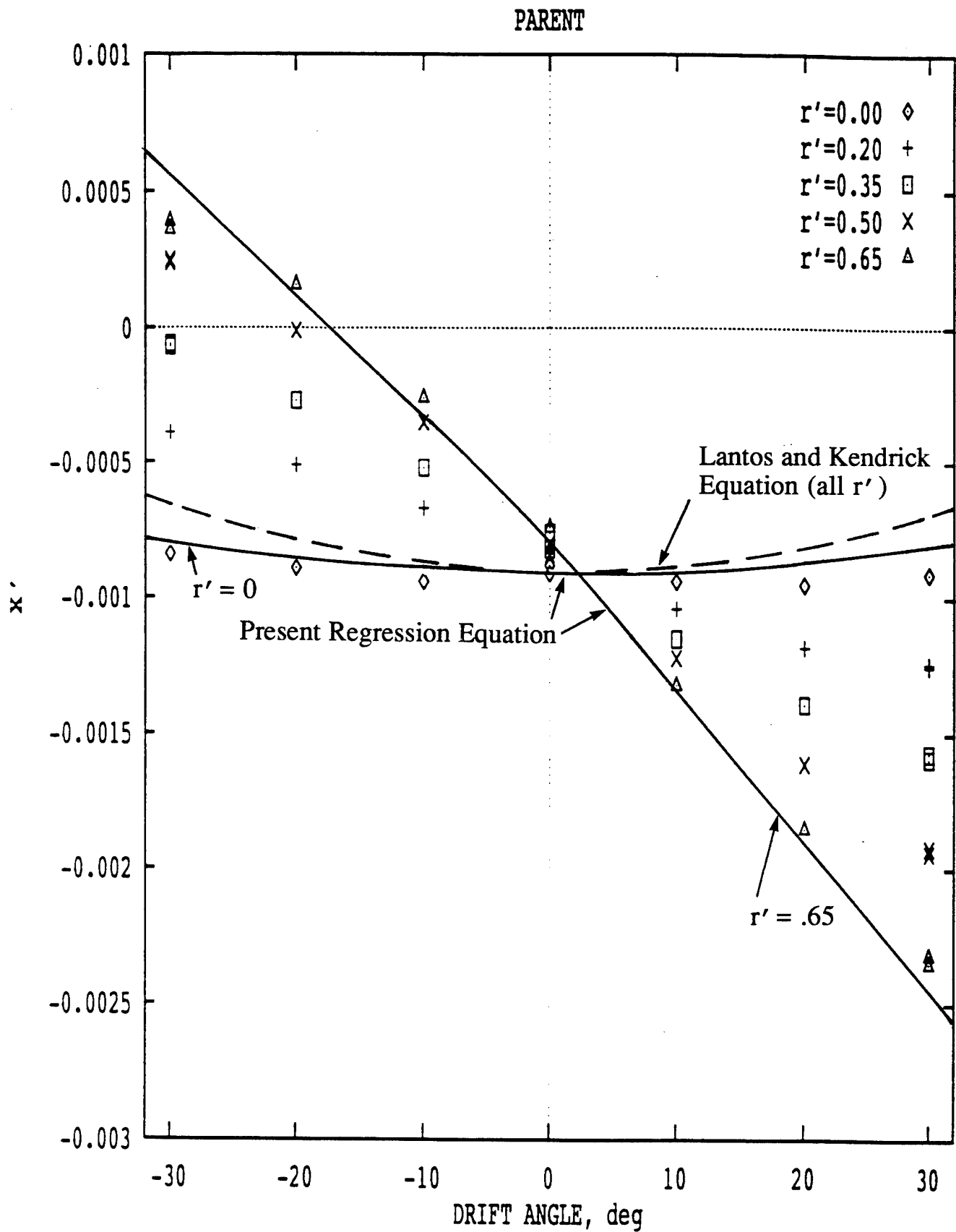


Figure 51. Comparison of Present Regression Equation and Canadian Model for Axial Force on Parent Model, data from [Klosinski and Lewandowski]

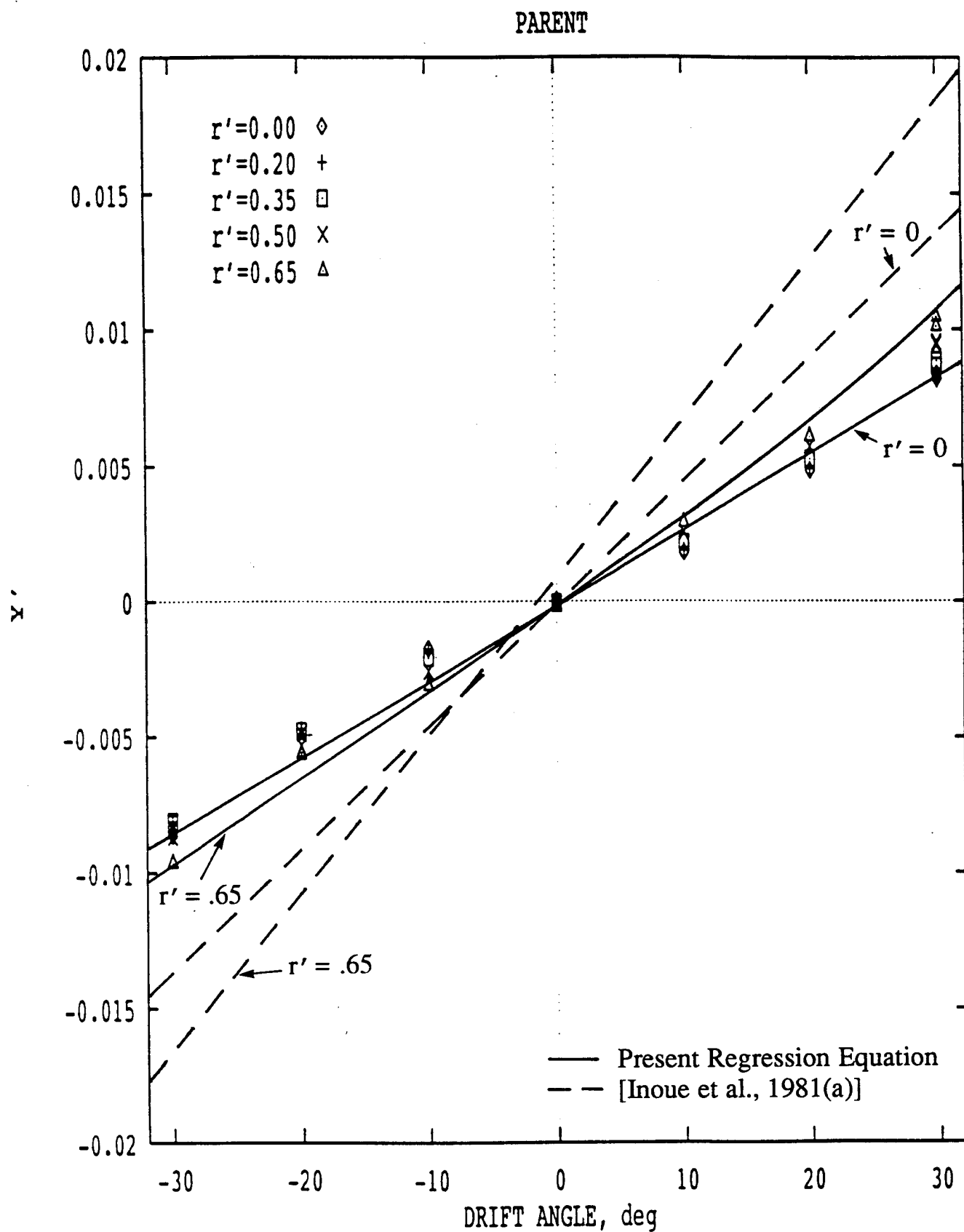


Figure 52. Comparison of Present Regression Equation and Inoue's Regression Equation for Side Force on Parent Model, data from [Klosinski and Lewandowski]

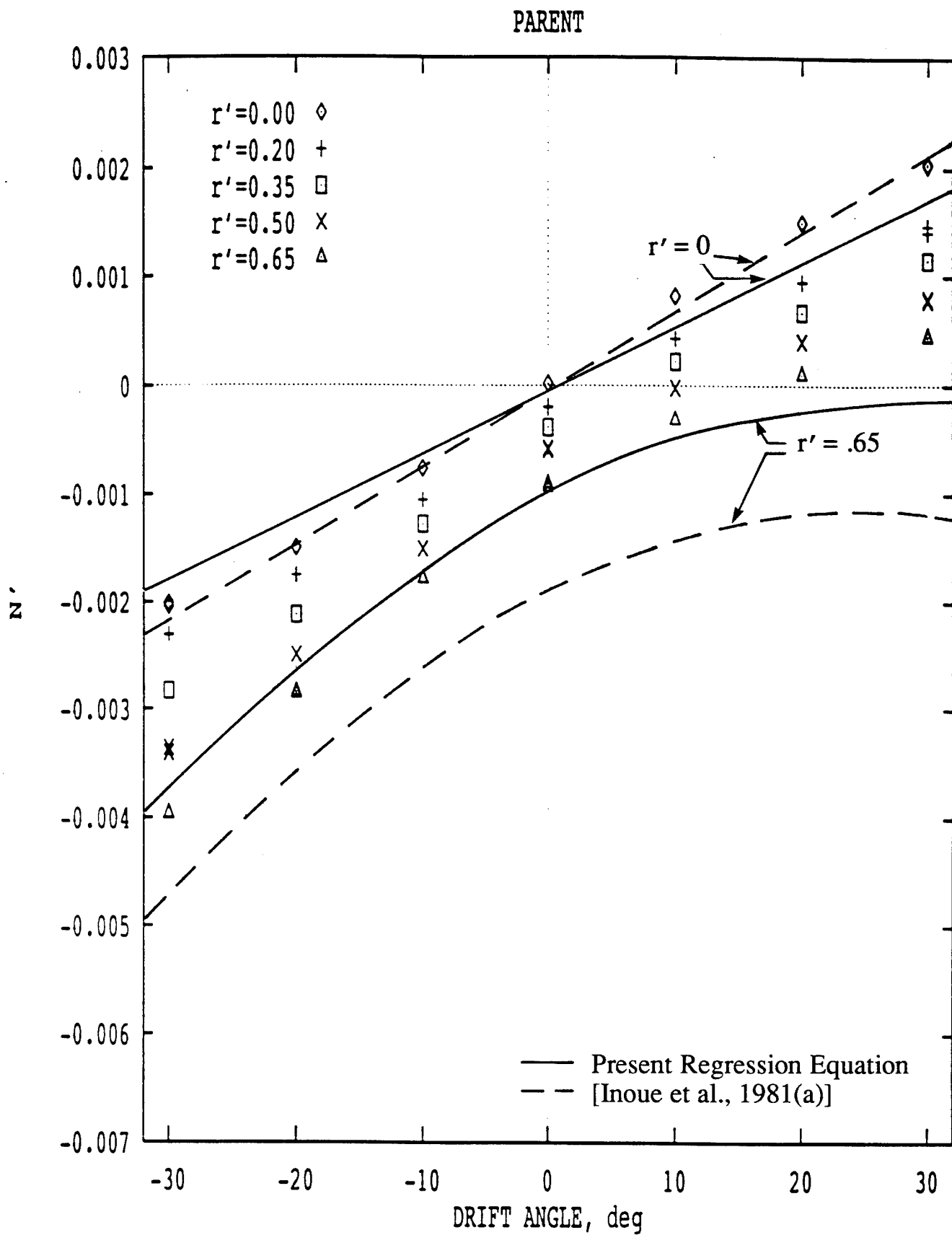


Figure 53. Comparison of Present Regression Equation and Inoue's Regression Equation for Yaw Moment on Parent Model, data from [Klosinski and Lewandowski]

$$X' = a_1 + a_2 r'^2 + a_3 \beta^2 + a_4 r'^3 + a_5 r' |\beta| + a_6 |r'| \beta$$

$$Y' = a_7 \beta + a_8 r' + a_9 \beta |\beta| + a_{10} \beta r' + a_{11} r' |r'|$$

$$N' = a_{12} \beta + a_{13} r' + a_{14} r' |r'| + a_{15} \beta r' + a_{16} \beta^2 r'$$

Coefficients $a_1 - a_{16}$ were obtained for each hull model by regression analysis. It was then determined that each of these coefficients could be expressed as a function of hull geometry as follows:

$$a_i = b_1 C_{fca} + b_2 C_{aca} + b_3 (L/B)^2 + b_4 (L/H)^2 + b_5 C_p + b_6 C_{fca}^2 + b_7 C_{aca}^2$$

The coefficients $b_1 - b_7$ for each of the a_i 's are listed in Table 2. The quality of fit is shown for the Parent model by the solid lines in Figures 51-53, and is seen to give considerable improvement over the Lantos and Kendrick model for x-force, and Inoue's equations for the y-force and yaw moment. (Curvefit results for the other models in the series are not plotted, but similar improvements are obtained). Thus, for $-30^\circ < \beta < +30^\circ$, $0.0 < r' < 0.65$, and within the geometrical parameters of Table 1, these equations can be used to obtain the basic hydrodynamic forces and moment on the hull. Forces and moments for $-.65 < r' < 0.0$ can be obtained by symmetry arguments as $F(\beta, -r') = -F(-\beta, r')$. Thus, the bare hull forces can be evaluated for low $|\beta|$ conditions typical of the standard maneuvers in the new IMO maneuvering regulations. Figures 47-50 show the general trends of force and moment data over the entire range of possible β values. These results were obtained at relatively high speed, $Fr = 0.17$, and may contain wavemaking effects at large $|\beta|$ values. It is recommended that these tests be repeated at a lower speed typical of high drift angle maneuvers.

Other researchers [Fedyayevskiy and Sobolev], [Strumpf, 1983], [Zilman] have used crossflow drag theory for large drift

Table 2

Coefficients for Present Equations

	b_1	b_2	b_3	b_4	b_5	b_6	b_7
a_1	+5.978E-4	-2.090E-3	+2.134E-6	+4.083E-7	-9.952E-4	-4.981E-4	+1.282E-3
a_2	+5.320E-2	-5.378E-2	+7.882E-5	-2.075E-6	+1.651E-3	-2.876E-2	+2.594E-2
a_3	+1.565E-1	-1.473E-1	-5.035E-5	-7.779E-7	+4.539E-3	-8.875E-2	+8.035E-2
a_4	+1.293E-1	-1.221E-1	-1.306E-4	+2.390E-6	-2.952E-3	-7.063E-2	+6.989E-2
a_5	-2.949E-1	+2.906E-1	+5.476E-5	+3.863E-7	-2.729E-3	+1.591E-1	-1.573E-1
a_6	+4.792E-2	-7.554E-2	+2.694E-5	+7.603E-6	-1.083E-3	-2.349E-2	+4.280E-2
a_7	+7.556E-1	-7.828E-1	+3.531E-5	-1.986E-5	-2.352E-2	-4.001E-1	+4.655E-1
a_8	+3.840E-1	-4.144E-1	+5.944E-5	-3.002E-6	-1.093E-2	-2.105E-1	+2.508E-1
a_9	-2.583E-1	+3.163E-1	+2.554E-4	-2.408E-5	-1.350E-2	+1.346E-1	-1.759E-1
a_{10}	+2.526E-1	-2.659E-1	+3.059E-5	-4.897E-6	-8.908E-3	-1.327E-1	+1.599E-1
a_{11}	-1.187E-1	+1.332E-1	-1.321E-5	-2.850E-6	+7.699E-3	+6.079E-2	-7.894E-2
a_{12}	-8.401E-2	+1.287E-1	-3.748E-5	-2.398E-5	+5.500E-3	+4.902E-2	-8.131E-2
a_{13}	-7.530E-2	+8.203E-2	-5.890E-6	+2.864E-6	+3.021E-3	+3.825E-2	-5.018E-2
a_{14}	-2.597E-2	+2.619E-2	-3.219E-6	-5.626E-7	+2.630E-3	+1.407E-2	-1.597E-2
a_{15}	-2.056E-1	+2.114E-1	-5.176E-5	+2.277E-6	+6.090E-3	+1.145E-1	-1.228E-1
a_{16}	-3.730E-1	+3.991E-1	-1.175E-4	+1.084E-5	+2.064E-2	+1.945E-1	-2.407E-1

angles to estimate sway force and yaw moment contributions at each longitudinal section. To get accurate results towards the stern, however, the effects of shed vorticity must be accounted for as described by [Hearn et al.]

David Taylor Research Center Test Program

The Coast Guard desired to assess possible scale effects on the small model bare-hull forces obtained at Stevens, despite the excellent agreement between small and large model rotating arm tests on a Destroyer hull form reported by [Strumpf]. A twenty-two foot model of a MARINER hull (as described in Table 3) was available at David Taylor Research Center (DTRC). This was tested in DTRC's linear towing tank and rotating arm facility at the same scaled draft and test conditions as the SIT tests. Again, centrifugal force effects were removed from the data to yield pure hydrodynamic forces and moment (about amidships). (In these tests, the centrifugal force and moment produced by the model and that portion of the dynamometer between the model and the block gages was determined by calculation, since the apparatus could not support the large model in air). Comparison of rotating arm data for the large and small model is shown in Figures 54-56. Agreement for the axial force and moment is generally good, but the side forces exhibit apparent scale effects except at $\beta = 0^\circ$ and $+10^\circ$.

It is unclear whether this discrepancy is a genuine scale effect, or some artifact of the calibration, experiment or analysis. However, the lack of fairness between DTRC's rotating arm and towing tank sway force data (shown in Figure 54) appears suspicious. It was initially suspected that the different centrifugal force correction methods used by SIT and DTRC may have been responsible, but both methods were carefully scrutinized and appear correct in principle. It is recommended that these tests be repeated at the same facility using the same

Table 3. Characteristics of Full-Scale MARINER and DTRC Model

	Full Scale	Model Scale
Length, L_{pp} (ft/m)	528.00 / 161.93	21.84 / 6.66
Length, L_{wl} (ft/m)	523.3 / 159.5	21.65 / 6.60
Beam (ft/m)	75.97 / 23.16	3.14 / 0.95
Draft (ft/m)	27.00 / 8.23	1.12 / 0.34
Displacement (LT/Tonnes)	18640 / 18939	1.28 / 1.30
Propeller Diam (ft/m)	22.00 / 6.71	0.91 / 0.28
Pitch/Diameter Ratio	1.046	
Expanded Area Ratio	0.562	
Mean Width Ratio	0.276	
Blade Tip Fraction	0.0474	
Scale Ratio, λ	24.175	

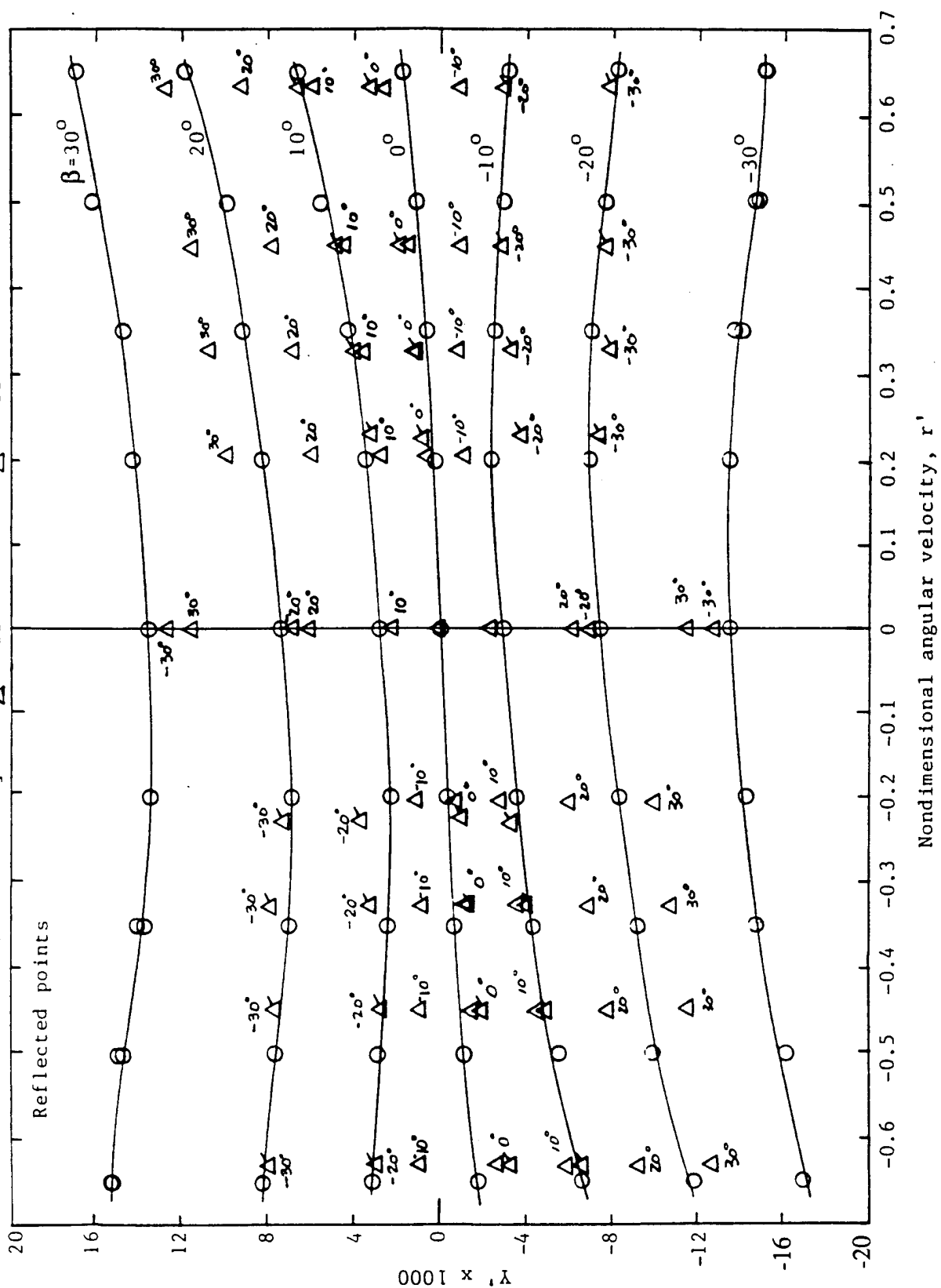


Figure 54. Effect of Model Scale on Side Force Data

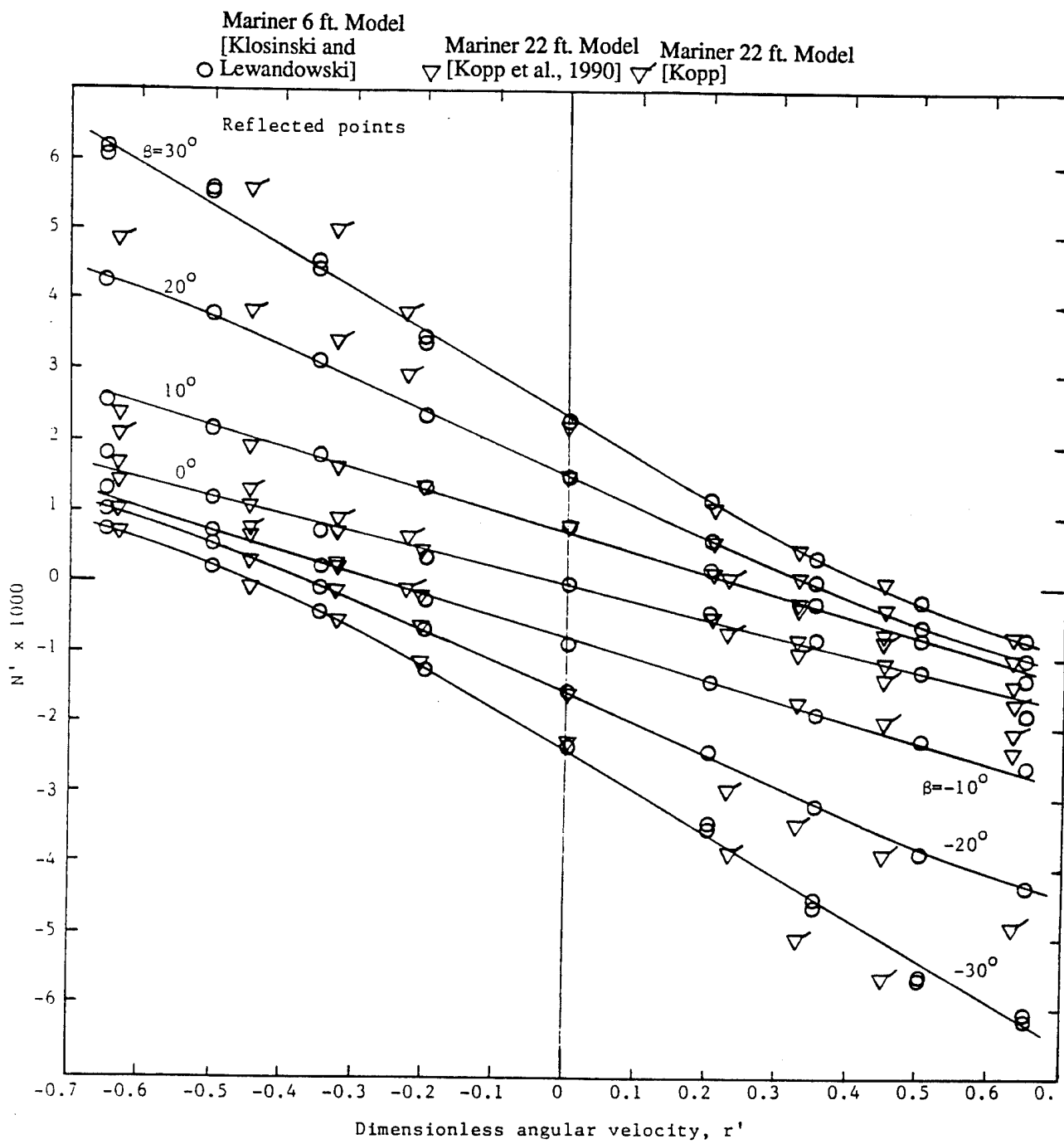


Figure 55. Effect of Model Scale on Yaw Moment Data

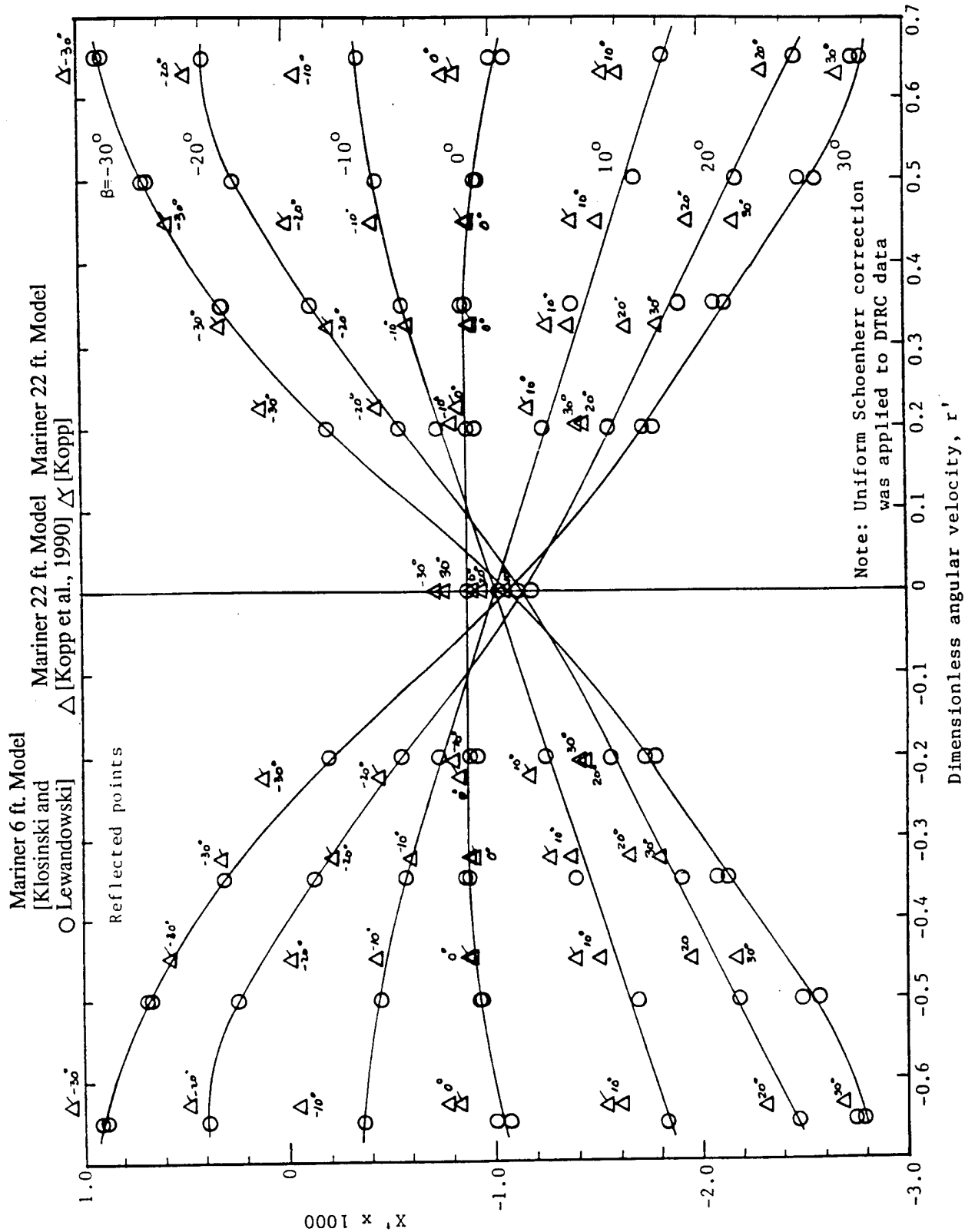


Figure 56. Effect of Model Scale on Axial Force Data

dynamometers and method of analysis for both the large and small models.

In a modular model, interaction effects, where the presence of one component induces or modifies the force on another, must be accounted for. Thus the Coast Guard tasked DTRC to perform a series of "stripping" tests to measure the forces and moment in the following additional configurations: hull with rudder and operating propeller, hull with rudder only, and hull with operating propeller only. Two types of rudders were used. An NACA-0025 airfoil rudder was built, whose stock passed through a hole in the hull without contacting the model and was attached directly to the carriage. Thus, the dynamometer attached to the hull measured hull forces in the presence of the rudder, but did not include forces on the rudder. It is shown in Figure 57 that the presence of the rudder, at an effective angle of attack, modifies the sway force and yaw moment on the hull. Additional data on this effect are given in [Kopp et al., 1990, figures 28-35]. The airfoil rudder was also fitted with five-hole pitot tubes at four different vertical locations (see Figure 58) to measure inflow velocity vectors at different locations along the rudder chord. Secondly, an unbalanced flat plate rudder (or "flag" rudder), with the stock at the leading edge, was constructed and left free to rotate to an angle which produced no net moment on the rudder. These tests are further described in [Kopp et al., 1990]. In the flat plate tests with hull and rudder only, the angle of zero moment was reduced compared to the geometric drift angle at the rudder, β_r . The tests with pitot tube rudder showed that this effect became less pronounced towards the bottom of the rudder. When the propeller was also included, there was a distinct increase in the axial flow velocity measured on the part of the rudder within the propeller race, resulting in additional flow straightening. These effects are illustrated schematically in Figure 59. (It should be noted that these effects are very significant for a single screw vessel, but become less pronounced and may even be negligible for

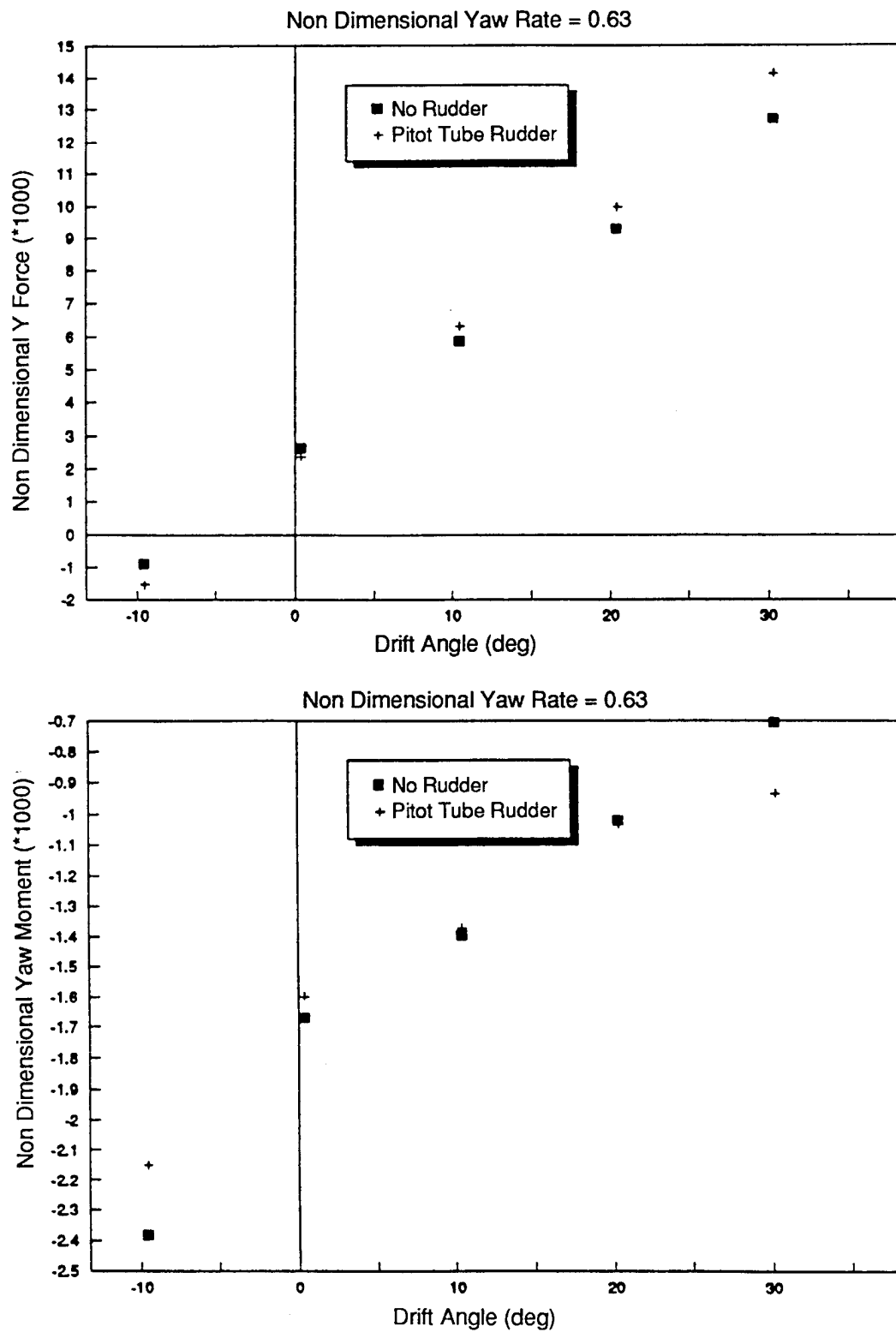
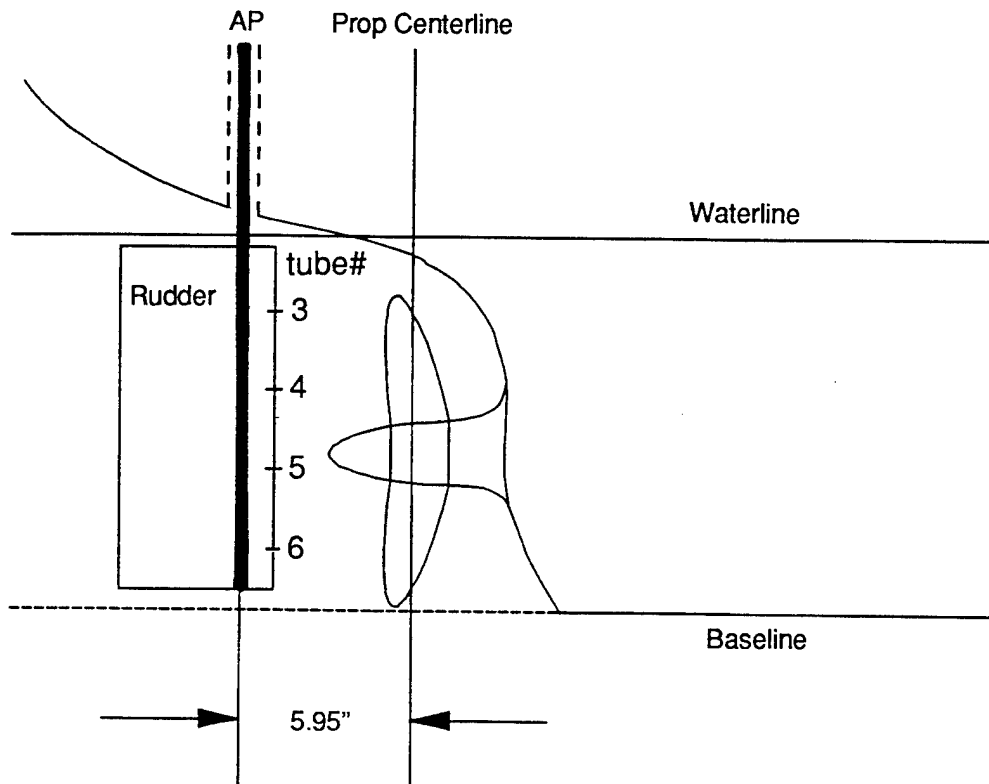


Figure 57. Effect of Rudder Angle of Attack on MARINER Side Force and Moment, from [Kopp et al. 1990]



Propeller Characteristics: $D = 22'$ $P/D = 1.05$ $EAR = .56$ # Blades = 4

Self-Propulsion Data:

$V = 17\text{Kts.}$ $w = .21$ $t = .17$ $J = .775$ $K_T = .18$ $K_Q = .031$

Figure 58. Stern Geometry with Pitot tube Rudder
Used in [Kopp et al., 1990], and Propulsion Data

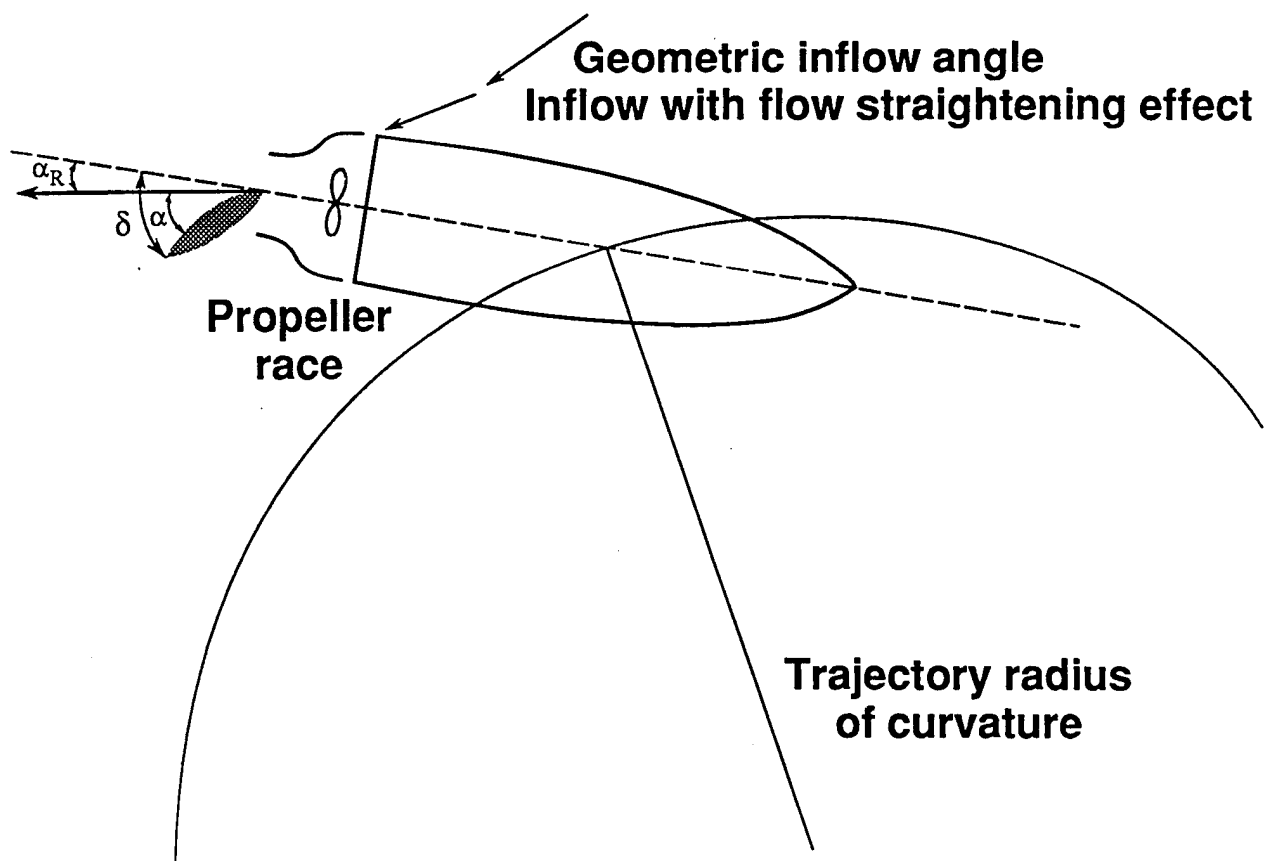


Figure 59. Schematic Illustration of Flow Straightening Effect

twin screw vessels whose propellers and rudders operate in relatively undisturbed flow).

An additional test series was performed with the unbalanced flat plate rudder. This rudder provided an indication of the effective neutral angle of attack. This is compared to the geometric rudder inflow angle without and with the propeller in Figure 60. It is seen that, even without the propeller, the neutral angle is less than the geometric inflow angle at the rudder. (Note that the geometric inflow angle at any axial location can be calculated as

$$\beta_x = \beta + \tan^{-1} [-x \cos(\beta) / (R - x \sin(\beta))] ,$$

where x is the distance of the desired location forward of the tow point. With the operating propeller, the flow straightening effect is even greater. It is also evident that, without or with the propeller, the flow-straightening effect revealed by the flag rudder is nearly independent of the yaw rate.

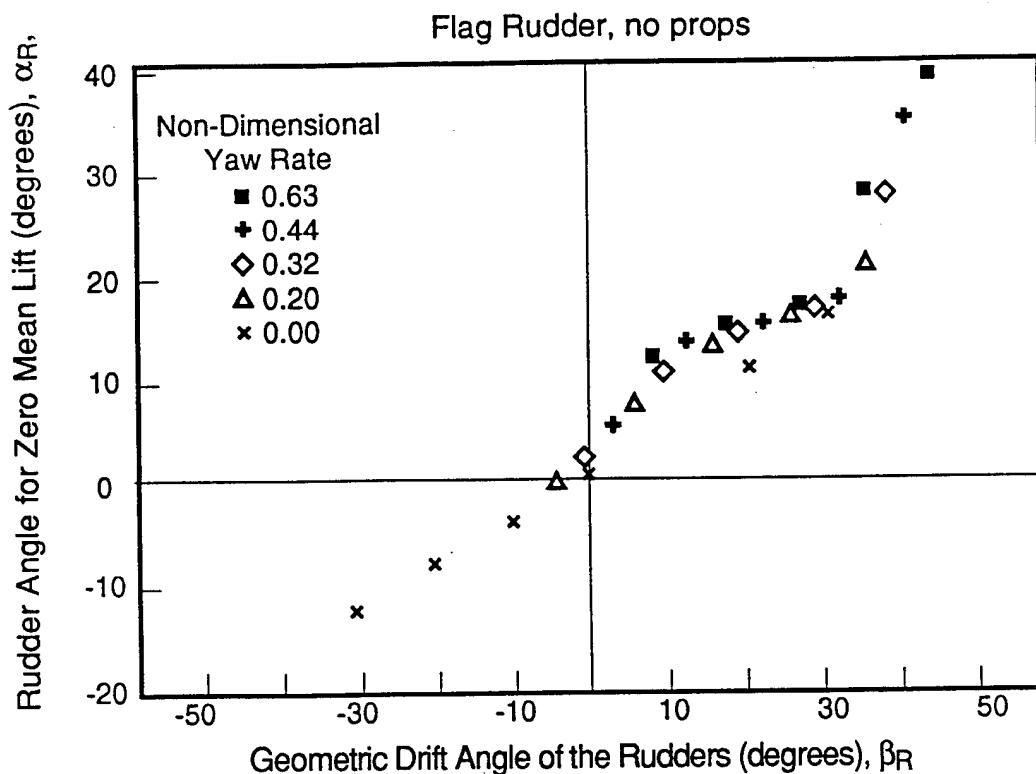
Propeller Inflow and Propeller Forces

The basic thrust force produced by a marine propeller in steady-state straight-ahead motion is well understood. An effective wake fraction, derived from self-propulsion tests, is used to calculate the effective inflow velocity to the propeller,

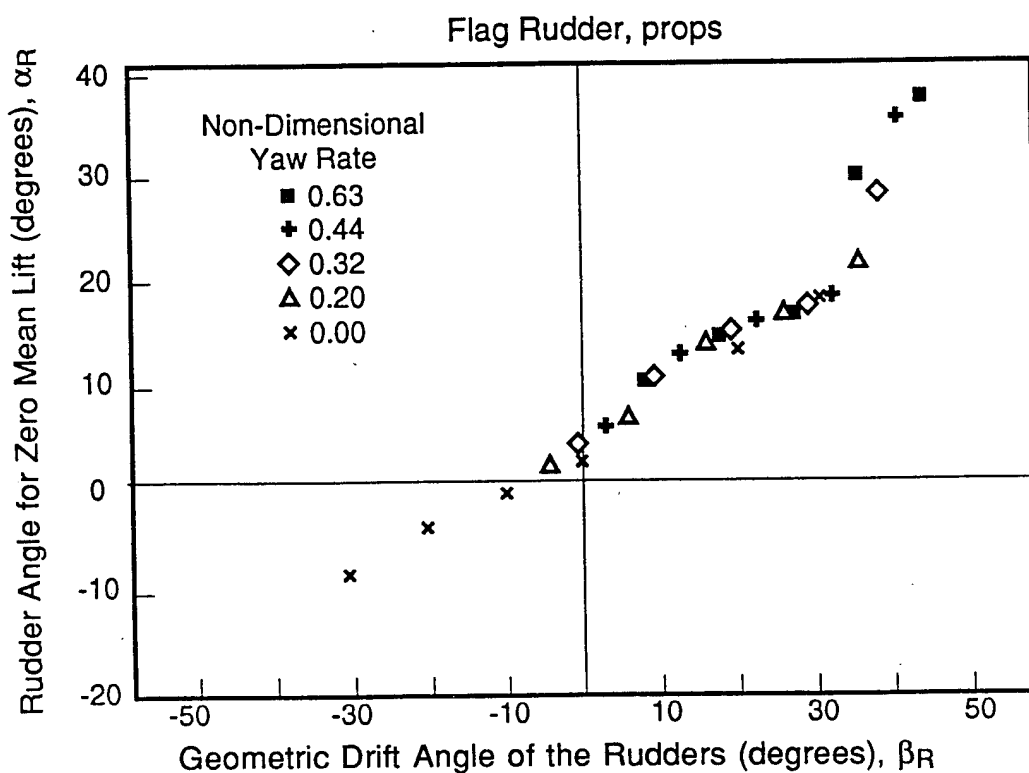
$$V_a = V (1-w_p)$$

For a known propeller RPM and diameter, the advance ratio is calculated,

$$J = V_a / (n D)$$



$$\alpha_R = 3.138 + .7781\beta_R - 1.433E-3\beta_R^2 - 6.929E-4\beta_R^3 + 5.369E-7\beta_R^4 + 4.115E-7\beta_R^5$$



$$\alpha_R = 3.248 + .6114\beta_R - 4.040E-3\beta_R^2 - 5.269E-4\beta_R^3 - 3.537E-6\beta_R^4 + 3.678E-7\beta_R^5$$

Figure 60. Flag Rudder Angle versus Geometric Rudder Drift Angle (with and without Propeller), from [Kopp et al. 1990]

Using results from systematic series of open water propeller tests [e.g. Oosterveld and van Oosanen] the thrust (and torque) coefficients can be obtained as functions of J . A minor correction for relative rotative efficiency is then applied, and full scale thrust and torque can then be calculated. Straight ahead and astern thrust can be determined from four-quadrant open-water data [e.g. Van Lammerman et al.], or from the method given by [Dand].

In straight motion, a propeller also produces a side force which acts to push the stern in the direction that the propeller tip is moving when it is straight up (12:00 o'clock). For a right-handed wheel, there is a tendency to turn to port when going ahead. (The tendency is even greater if the propeller shaft is inclined). This "paddlewheel" or "Hovgaard effect" is discussed in [Saunders]. It is quite complicated and not amenable to theoretical prediction, but the force and associated moment can be significant. During astern maneuvering, this effect accelerates turning to port, but makes backing to starboard difficult or even impossible.

During maneuvering, the flow into the propeller is oblique, as shown in Figure 59, and significant additional side forces may be generated. Early studies of propeller side forces in oblique flow are given by [Gutsche] and [Ribner]. [Peck and Moore] present extensive open water test measurements including vertical and horizontal forces produced by model propellers in oblique flow ($-15^\circ < \alpha_p < +15^\circ$).

In order to use the results of [Peck and Moore], the velocity and direction of inflow to the propeller (averaged over the propeller disk) must be known. Rough estimates of these quantities may be made by averaging the DTRC pitot tube data [Kopp et al., 1990, Table 11] (without propeller, $\delta = 0$). These averaged velocity and inflow angles are shown in Figures 61-62, respectively. The flag rudder inflow angles (without

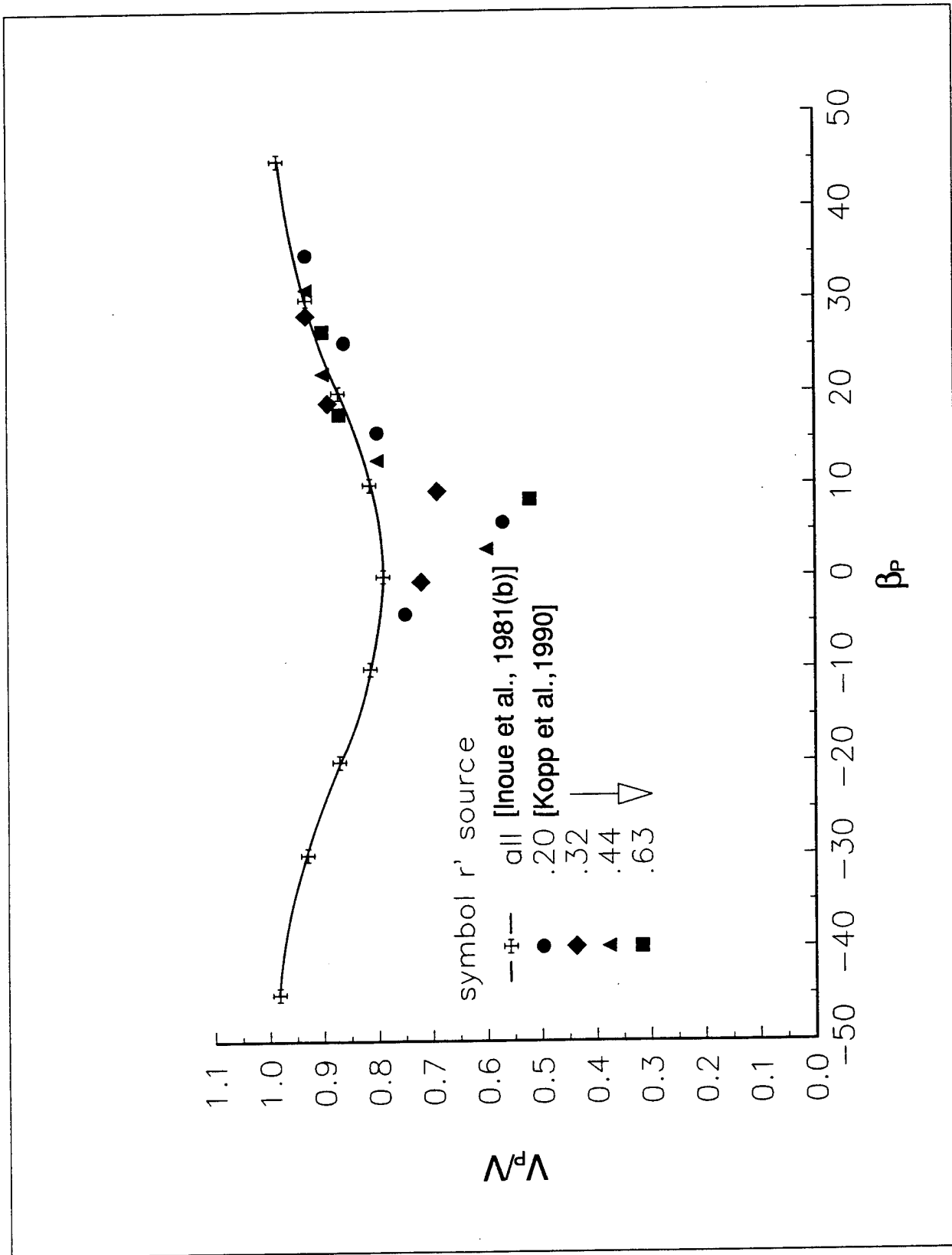


Figure 61. Propeller Inflow Velocity versus Geometric Propeller Drift Angle

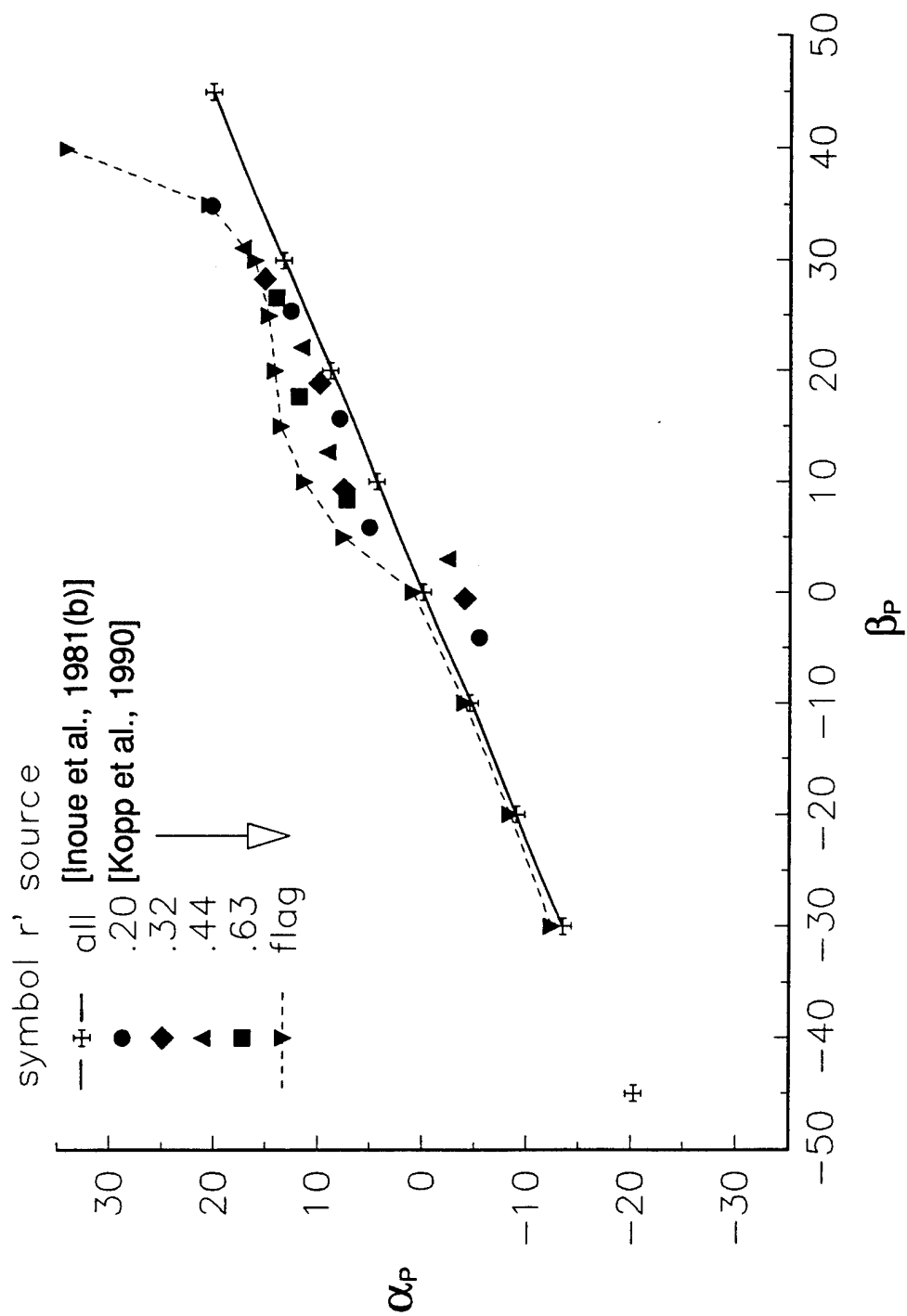


Figure 62. Propeller Inflow Angle versus Geometric Propeller Drift Angle

propeller) are also shown in Figure 62 for comparison. Neither inflow velocity or angle shows any clear dependence on r' . It may be seen that at high absolute values of drift angle, the inflow velocity to the propeller is nearly the same as the ship speed, V , but that it drops substantially at low drift angles. Also, the minimum inflow velocity appears at β_p values between $+5^\circ$ and $+10^\circ$. The inflow angles from the flag rudder data agree well with those from the averaged pitot tube data, including the marked deviation from linearity at positive β_p angles.

The Japanese MMG method, as described in [Lantos and Kendrick], uses an effective axial inflow velocity to the propeller to calculate the thrust from standard open water diagrams. This velocity is calculated from an effective axial wake fraction, w_p , which depends on the effective wake in the straight ahead condition, w_{po} , as

$$w_p = w_{po} e^{-4.0 \beta_p^2}$$

This equation is used to determine V_p/V , and plotted in Figure 61. It is clear that the minimum DTRC inflow velocities are substantially less than those given by the MMG equation, but this difference is expected. The DTRC data represents nominal velocities along the centerplane of the ship where the velocity defect due to boundary layer effects is greatest. Other areas of the propeller disk will experience somewhat higher velocities. The MMG curve shows the effective axial velocity as found from self-propulsion tests using the thrust identity method. Since effective wake fraction is generally less than nominal, (i.e. effective velocity greater than nominal) it is not surprising that the MMG curve lies above much of the DTRC data. Nonetheless, both sources show similar inflow velocities at larger absolute values of drift angle.

Although the MMG method does not take account of oblique flow when computing propeller forces, it does define a ship hull flow rectification coefficient, (equal to $.45 \times \beta_R$ when $\beta_R < 63^\circ$, and $.5 \times \beta_R$ when $\beta_R > 63^\circ$). Since the separation between propeller and rudder is small, differences between β_R and β_P may be neglected. Thus, the MMG propeller inflow angles after hull rectification can be compared to the rudder inflow angles (without propeller) from the DTRC data, as shown in Figure 62. While qualitatively similar, significant differences between the two curves are evident, particularly for positive values of β_P . (It should also be noted that the MMG's expression for $\beta_P = \beta - x_P r'$ is an approximation, rather than the exact expression given for β_x given on page 76. (The exact expression has been used to calculate the β_P for the x-axis of figures 61 and 62).

Thus, the MMG method does not account for the propeller side force developed in oblique flow. It predicts propeller inflow velocities and directions which are qualitatively similar, but quantitatively somewhat different from the DTRC results.

Rudder Inflow Velocity and Direction

The MMG method also determines an effective flow velocity and inflow angle at the rudder. The details of the model tests used to derive the MMG equations are not available in English, and are thus somewhat unclear. It is inferred that the rudder lift force was measured at various angles. The angle of zero lift can then be interpolated, and the effective inflow velocity determined by comparison to low aspect airfoil lift data taken at similar Reynolds numbers. The MMG regression equations for calculating inflow velocity and direction [see Lantos and Kendricks] are somewhat lengthy, and will not be repeated here. One of the input quantities for this calculation is the rudder wake fraction in straight ahead operation, w_{RO} , but no means is given for

estimating this quantity. [Kajima and Nakiri] do give a formula for calculating w_{RO} from w_{PO} , but it gives values of w_{RO} for the MARINER which are nearly twice w_{PO} . This does not make sense since the propeller race will increase the velocities downstream, (i.e. decrease the wake fraction). Therefore, a value of $w_{RO} = w_{PO} - .05$ was assumed. It should be noted that the MMG calculation also contains an anomaly in the calculation of the geometric inflow angle at the rudder, given as

$$\beta_R = \beta - 2 x_R r'$$

where the empirically determined factor of 2 yields incorrect geometric inflow angles. Nonetheless, the MMG method, using the formula above, was applied to the MARINER model tested by DTRC. The results are shown in figures 63 and 64, but are plotted against the correct values of β_R (as calculated from the formula for β_x given on page 76), so they can be compared to the DTRC data. The rudder inflow velocities, averaged from the DTRC pitot tube data (with propeller, $\delta=0$) are also shown in Figure 64. Agreement is only fair, but no systematic differences are apparent.

The mean axial velocity induced downstream by an actuator disk can be calculated from simple momentum theory, as shown in Figure 65. Using the MARINER test conditions, it is found that the velocity induced by the propeller during steady straight ahead motion equals 0.12 V, at the propeller, and 0.21 V at the rudder. Comparing Figures 61 and 64, it is seen that rudder inflow velocities from the DTRC data are correspondingly higher than those at the propeller, whereas the MMG velocities show little change.

Figure 63 compares three different sources of data for rudder inflow angles: the DTRC flag rudder data (with propeller), the averaged values of the DTRC pitot tube data (with

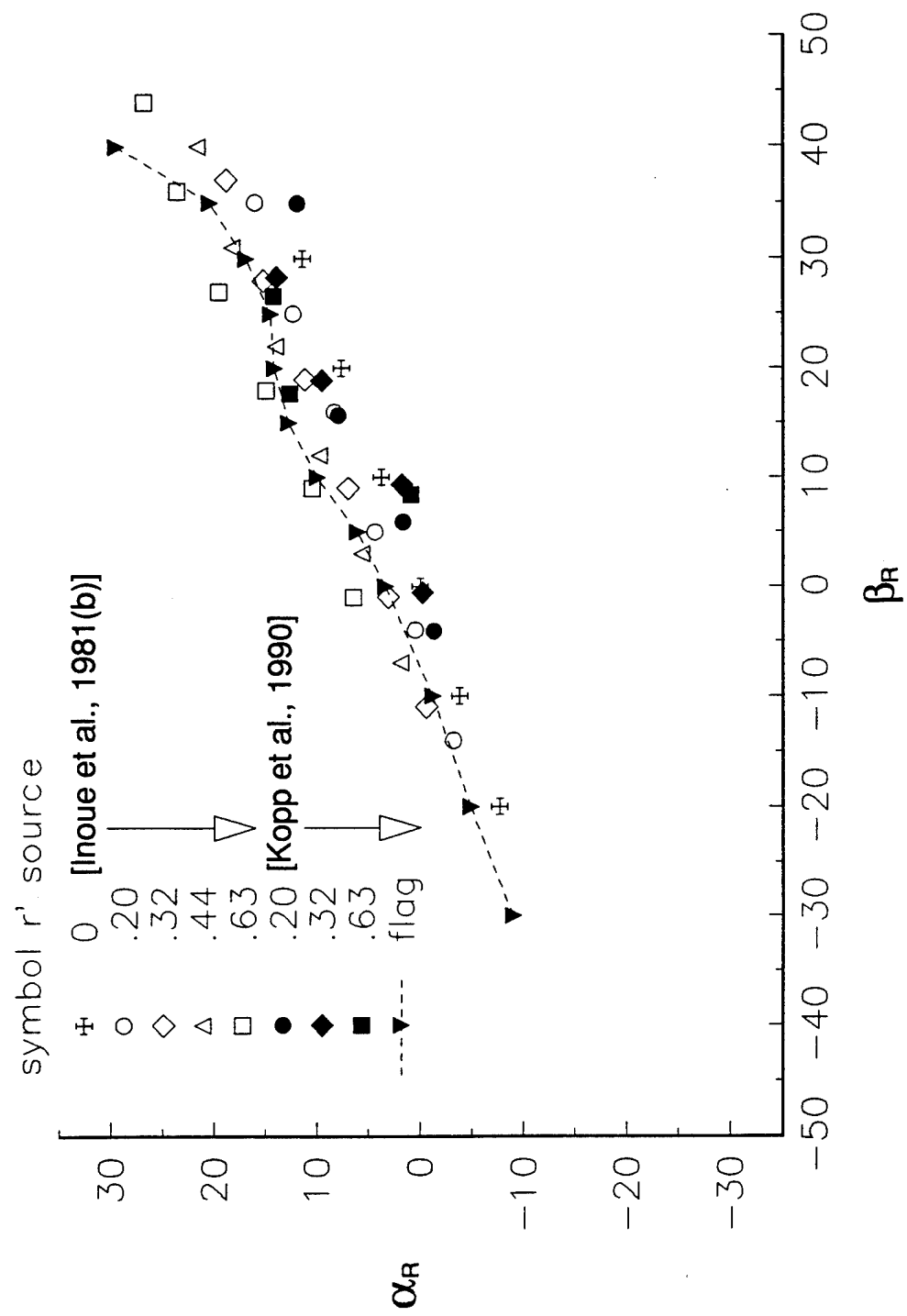


Figure 63. Rudder Inflow Angle versus Geometric Rudder Drift Angle

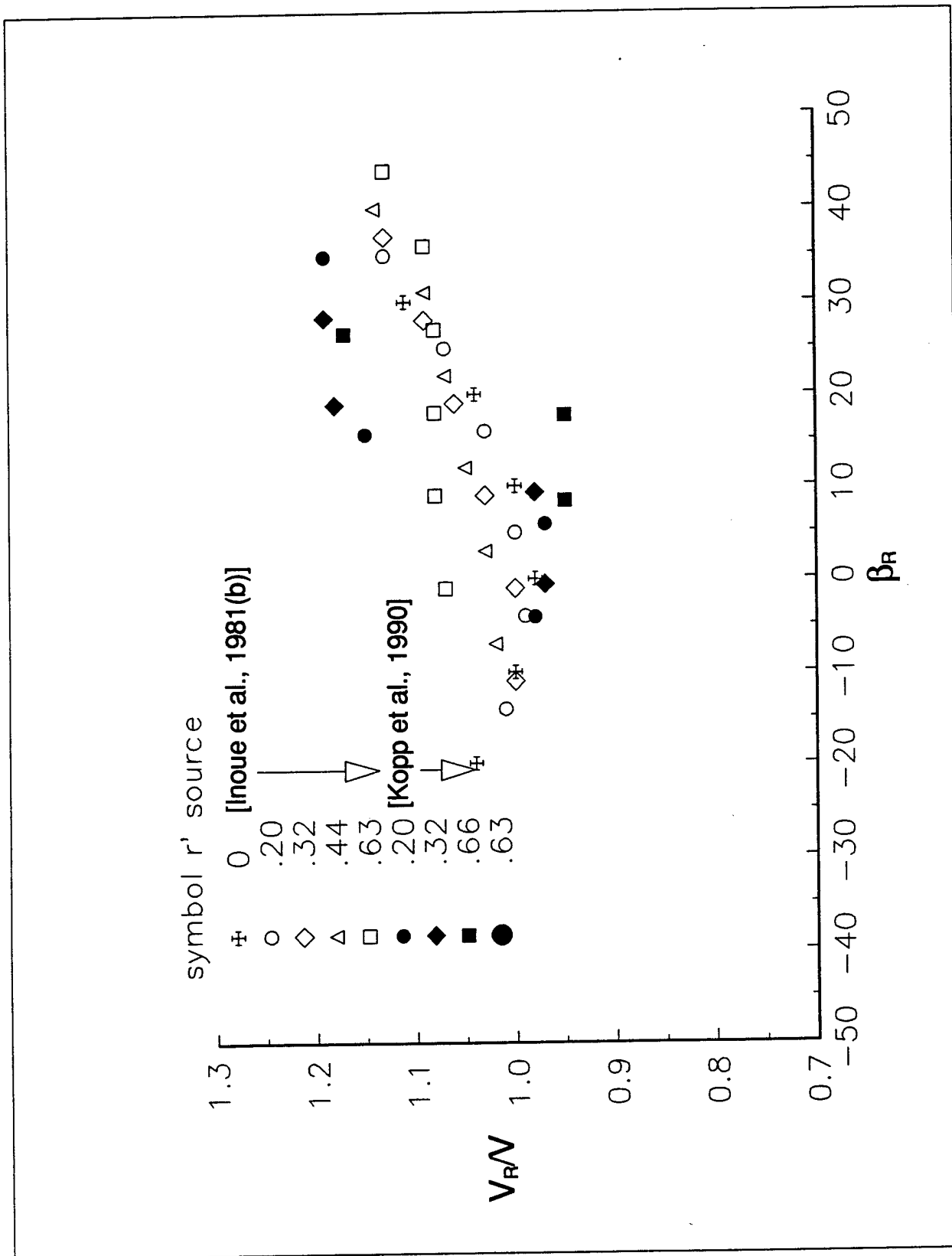
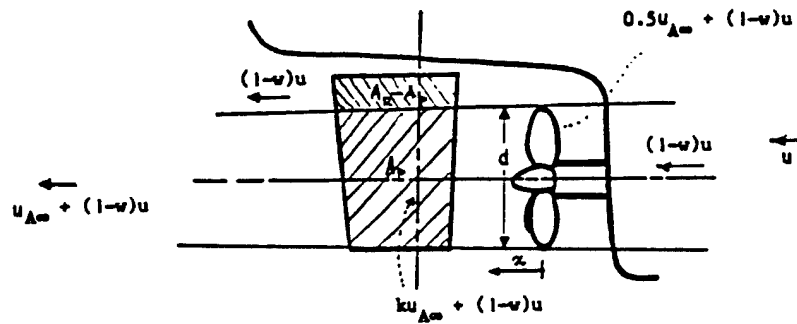
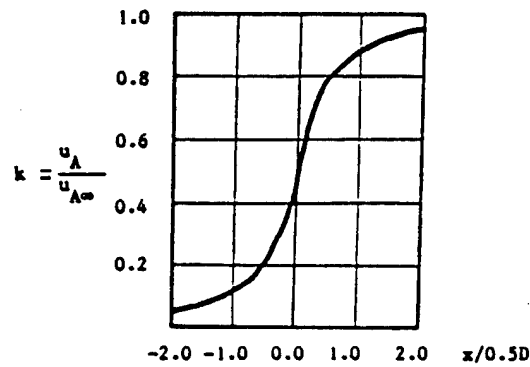


Figure 64. Rudder Inflow Velocity versus Geometric Rudder Drift Angle



Geometrical relationship between the propeller and the rudder.
Propeller race according to momentum theory



Mean axial velocity induced by a semi-infinite tube of ring vortices
determined by the law of Biot-Savart [Smitt and Chislett, 1974]

Far behind the propeller disk, the induced axial velocity $u_{A\infty}$ is:

$$u_{A\infty} = -(1-w)u + \sqrt{(1-w)^2u^2 + \frac{8}{\pi}K_T(nD)^2} \quad (1)$$

At a general position x , the induced mean axial velocity u_A is acquired by multiplying $u_{A\infty}$ (by) a factor k , which is a function of the axial distance x from the propeller disk to the point of interest. In this case x is the location of the quarter mean chord of the rudder. An infinite-blade propeller is used to find the functional relationship between k and x . See Fig. 21. The mean squared velocity c^2 over the rudder is now evaluated as a weighted sum of $(1-w)^2u^2$ and u_A^2 :

$$c^2 = \frac{A_P}{A_R} [(1-w)u = ku_{A\infty}]^2 + \frac{A_R - A_P}{A_R} (1-w)^2u^2 \quad (2)$$

Figure 65. Axial Velocity Induced by the Propeller on the Rudder, from [Abkowitz et al.]

propeller, $\delta=0$), and the rudder inflow angles from the MMG method. Agreement is generally good, but the DTRC inflow angles are slightly higher, and distinctly non-linear for positive values of β_r .

Despite the difficulties of comparing data from two different types of experiments, it can be concluded that the DTRC data and the MMG equations show qualitatively similar trends for inflow velocities and angles to the propeller and rudder. There are sufficient differences, however, to warrant additional experiments. Direct measurement of propeller thrust and RPM, and of rudder forces, during rotating arm experiments would yield additional data on effective inflow angles and velocities which could be compared directly to the MMG results.

Rudder Forces and Moment

Once an effective rudder inflow angle is known, the hydrodynamic angle of attack of the rudder, producing a lift force on the port side, is

$$\alpha = (\delta - \delta_o) - \alpha_R,$$

where the rudder angle, δ , is positive to starboard, and the neutral rudder angle, δ_o , is usually small and positive to starboard for a right-handed propeller. (See Figure 59).

Numerous data are then available for calculating the forces developed on a low aspect ratio foil with a known effective inflow velocity, e.g. [Jones], [Whicker and Fehlner], [Lewandowski], and [Fuji and Tsuda]. Due account of Reynolds number effects must, of course, be taken when predicting full scale forces. Thus, rudder forces can be calculated and trigonometrically resolved into their contributions to the surge, sway and yaw equations.

All significant terms on the right hand sides of the equations of motion can therefore be calculated for low drift angle maneuvers. (Some suggestions on how these terms can be extended to higher drift angles have also been given). Numerical integration of these equations can then be performed to predict a vessel's response to any arbitrary maneuver.

Simplified Steady State Turning Circle Predictions

The experimental data discussed above was originally intended to provide input for solving Dr. Asinovsky's equations for prediction of the "diagram of steering." This diagram provides information on steady turning performance, and on controls-fixed course stability. These quantities are obtained from an iterative solution of the full non-linearized equations of motion. Background, references, and worked examples of this application are provided in Appendix D.

A Desktop Ship Maneuvering Simulator (DSMS)

During the conduct of the experiments described above, the Coast Guard R&D Center identified a PC-based maneuvering simulator based on modular principles. This Desktop Ship Maneuvering Simulator (DSMS) was developed by Dr. Gregory Zilman, formerly of the Leningrad Shipbuilding Institute. It was considered cost-effective to license this software for evaluation, rather than to develop new software using the approaches described above.

This software has degrees of freedom in surge, sway, yaw, roll and machinery RPM. It can simulate arbitrary maneuvers over the entire range of drift angles. Because of its modular nature, numerous combinations of hull forms, engine types, propeller types, and rudder geometries can be examined during preliminary

design. Different map files can be developed so that maneuvers can be simulated in a particular harbor or channel. Wind, wave, current and shallow water effects can be included, (but cannot presently be varied from one part of the course to the next). Two versions of the program exist, one for simulating high-speed low block coefficient forms such as break bulk or container ships, and another for simulating low-speed high block coefficient forms such as tankers. Minimum hardware is a 386 IBM compatible PC with a Video Graphics Adaptor (VGA). The program can be operated in real time from the keyboard, or programmed to perform standard maneuvers automatically. It does not currently have the capability to include bank effects, ship/ship interactions or multiple ships. An Operator's Manual, and Technical Documentation of the program's algorithms, are available in [Zilman].

Full-Scale Trials

Previous ship trials data for the MARINER class "Compass Island" were available [Morse and Price], but included a bow sonar dome, and were performed at a different draft than the experiments described above. Therefore, personnel at DTRC were tasked by the USCG to perform full-scale maneuvering trials on a MARINER type hull form, the USNS "Observation Island" (T-AGM 23). Tests included acceleration/deceleration straight line tests, turning circles with pullouts, and zig-zag tests. A summary of test conditions, methods and results is given by [Kopp and Rossignol].

Comparison of Simulation to Full-Scale Trials

The DSMS program was used to configure a vessel to match the trial conditions of the Navy's MARINER hull form. Selected maneuvers were then simulated and compared to DTRC's trial

results. Initial comparisons showed that the turning circle diameter was substantially under-predicted. The rudder force model was then modified to account for the ratio of fixed to moveable areas on the actual MARINER rudder. Figure 66 compares turning circles from both sets of full-scale trials, and from the revised DSMS simulations. Agreement between prediction and trials is much improved, but the predicted turning circle diameter is still about 8% less than the DTRC trials data. Figures 67 and 68 compare zig-zag maneuver results from the DTRC trials to the revised DSMS simulation. Agreement is fair, but the predicted first overshoot angle and time to first overshoot are somewhat less than the trial values. This may be because the predicted rudder efficiency was still somewhat greater than the actual, as evidenced by the turning circle results. It may also be due to small errors in time of execution and differences between ordered and achieved rudder angles during the actual trials. Finally, when a simulation model is adjusted to match a particular trial, it is difficult to be sure that the adjustment is physically correct. For example, a larger turning circle will be predicted if either the rudder's effectiveness is decreased, or if the hull's resistance to turning is increased. Only extensive model and full scale measurements of component forces can determine which part of the simulation model needs to be revised.

Thus, it can be concluded that the final simulation results for this particular ship form are in reasonable agreement with the trials, and could probably be further improved by additional modification of the mathematical model. This type of verification should also be carried out for a variety of different ship forms to assess the robustness of the model's predictive capability. Even then, predictions for ship designs outside the range of test parameters should be treated cautiously.

Rudder Angle 12 Degrees
Approach Speed = 20 Knots

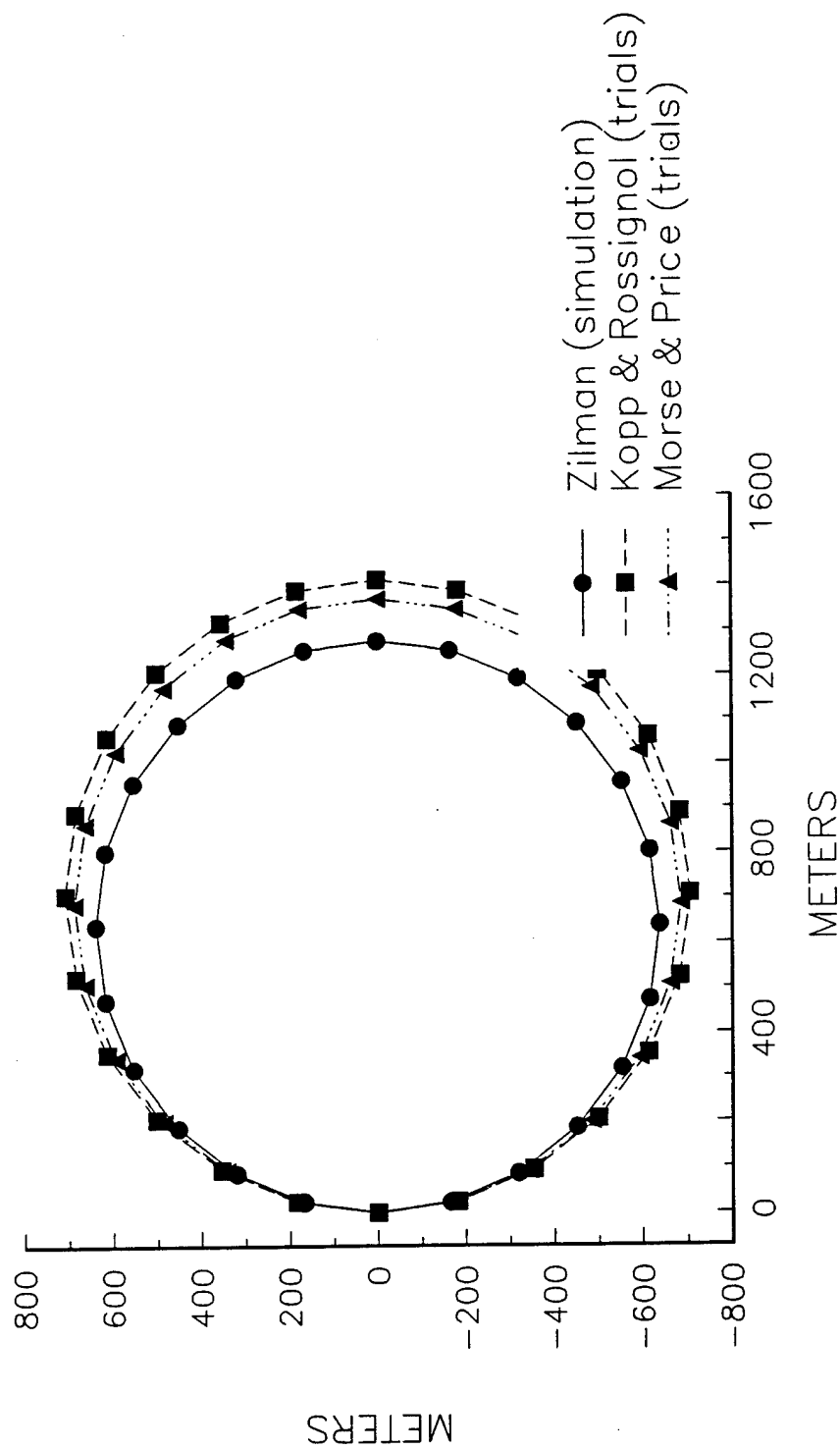


Figure 66. Comparison of Predicted and Measured Turning Circles

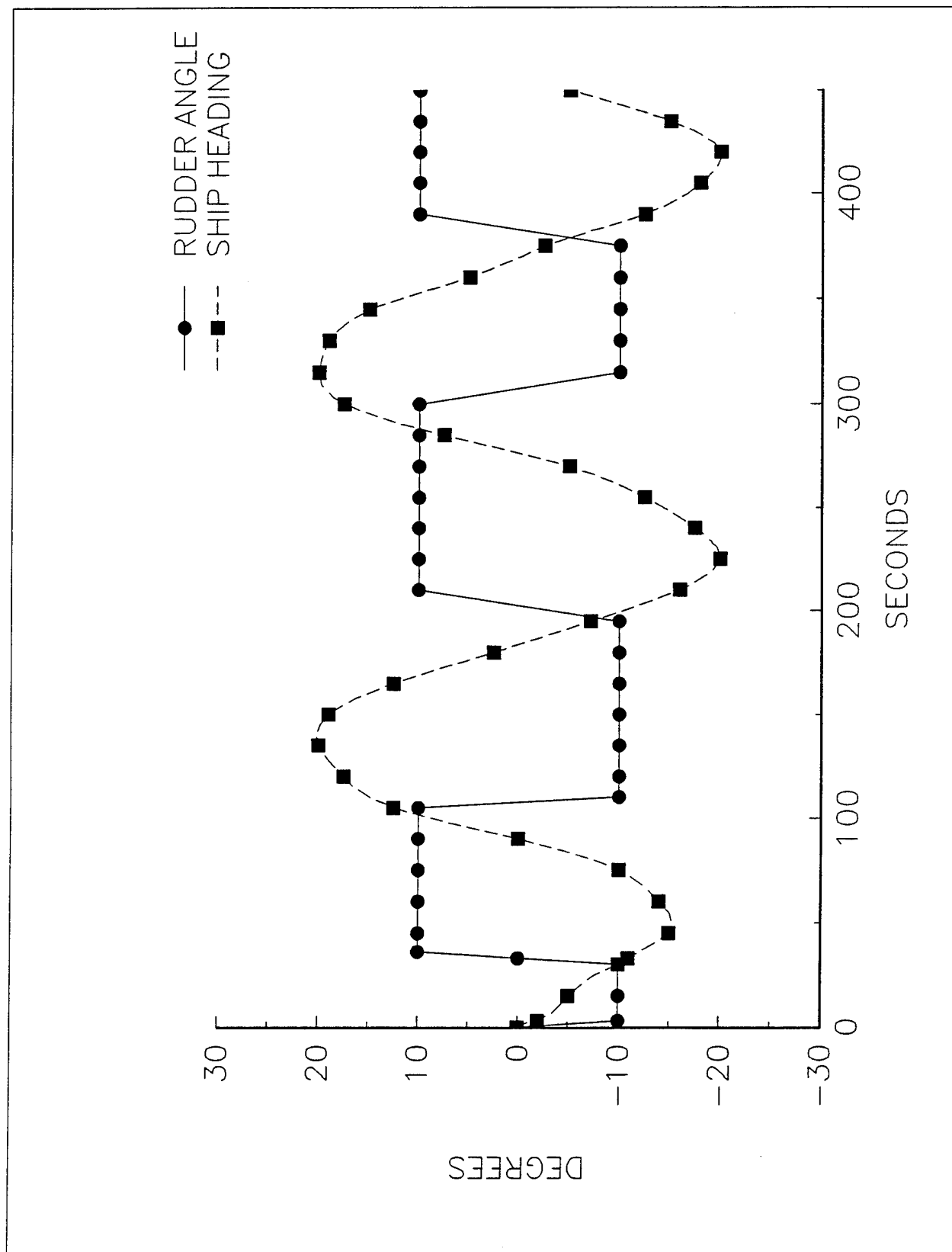


Figure 67. Predicted 10-10 Zig-Zag (20 Knot Approach Speed), by [Zilman]

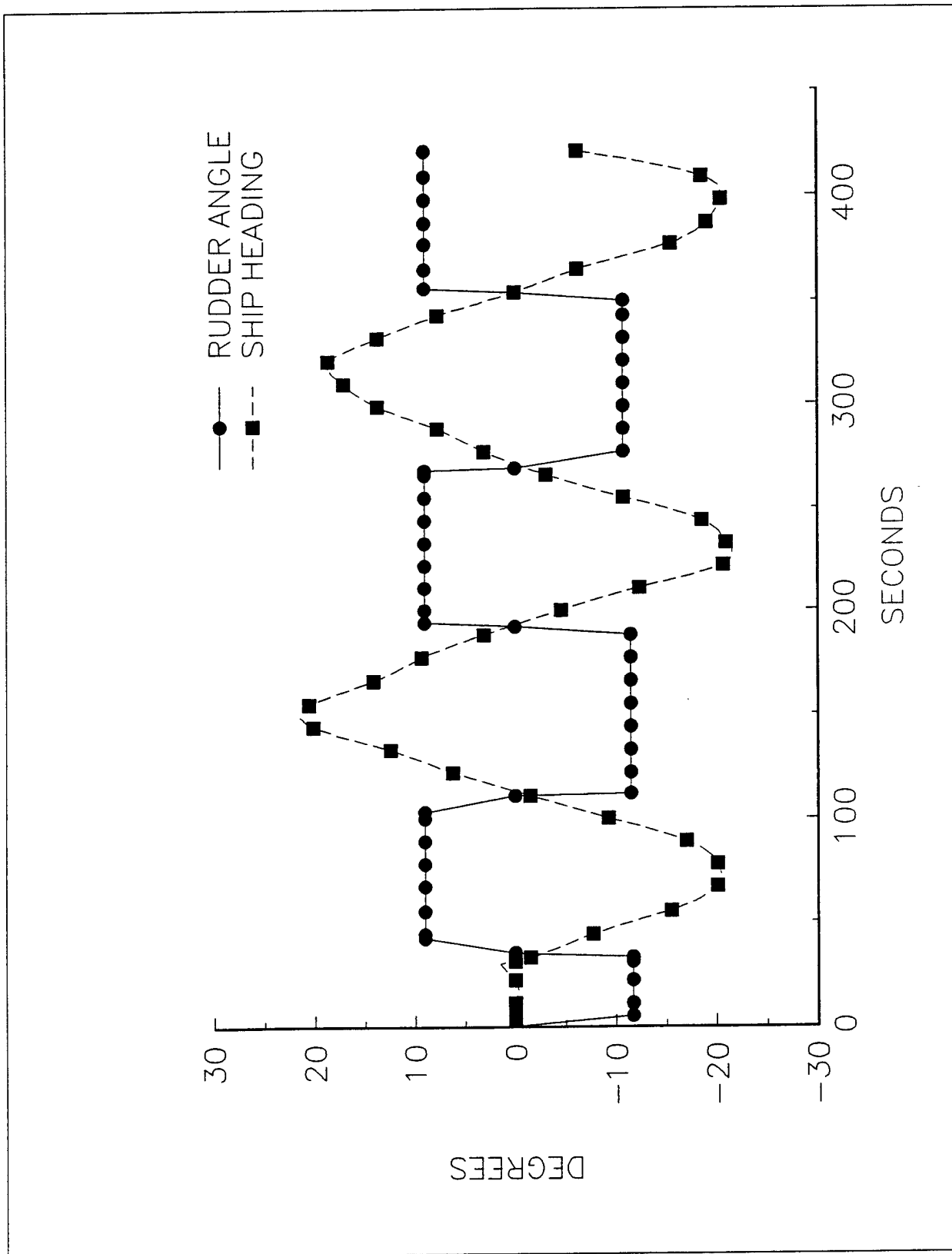


Figure 68. Measured 10-10-10 Zig-Zag (20 Knot Approach Speed), from [Kopp & Rossignol]

Conclusions

"Modular" maneuvering models can simulate a wide range of ship configurations and operating conditions. This makes them ideal for assessing and improving maneuverability during preliminary design, and for pilot training. It also offers greater flexibility in designing waterways which to be used by many different vessel types.

The Japanese MMG model is widely and successfully used to predict "standard" maneuvers (low forward speed and low drift angles). Data from the present study shows good qualitative agreement with the MMG model, but there are some quantitative differences, particularly in the prediction of bare hull forces and moment. There are also differences in the inflow velocities and angles to the propeller, but these may be due to the different methods used to determine these quantities.

The DSMS program uses some of the MMG algorithms, but is able to simulate maneuvers over a much wider range of drift angles and yaw rates, including astern operations. The Hovgaard effect is well modeled, both ahead and astern. The model is based on sound physical principles, and shows reasonable agreement with the full-scale trials data from the present study.

"Modular" techniques are superior other simulation models in that they allow a greater variability in hull and appendage configuration, and thus can be used to predict maneuvering performance during preliminary design. Nonetheless, further development and verification of modular models is needed to fully realize this potential.

Recommendations

Additional studies of possible scale effects, and systematic measurements of bare hull forces at large drift angles and low speeds are clearly indicated.

Also, instrumentation should be developed to directly measure axial and side forces transmitted by the propeller and rudder to the hull during rotating arm tests. Presently, a modular model may be tuned to match full-scale trials by adjusting any of several terms. Only with such instrumentation can one rationally determine which terms need adjustment.

Maneuvering models for twin screw ships, and other types of vessels, such as tankers, multihulls and planing craft should be developed.

Maneuvering models which account for shallow water, bank effects and ship/ship interactions should be identified and verified.

The Coast Guard should continue to monitor development of maneuvering simulators and validate them using full-scale data. This will enhance Coast Guard capabilities for contributing to the development of effective maneuvering criteria, performing plan reviews which include maneuvering predictions of new ship designs, and designing safer ships and waterways.

REFERENCES

Abkowitz, M., Stability and Motion Control of Ocean Vehicles, The MIT Press, Cambridge, 1969

Abkowitz, M., Measurement of Hydrodynamic Characteristics from Ship Maneuvering Trials, SNAME Transactions, 1980

Asinovsky, V., On Maneuverability Criterion for Determining Ship Response to Rudder Angle Change, SNAME Chesapeake Section Meeting, May 17, 1983

Asinovsky, V., Statistical Analysis of Yaw and Yaw Caused Speed Drop in Calm Water Conditions, Transactions of SNAME Spring Meeting/STAR Symposium, May 27-30, 1987

Chislett, M. (editor), Prediction of Maneuverability of A Ship, SNAJ Bulletin No. 668, Feb. 1985. Translated by T. Bundgaard for Danish Maritime Institute, 1986

Dand, I. W., On Modular Maneuvering Models, RINA International Conference on Ship Maneuverability, London, 1987

Davidson, K., On the Turning and Steering of Ships, SNAME Transactions, Vol. 52, 1944

Davidson, K and Schiff, L., Turning and Course-Keeping Qualities of Ships, SNAME Transactions, Vol. 54, 1946

Fedyayevskiy, K. K. and Sobolev, G. V., Control and Stability in Ship Design, State Union Shipbuilding Industry Publishing House, Leningrad, 1963

Flax and Lawrence, The Aerodynamics of Low-Aspect Ratio Wings and Wing-Body Combinations, Cornell Aerodynamics Laboratory Report, Buffalo, N.Y., September, 1951

Fuji, H., and Tsuda, T., Experimental Researches on Rudder Performance (2nd Report), JSNAJ Vol. 110, December, 1961

Gutsche, F., Untersuchung von Schiffsschrauben Anstromung, Schiffbauforschung, March, 1964, (DTMB Translations)

Goodwin, A., Irvine, J., and Forrest, J., The Practical Application of Computers in Marine Engineering, Transactions of the Institute of Marine Engineers, 1968

Harvaldt, S., Wake and Thrust Deduction at Extreme Propeller Loadings for a Ship Running in Shallow Water, RINA Transactions, 1977

Hearn, G., Clarke, D., Chan, H., Incecik, A., and Varyani, K., The Influence of Vorticity upon Estimation of Maneuvering Derivatives, 20th Naval Hydrodynamics Symposium, Santa Barbara, California, 1994

Hirano, M., Takashina, J., and Moriya, S., A Practical Method of Ship Maneuvering Motion and its Application, RINA International Conference on Ship Maneuverability, London, 1987

Inoue, S., Hirano, M., Kijima, K., Hydrodynamic Derivatives on Ship Maneuvering, International Shipbuilding, Vol. 28, No. 321, 1981 (a)

Inoue, S., Hirano, M., Kijima, K., and Takashina, A., A Practical Calculation Method of Ship Maneuvering, International Shipbuilding Progress, Vol. 28, No. 325, 1981 (b)

Kijima, K., Katsuno, T., Nakiri Y., and Furakawa, Y., On The Maneuvering Performance of a Ship with the Parameter of Loading Condition, Journal of the SNAJ, Vol. 168, Novemeber, 1990

Klosinski, W. and Lewandowski, E., Systematic Series Model Tests, Davidson Laboratory, Technical Report SIT-DL-93-9-2689, October, 1993

Kopp, P., Bishop, R., and Motter, L., Experimental Study of the Rudder Flow Field and its Effect on Hull Forces, DTRC/SHD 1341-01, August 1990

Kopp, P., Captive Model Rotating Arm Test on the Bare Hull T-AG(S) 38 Represented by Model 4414, DTRC/SHD-1341-02, February, 1991

Kopp, P. and Rossignol, G., Summary of a Full-Scale Maneuvering Trial on the USNS Observation Island (T-AGM-23), Carderock Division, Naval Surface Warfare Center, CRDKNSWC-HD-1432-01, October, 1993

Lantos, S. and Kendrick, A., Development of Canadian and International Maneuvering Standards, German and Milne, Prepared for Transportation Development Center Policy and Coordination Group, Transport Canada, TP9551E, January, 1989

Lewandowski, E., The Effects of Reynolds Number, Section Shape, and Turbulence Stimulation on the Lift of a Series of Model Control Surfaces, 22nd ATTC Conference Proceedings, August, 1989

Martinussen, K. and Linnerud, I., Techniques for Predicting Maneuvering Characteristics of Ships at the Design Stage, RINA International Conference on Ship Maneuverability, London, 1987

Molland, A., A Method for Determining the Free-Stream Characteristics of Ship Skeg-Rudders, ISP Vol. 32, No. 370, June, 1985

Moor, D., An Investigation of Tug Propulsion, RINA Transactions, 1963

Morse, R. and Price, D., Maneuvering Characteristics of the Mariner Type Ship (USS COMPASS ISLAND) in Calm Seas, Sperry Gyroscope Company, Syosset N.Y., 1961

Motora, M., On the Measurement of Added Mass and Moment of Inertia of Ships in Steering Motion, First Symposium on Ship Maneuverability, David Taylor Model Basin Report 1461, May, 1960

Newman, J. N., Marine Hydrodynamics, The MIT Press, Cambridge, 1977

Norrie, D. H., The Virtual Inertia of Propellers Under Load, Journal of Ship Research, 1965

Oltmann, P. and Sharma, S., Simulation of Combined Engine and Rudder Maneuvers Using an Improved Model of Hull-Propeller-Rudder Interactions, Fifteenth Symposium on Naval Hydrodynamics, National Academy Press, Washington, D.C., 1985

Oosterveld, M., and van Oossanen, P., Further Computer Analysed Data of the Wageningen B-Screw Series, International Shipbuilding Progress, July, 1975

Parker, M. and Dawson, J., Tug Propulsion Investigation, RINA Transactions, 1962

Peck J., and Moore, D., Inclined-Shaft Propeller Performance Characteristics, SNAME Spring Meeting, Buena Vista, Fla., April 1973

Ribner, H., Proposal for a Propeller Side Force Factor, NACA Restricted Bulletin 3L02, 1943

Saunders, H., Hydrodynamics in Ship Design, , Volumes I-III, SNAME, 1965

Soding, H., Forces on Rudder behind a Maneuvering Ship, Proceedings of the 3rd International Conference on Numerical Ship Hydrodynamics, Paris, France, June, 1981

Strumpf, A., Analysis and Correlation of Captive Model Rotating Arm Test Results of a Destroyer, Davidson Lab Report SIT-DL-82-9-2264, February, 1982

Strumpf, A., Calculation of Hydrodynamic Side Forces and Yaw Moments of Merchant Ships, MarAd Report MA-RD-940-83065, July, 1983

van Lammerman, W., van Manen, J., and Oosterveld, M., The Wageningen B-Screw Series, Sname Transactions, 1969

Whicker, L., and Fehlner, L., Free Stream Characteristics of a Family of Low Aspect Ratio, All Movable Control Surfaces for Application to Ship Design, DTMB Report 933, December, 1958

Zilman, G., Desktop Maneuvering Simulator (DSMS), Users Guide and Technical Documentation, October, 1992, (to be published as Coast Guard report)

APPENDIX A

ASSEMBLY - 18th session
Agenda item 11

IMO RESOLUTION A.751(18)
adopted on 4 November 1993

INTERIM STANDARDS FOR SHIP MANEUVERABILITY

THE ASSEMBLY,

RECALLING Article 15(j) of the Convention on the International Maritime Organization concerning the functions of the Assembly in relation to regulations and guidelines concerning maritime safety and the prevention and control of marine pollution from ships,

RECALLING FURTHER that by MSC/Circ. 389 the Maritime Safety Committee approved interim guidelines for estimating manoeuvring performance in ship design, whereby Member Governments were invited to apply the guidelines on a trial basis so that they may be assessed in the light of practical experience gained with a view to their possible further development,

RECALLING ALSO resolutions A.160(ES.IV), A.209(VII) and A.501(15) concerning information on ship manoeuvring,

RECOGNIZING the manoeuvring capability of ships to be an important contribution to the safety of navigation,

BELIEVING that the development and implementation of standards for ship manoeuvrability, particularly to large ships and ships carrying dangerous goods in bulk, will improve maritime safety and enhance marine environment protection,

HAVING CONSIDERED the recommendations made by the Maritime Safety Committee at its sixty-second session,

1. ADOPTS the Interim Standards for Ship Manoeuvrability, set out in the Annex to the present resolution;
2. RECOMMENDS Governments to encourage those responsible for the design, construction, repair and operation of ships to apply the Standards;
3. INVITES Governments to collect data obtained by the application of the Standards and report them to the Organization;
4. REQUESTS the Maritime Safety Committee to keep the Standards under review on the basis of the information and data collected;
5. AUTHORIZES the Maritime Safety Committee to amend the Standards as necessary.

ANNEX

INTERIM STANDARDS FOR SHIP MANOEUVRABILITY

1. Principles

1.1 The standards should be used with the aim of improving ship manoeuvring performance and with the objective of avoiding building ships that do not comply with the criteria.

1.2 The standards contained in this document are based on the understanding that the manoeuvrability of ships can be evaluated from the characteristics of conventional trial manoeuvres. The following two methods can be used to demonstrate compliance with these standards:

- .1 Scale model tests and/or computer predictions using mathematical models can be performed to predict compliance at the design stage. In this case full-scale trials should be conducted to validate these results. The ship should then be considered to meet these standards regardless of full-scale trial results, except where the Administration determines that the prediction efforts were substandard and/or the ship performance is in substantial disagreement with these standards;
- .2 The compliance with the standards can be demonstrated based on the results of the full-scale trials conducted in accordance with the standards. If a ship is found in substantial disagreement with the interim standards, then the Administration may require remedial action.

1.3 The standards presented herein are considered interim for a period of 5 years from the date of their adoption by the Assembly. The standards and method of establishing compliance should be reviewed in the light of new information and the results of experience with the present standards and ongoing research and developments.

2 Application

2.1 The standards should be applied to ships of all rudder and propulsion types, of 100 m in length and over, and chemical tankers and gas carriers regardless of the length, which are constructed on or after 1 July 1994.

2.2 In case ships referred to in paragraph 2.1 undergo repairs, alterations and modifications which in the opinion of the Administration may influence their manoeuvrability characteristics the continued compliance with the standards should be verified.

2.3 Whenever other ships, originally not subject to the standards, undergo repairs, alterations and modifications, which in the opinion of the Administration are of such an extent that the ship may be considered to be a new ship, then that ship should comply with these standards. Otherwise, if the repairs, alterations and modifications in the opinion of the Administration may influence the manoeuvrability characteristics, it should be demonstrated that these characteristics do not lead to any deterioration of the manoeuvrability of the ship.

2.4 The standards should not be applied to the high speed craft as defined in the relevant Code.

3 Definitions

3.1 Geometry of the ship

- .1 Length (L) is the length measured between the aft and forward perpendiculars;
- .2 Midship point is the point on the centerline of a ship midway between the aft and forward perpendiculars;
- .3 Draught (T_a) is the draught at the aft perpendicular;
- .4 Draught (T_f) is the draught at the forward perpendicular;
- .5 Mean draught (T_m) is defined as $T_m = (T_a + T_f)/2$.

3.2 Standard manoeuvres and associated terminology

Standard manoeuvres and associated terminology are as defined below:

- .1 The test speed (V) used in the standards is a speed of at least 90% of the ship's speed corresponding to 85% of the maximum engine output.
- .2 Turning circle manoeuvre is the manoeuvre to be performed to both starboard and port with 35° rudder angle or the maximum rudder angle permissible at the test speed, following a steady approach with zero yaw rate.
- .3 Advance is the distance travelled in the direction of the original course by the midship point of a ship from the position at which the rudder order is given to the position at which the heading has changed 90° from the original course.

- 4 Tactical diameter is the distance travelled by the midship point of a ship from the position at which the rudder order is given to the position at which the heading has changed 180° from the original course. It is measured in a direction perpendicular to the original heading of the ship.
- .5 Zig-zag test is the manoeuvre where a known amount of helm is applied alternately to either side when a known heading deviation from the original heading is reached.
- .6 $10^\circ/10^\circ$ zig-zag test is performed by turning the rudder alternately by 10° to either side following a heading deviation of 10° from the original heading in accordance with the following procedure:
 - .1 after a steady approach with zero yaw rate, the rudder is put over to 10° to starboard/port (first execute);
 - .2 when the heading has changed to 10° off the original heading, the rudder is reversed to 10° to port/starboard (second execute);
 - .3 after the rudder has been turned to port/starboard, the ship will continue turning in the original direction with decreasing turning rate. In response to the rudder, the ship should then turn to port/starboard. When the ship has reached a heading of 10° to port/starboard of the original course the rudder is again reversed to 10° to starboard/port (third execute).
- .7 The first overshoot angle is the additional heading deviation experienced in the zig-zag test following the second execute.
- .8 The second overshoot angle is the additional heading deviation experienced in the zig-zag test following the third execute.
- .9 $20^\circ/20^\circ$ zig-zag test is performed using the procedure given in .6 above using 20° rudder angles and 20° change of heading, instead of 10° rudder angles and 10° change of heading, respectively.
- .10 Full astern stopping test determines the track reach of a ship from the time an order for full astern is given until the ship stops in the water.
- .11 Track reach is the distance along the path described by the midship point of a ship measured from the position at which an order for full astern is given to the position at which the ship stops in the water.

4 Standards

4.1 The standard manoeuvres should be performed without the use of any manoeuvring aids, which are not continuously and readily available in normal operation.

4.2 Conditions at which the standards apply

In order to evaluate the performance of a ship, manoeuvring trials should be conducted to both port and starboard and at conditions specified below:

- .1 deep, unrestricted water;
- .2 calm environment;
- .3 full load, even keel condition;
- .4 steady approach at the test speed.

4.3 Criteria

The manoeuvrability of the ship is considered satisfactory, if the following criteria are complied with:

.1 Turning ability

The advance should not exceed 4.5 ship lengths (L) and the tactical diameter should not exceed 5 ship lengths in the turning circle manoeuvre;

.2 Initial turning ability

With the application of 10° rudder angle to port/starboard, the ship should not have travelled more than 2.5 ship lengths by the time the heading has changed by 10° from the original heading;

.3 Yaw checking and course keeping abilities

- .1 The value of the first overshoot angle in the 10°/10° zig-zag test should not exceed:

- 10°, if L/V is less than 10 seconds;
- 20°, if L/V is 30 seconds or more; and
- $(5 + \frac{1}{2} (L/V))$ degrees, if L/V is 10 seconds or more but less than 30 seconds

where L and V are expressed in m and m/s, respectively;

2 The value of the second overshoot angle in the 10°/10° zig-zag test should not exceed the above criterion values for the first overshoot by more than 15°;

.3 The value of the first overshoot angle in the 20°/20° zig-zag test should not exceed 25°;

.4 Stopping ability

The track reach in the full astern stopping test should not exceed 15 ship lengths. However, this value may be modified by the Administration where ships or large displacement make this criterion impracticable.

5 Additional considerations

5.1 In case the standard trials are conducted at a condition different from those specified in 4.2.3 necessary corrections should be made in accordance with the guidelines contained in the explanatory notes on the standards for ship manoeuvrability developed by the Organization.

5.2 Where standard manoeuvres indicate dynamic instability, alternative test may be conducted to define the degree of instability. Guidelines for alternative tests such as a spiral test or pull-out manoeuvre are included in the explanatory notes on the standards for ship manoeuvrability developed by the Organization.

Appendix B

Added Mass Values:

It is known that hydrodynamic added mass is generally frequency dependent. However, numerous researchers have shown that reasonable maneuvering simulations can be achieved by using the asymptotic zero-frequency values of added mass. Several alternative sources have been used to estimate added mass values for a Mariner type hull form. These values are shown in Table 2 below.

Added Mass Values

	[Fedyayevskiy and Sobolev] (ellipsoid)	[Newman] (prolate spheroid)	[Matora] (ship models)	[SMP]* (180' WLB)
m_{11}/m	0.053	0.033	0.031	0.24
m_{22}/m	1.18	0.95	0.99	1.14
m_{66}/I_{xx}	1.80	0.83	1.50	1.44

* SMP is the U.S. Navy "Ship Motion Program"

Exact agreement of values is not expected, since each reference is for a different shape with approximately the same principal dimension ratios as the Mariner. It is noted that SMP's value of m_{11}/m is unrealistically high, probably due the application of strip theory in a direction where the body is anything but long and slender. Otherwise, the figures above are sufficiently close that an average value can be used for

practical calculations. With fore and aft symmetry, m_{26} is zero, (and is often considered negligible, even in the absence of such symmetry).

Appendix C

Partial List of Commercially-Available PC-Based Ship Maneuvering Simulators

<u>Program Name</u>	<u>Source</u>	<u>Location</u>
Officer of the Watch	PC Maritime	U.K.
Portsim	SSPA	Sweden
Rembrandt	BMT CORTEC	U.K.
Mathman	Burness, Corlett and Partners	U.K.
DSMS	Dr. Gregory Zilman	U.S.
Shipboard Maneuvering Assistance & Training Program	Advanced Marine Enterprises	U.S.
DynaSim	Dynaflow, Inc.	U.S.

Appendix D

Steady-State Diagram of Steering

The "diagram of steering" shows calculated yaw rates (and various other steady-state turning performance parameters) as a function of rudder angle. Thus, the results of a Dieudonne' spiral maneuver can be calculated, where the absence or presence of a hysteresis loop indicates whether the vessel possesses controls-fixed course stability or not. Methods for solving the equations for steady turning were suggested by [Davidson], and further developed by [Fedyayevskiy and Sobolev] and [Asinovsky, 1983 and 1987], among others. The diagram of steering shows steady state values of drift angle, ship angular velocity, speed loss, and steady turning diameter as a function of rudder angle. In order to obtain the turning performance of any particular vessel, either a model must be built and tested, or the equations of motion must be solved for each rudder angle. One objective of the model/full-scale testing program described herein was to develop a data base from which design tools could be developed to predict the diagram of steering. In solving the equations of steady turning motion, it has been common practice to linearize the equations, estimate or calculate the various coefficients, and solve the system analytically. This procedure is incorrect since it yields a yaw rate of zero for a rudder angle of zero when the ship is non-asymptotically stable against a change of angular velocity (i.e. dynamically unstable). [Asinovsky, 1987] describes an iterative solution of the complete non-linear equations using a modular approach. The modular approach calculates the various forces and moments on the hull and appendages separately [Fedyayevskiy and Sobolev]. These equations were coded into a computer program which iteratively solves them, using the hull force and moment data from the present MARINER model tests, and modular estimates for rudder and propeller forces and moments.

The horn rudder configuration on the MARINER presents certain difficulties in the analysis. Data in [Whicker and Fehlner] can be used to determine the lift gradient, $dC_L/d\alpha$, for an all moveable rudder of a particular aspect ratio against a groundboard. This lift gradient for a rudder of the MARINER's aspect ratio is 2.6 rad^{-1} . Data in [Whicker and Fehlner] further suggest that this is degraded by 10% for a typical skeg-rudder combination for a skeg at zero angle of attack, giving a lift gradient of 2.2 rad^{-1} . [Molland] presents similar data for skeg angles of attack of +5, 0 and -5 degrees. These can be used to interpolate/extrapolate a reduction factor (relative to zero degrees) for a particular skeg angle of attack. Note that the skeg in a steady turn may develop a negative angle of attack, i.e. the skeg actually opposes the turn. By iteratively determining the geometric drift angle at the rudder associated with a particular rudder angle, and estimating the actual skeg angle of attack as a fraction of this drift angle, a reduction factor can be obtained. For example, with a geometric drift angle at the rudder of 13° , taking the actual skeg angle of attack as $.44 \times \beta_R$, we get a skeg angle of attack of -5.7° . The associated reduction factor from [Molland] is .84, so the lift gradient is $2.2 \times .84 = 1.84 \text{ rad}^{-1}$. This accounts for the effect of the horn.

As the moveable part of the rudder is turned, a gap is opened between the rudder and the stool above it, effectively decreasing the aspect ratio of the rudder and further reducing its lift gradient. This gap effect is shown in Figure 153, page 315, Vol. III of Principles of Naval Architecture. For a rudder angle of 15° or greater, the presence of the gap reduces the lift gradient by 37%. (While Figure 153 is strictly for a skeg angle of attack of $-.25^\circ$, it is assumed that this gap effect applies to other skeg angles of attack). Thus, with 15 degrees rudder, at the assumed steady turning rate of the MARINER, the lift gradient

of the horn rudder is estimated as $1.84 \times .63 = 1.17 \text{ rad}^{-1}$. This is used as input to the diagram of steering calculations shown in Table D-1, with the understanding that results will be increasingly inaccurate at lower rudder angles.

The calculated turning diameter/ ship length ratio, at an approach speed of 20 knots and a rudder angle of 12° , can be compared to the trials values shown on Figure 66 of the main report. The interpolated value from Table D-1 is 8.4, which compares well to the trials values of 8.6 - 8.9. Plotting yaw rate vs. rudder angle, as in the Dieudonne' spiral test diagram, shows no hysteresis loop, so the vessel is predicted to possess controls-fixed course stability.

A similar set of calculations is shown in Table D-2, except that the rudder area and aspect ratio have been reduced by removing 100 square feet from the bottom of the rudder. Plotting yaw rate vs. rudder angle now reveals a hysteresis loop with a width of almost 2° , and a height of .08 degrees/second.

Thus, this program can be used to predict turning circle characteristics, and to determine which rudder sizes and shapes will produce controls-fixed stability on a particular hull. Object code for the present version of this program has been posted on the SNAME electronic bulletin board. It is intended to modify the program to include the present regression equations for the Asinovsky systematic series. Object code for the modified version will also be posted upon its completion.

Table D-1

Diagram of Steering Program (STRDGM06) - Input Echo

```

TITLE - MARINER
SHIP DRAFT IN FEET ----- 27.0000
SHIP LOAD WATERLINE IN FEET ----- 520.0000
SHIP BEAM IN FEET ----- 76.0000
SHIP TRIM BY THE STERN ----- 0.0000
SHIP DISPLACEMENT IN LONG TONS ----- 18674.0000
MIDSHIP SECTION COEFFICIENT ----- 0.9807
DISTANCE BETWEEN LCG AND RUDDER STOCK IN FEET ----- 260.4000
CENTERPLANE AREA FWD OF MIDSHIPS (sq.ft.) ----- 7020.0000
CENTERPLANE AREA AFT OF MIDSHIPS (sq.ft.) ----- 6669.0000
INITIAL SPEED IN KNOTS ----- 20.0000
RESISTANCE IN POUNDS AT INITIAL SPEED ----- 159571.0000
THRUST DEDUCTION FACTOR AT INITIAL SPEED ----- 0.1600
PROPELLER WAKE FRACTION AT INITIAL SPEED ----- 0.2300
NUMBER OF PROPELLERS ----- 1.0000
PROPELLER DIAMETER IN FEET ----- 22.0000
RUDDER AREA FOR ONE RUDDER (sq.ft.) ----- 325.0000
AREA OF RUDDER IN PROPELLER RACE (sq.ft.) ----- 250.0000
ASPECT RATIO OF RUDDER (span^2/area) ----- 2.0000
NUMBER OF RUDDERS ----- 1.0000
RUDDER WAKE FRACTION AT INITIAL SPEED ----- 0.1200
GRADIENT OF RUDDER SIDE FORCE (1./RADIANS) ----- 1.1700
HULL INFLN COEFF ON DRFT ANGL AT RUDDER (kappa) -- 0.4400
LATERAL AREA OF SONAR DOME (ENTER 0 IF NO DOME) -- 0.0000
SONAR DOME SIDE FORCE GRADIENT (1./RADIANS) ----- 0.0000
DISTANCE FROM DOME TO LCG IN FEET ----- 0.0000

```

Results From Non-Linear Analysis of Kinetics and Kinematics
(Mariner Model Test Data)

RUDDER ANGLE	BETA-G (BT)	BETA-R (BR)	ALPHA (AR)	DIAM/L (RD)	V/V0 (Vn)	OMEGA (Rn)	ANGVEL (r)	RSFCE (CYR)	BT/Rn
35.00	10.04	19.70	26.33	5.62	0.8164	0.3560	1.0819	0.54	0.4922
30.00	9.47	18.49	21.87	6.06	0.8444	0.3300	1.0372	0.45	0.5009
25.00	8.86	17.27	17.40	6.54	0.8701	0.3060	0.9910	0.36	0.5054
20.00	8.16	15.88	13.01	7.17	0.8981	0.2790	0.9327	0.27	0.5105
15.00	7.33	14.24	8.73	8.06	0.9282	0.2480	0.8568	0.18	0.5159
10.00	6.25	12.15	4.65	9.52	0.9598	0.2100	0.7502	0.10	0.5195
9.00	6.00	11.63	3.88	10.00	0.9667	0.2000	0.7197	0.08	0.5236
8.00	5.70	11.06	3.13	10.53	0.9731	0.1900	0.6882	0.06	0.5236
7.00	5.36	10.45	2.40	11.11	0.9787	0.1800	0.6558	0.05	0.5197
6.00	5.04	9.85	1.67	11.76	0.9837	0.1700	0.6225	0.03	0.5174
5.00	4.63	9.08	1.00	12.74	0.9890	0.1570	0.5780	0.02	0.5147
4.00	4.12	8.10	0.44	14.29	0.9941	0.1400	0.5181	0.01	0.5136
3.00	3.50	6.92	-0.04	16.67	0.9978	0.1200	0.4457	-0.00	0.5091
2.00	2.90	5.76	-0.53	20.00	0.9994	0.1000	0.3720	-0.01	0.5062
1.00	1.80	3.52	-0.55	33.33	1.0000	0.0600	0.2233	-0.01	0.5236
0.50	1.05	1.91	-0.34	66.67	1.0000	0.0300	0.1117	-0.01	0.6109
-0.50	999.99								(no simultaneous solution for force and moment equations)

BT - DRIFT ANGLE AT CENTER OF GRAVITY (degrees)
 BR - DRIFT ANGLE AT RUDDER (degrees)
 AR - RUDDER ANGLE OF ATTACK (degrees)
 RD - NON-DIMENSIONAL STEADY TURNING DIAMETER (diam./LWL)
 Vn - NON-DIMENSIONAL RELATIVE SPEED DROP (V/Vo)
 Rn - ANGULAR VELOCITY OF TURNING MOTION ($r \cdot (3.14159/180) \cdot L/V$)
 r - ANGULAR VELOCITY OF TURNING MOTION (deg./sec.)
 CYR - RUDDER SIDE FORCE COEFFICIENT
 V - STEADY LINEAR VELOCITY (ft/sec)
 Vo - APPROACH LINEAR VELOCITY (ft/sec)

Table D-2

Diagram of Steering Program (STRDGM06) - Input Echo

TITLE - MARINER	27.0000
SHIP DRAFT IN FEET -----	520.0000
SHIP LOAD WATERLINE IN FEET -----	76.0000
SHIP BEAM IN FEET -----	0.0000
SHIP TRIM BY THE STERN -----	18674.0000
SHIP DISPLACEMENT IN LONG TONS -----	0.9807
MIDSHIP SECTION COEFFICIENT -----	260.4000
DISTANCE BETWEEN LCG AND RUDDER STOCK IN FEET -----	7020.0000
CENTERPLANE AREA FWD OF MIDSHIPS (sq.ft.) -----	6669.0000
CENTERPLANE AREA AFT OF MIDSHIPS (sq.ft.) -----	20.0000
INITIAL SPEED IN KNOTS -----	159571.0000
RESISTANCE IN POUNDS AT INITIAL SPEED -----	0.1600
THRUST DEDUCTION FACTOR AT INITIAL SPEED -----	0.2300
PROPELLER WAKE FRACTION AT INITIAL SPEED -----	1.0000
NUMBER OF PROPELLERS -----	22.0000
PROPELLER DIAMETER IN FEET -----	225.0000
RUDDER AREA FOR ONE RUDDER (sq.ft.) -----	150.0000
AREA OF RUDDER IN PROPELLER RACE (sq.ft.) -----	1.5000
ASPECT RATIO OF RUDDER (span ² /area) -----	1.0000
NUMBER OF RUDDERS -----	0.1200
RUDDER WAKE FRACTION AT INITIAL SPEED -----	1.3000
GRADIENT OF RUDDER SIDE FORCE (1./RADIANS) -----	0.4400
HULL INFLN COEFF ON DRFT ANGL AT RUDDER (kappa) --	0.0000
LATERAL AREA OF SONAR DOME (ENTER 0 IF NO DOME) --	0.0000
SONAR DOME SIDE FORCE GRADIENT (1./RADIANS) -----	0.0000
DISTANCE FROM DOME TO LCG IN FEET -----	0.0000

Results From Non-Linear Analysis of Kinetics and Kinematics
(Mariner Model Test Data)

RUDDER ANGLE	BETA-G (BT)	BETA-R (BR)	ALPHA (AR)	DIAM/L (RD)	V/V0 (Vn)	OMEGA (Rn)	ANGVEL (r)	RSFCE (CYR)	BT/Rn
35.00	9.27	18.11	27.03	6.19	0.8519	0.3230	1.0243	0.61	0.5009
30.00	8.80	17.14	22.46	6.60	0.8732	0.3030	0.9849	0.51	0.5069
25.00	8.22	15.97	17.97	7.14	0.8971	0.2800	0.9350	0.41	0.5124
20.00	7.61	14.79	13.49	7.75	0.9188	0.2580	0.8824	0.31	0.5148
15.00	6.85	13.29	9.15	8.70	0.9440	0.2300	0.8082	0.21	0.5198
10.00	5.92	11.52	4.93	10.05	0.9674	0.1990	0.7166	0.11	0.5192
9.00	5.70	11.06	4.13	10.53	0.9731	0.1900	0.6882	0.09	0.5236
8.00	5.40	10.49	3.39	11.11	0.9787	0.1800	0.6558	0.08	0.5236
7.00	5.10	9.91	2.64	11.76	0.9837	0.1700	0.6225	0.06	0.5236
6.00	4.80	9.33	1.89	12.50	0.9879	0.1600	0.5883	0.04	0.5236
5.00	4.44	8.70	1.17	13.33	0.9914	0.1500	0.5535	0.03	0.5166
4.00	3.85	7.55	0.68	15.38	0.9962	0.1300	0.4821	0.02	0.5169
3.00	3.51	6.93	-0.05	16.67	0.9978	0.1200	0.4457	-0.00	0.5105
2.00	2.90	5.76	-0.53	20.00	0.9994	0.1000	0.3720	-0.01	0.5062
1.00	1.80	3.52	-0.55	33.33	1.0000	0.0600	0.2233	-0.01	0.5236
0.50	1.30	2.45	-0.58	50.00	1.0000	0.0400	0.1489	-0.01	0.5673
-0.50	0.50	0.61	-0.77	500.01	1.0000	0.0040	0.0149	-0.02	2.1821
-1.00	999.99								(no simultaneous solution for force and moment equations)

BT - DRIFT ANGLE AT CENTER OF GRAVITY (degrees)
 BR - DRIFT ANGLE AT RUDDER (degrees)
 AR - RUDDER ANGLE OF ATTACK (degrees)
 RD - NON-DIMENSIONAL STEADY TURNING DIAMETER (diam./LWL)
 Vn - NON-DIMENSIONAL RELATIVE SPEED DROP (V/Vo)
 Rn - ANGULAR VELOCITY OF TURNING MOTION ($r \cdot (3.14159/180) \cdot L/V$)
 r - ANGULAR VELOCITY OF TURNING MOTION (deg./sec.)
 CYR - RUDDER SIDE FORCE COEFFICIENT
 V - STEADY LINEAR VELOCITY (ft/sec)
 Vo - APPROACH LINEAR VELOCITY (ft/sec)